AN ABSTRACT OF THE DISSERTATION OF

S. Morgaine McKibben for the degree of Doctor of Philosophy in Oceanography presented on December 20, 2016.

Title: Above and Below: Oregon Coastal Phytoplankton Bloom Dynamics from Sea and Space

Abstract approved: _____

Angelicque E. White

Phytoplankton are a sentinel class of organisms in the marine environment. Through their photosynthetic activity in sunlit waters worldwide, phytoplankton shape the health and productivity of marine ecosystems and impact the global climate. In this work a range of ocean sensing technologies (via ships, surf zone sampling, moorings, gliders, and satellites) are applied to investigate phytoplankton bloom dynamics from event to regional and climate scales along the Oregon coastal region, a productive eastern boundary upwelling regime.

Chapters 2 and 3 investigate patterns in, and mechanisms behind, Oregon coastal harmful algal blooms (HABs). Chapter 2 presents the temporal and spatial occurrence of HAB events in this region and investigates ecological conditions associated with them. Elevated HAB activity was observed in 2009-2010 and coincided with anomalously warm ocean conditions, specifically a brief change in the Pacific Decadal Oscillation (PDO) to a warm phase and a coincident El Niño event. Through these analyses, key parameters came to the forefront as informative to future monitoring efforts such as wind stress, a metric for when putative blooms

may move on/off shore, particulate dissolved domoic acid in surface waters, and the abundance of *Alexandrium* spp. which appear to be strongly predictive of potential saxitoxin contamination of shellfish.

Chapter 3 provides the first evidence of climatic regulation of domoic acid in shellfish over the past 20 years in the Northern California Current regime. The timing of elevated domoic acid and changes in plankton communities are found to be strongly related to warm phases of the PDO and the Oceanic Niño Index, an indicator of El Niño events. Based on these findings, a risk assessment model is developed to forecast bloom events.

Chapter 4 explores patterns in the surface (horizontal) and depth (vertical) distribution of phytoplankton based on the universal autotrophic pigment chl-a. Results were considered with respect to season (upwelling or downwelling) and region (high chl-a nearshore to low chl-a offshore). Applications of glider-based primary productivity models to evaluating satellite-based estimates of ocean primary productivity are discussed. The research presented in this dissertation shows the power of long-term ocean observations from a variety of vantage points to describe the patterns and processes in the vast ocean that affect the tiniest of Earth's photosynthetic life.

Above and Below: Oregon Coastal Phytoplankton Bloom Dynamics from Sea and Space

by

S. Morgaine McKibben

A DISSERTATION

submitted to

Oregon State University

in partial fulfillment of
the requirements for the
degree of

Doctor of Philosophy

Presented December 20, 2016
Commencement June 2017

Doctor of Philosophy dissertation of S. Morgaine McKibben presented on December 20, 2016

APPROVED:

Major Professor, representing Oceanography

Dean of the College of Earth, Ocean, and Atmospheric Sciences

---

Dean of the Graduate School

I understand that my dissertation will become part of the permanent collection of Oregon State University libraries. My signature below authorizes release of my dissertation to any reader upon request.

S. Morgaine McKibben, Author

ACKNOWLEDGEMENTS

There are many that I have to thank for helping me during the journey to achieving this lifelong career goal.

First, my advisor, Angel. Thank you for taking on the task of having me as a student and seeing me through two graduate degrees. You have advised me with patience and determination, a sense of humor, and (necessarily) ruthless editing. Thank you for your guidance, I am a better scientist because of it.

To Katie Watkins-Brandt, I don't think I've spent more time at sea with, or more hours dancing with (Zumba!), any other person on this planet! We were an unstoppable team all those times at sea (BGSD!). Your lab expertise helped me more times than I can count. Beyond work you are a great friend, willing at anytime to lend an ear or share a laugh. Thank you for your friendship.

An especially huge thank you to Bill Peterson for always giving thoughtful feedback on manuscripts and for being so positive to work with. Your willingness to share your wealth of NH-line data with me for my research efforts is so greatly appreciated. You have been a great colleague to work with.

I extend great appreciation to the OSU Glider Group, to Kipp Shearman and Jack Barth for sharing your Slocum glider dataset so I could conduct my research. Thank you to Anatoli Erofeev for taking the time to process (and reprocess) the data for for me and answering my many questions about it. Thank you to Zen Kurokawa for extensive help in conducting the in-lab glider experiments.

Thank you to Lori Hartline for all the great grad school advice over the years. You and Katie are the most fun people on Earth to go to sea with, thanks for all the help on the cruises. I will always fondly remember our hard-working days at sea, punctuated by laughs, naps, bean bags, and pirate's booty.

Thank you to Robert Allan, you have always been so approachable and helpful with graduate student questions. Your encouragement, humor, positive attitude, and great advice over the years helped me get through grad school.

Thank you to all coauthors and collaborators for your input and assistance throughout the MOCHA project (Bill Peterson, Michelle Wood, Matt Hunter, Zach Forster, Alyssa Hopkins, Xiuning Du). Thank you to Captain Mike Kriz of the R/V Elakha and first mate Cody for taking us to sea to collect our numerous MOCHA samples. I also thank the many cruise volunteers that came on MOCHA cruises and helped collect samples.

Going back to my undergraduate career at UC Santa Cruz, a handful of people stand out as instrumental in my educational and, ultimately, career path. Thank you to Prof. Donald Potts, who provided me with my first experience working with a research lab and also my first cruise expedition on a global class research vessel. Through volunteer work aboard the R/V Martin with then graduate student Kelly Newton on the Wind to Whales project I discovered my love for oceanographic field work that persists even now. In Prof. Raphael Kudela's Introductory Oceanography class I discovered my passion for in biological oceanography and satellite remote sensing. Also so many thanks to Sherry Palacios, who I first met as a TA for that course. You recognized my interest and encouraged me to volunteer in the Kudela Lab where I obtained further lab and cruise experience and made connections that persist through today. In the years since, you've continued to offer advice whenever I've tossed various questions your way, thank you so much for that. And, finally, for aiding in my the transition to graduate school at Oregon State I am indebted to Pete Strutton, my first and most brief advisor, and Tawnya Peterson.

For my family tributes, it feels there are no words to capture my gratitude and love, but I'll try. Thank you to my Dad for being a model of the persistence it takes through graduate school. Thank you for supporting me and believing in me.

Thank you to my Mom for instilling in me values of independence, skepticism, and passion. All of those qualities are vital to getting through grad school, as well as life in general. You have always been my biggest cheerleader. You've helped me get back up and keep going after so many hard times in life. I would not be who I am today without your unconditional love and support.

Last, and the inverse of least, thank you to my husband and our daughter. Lili, you are my sweet pride and joy, you bring sunshine and inspiration into my every day with your curiosity, intelligence, and sweet giggles. Chris, you have been my foundation through the ups and downs of graduate school. You are a consistent source of peace and stability (not to mention those fantastic meals) that so perfectly balances my spirited and chaotic nature. Thank you for being such a wonderful partner in life together and standing with me through graduate school. Whew, it's finally over. I look forward to starting our next adventure together in California!

CONTRIBUTION OF AUTHORS

Angelicque E. White provided intellectual contributions and editing for all chapters of this manuscript. William T. Peterson, A. Michelle Wood, Matthew V. Hunter, and Vera T. Trainer provided feedback and editing for Chapters 2 and 3 and are each coauthors on one or both chapters. William T. Peterson provided data and intellectual contributions for Chapter 3. Katie S. Watkins-Brandt, Zach Forster, Alyssa Hopkins, Xiuning Du, Bich-Thuy Eberhart, provided sample processing efforts, feedback, and/or editing on Chapter 2 and are coauthors on that chapter.

TABLE OF CONTENTS

TABLE OF CONTENTS (Continued)

TABLE OF CONTENTS (Continued)

LIST OF FIGURES

LIST OF FIGURES (Continued)

LIST OF TABLES

ABOVE AND BELOW: OREGON COASTAL PHYTOPLANKTON BLOOM DYNAMICS FROM SEA AND SPACE

1. INTRODUCTION

Phytoplankton are unicellular, photosynthetic organisms that inhabit the sunlit surface layer of the world's oceans. As the ocean's primary producers they use carbon dioxide, water, and energy from the sun to synthesize oxygen and organic molecules (sugars). The energy biochemically captured by this process is transferred to other organisms through the marine food web, ultimately providing the fuel necessary for cellular respiration to most organisms in the marine environment. Considering that over 70% of the Earth's surface is sunlit ocean inhabited by phytoplankton and one liter of water can have thousands to millions of phytoplankton cells, the photosynthetic activity of these microbes extends beyond their role as the base of the marine foodweb in their local ecosystem; phytoplankton are responsible for up to half of global net primary productivity (Field et al., 1998). Marine ecosystems, the global climate, and atmosphere are all affected to a significant degree by phytoplankton photosynthesis. As microscopic organisms with global-scale impact, phytoplankton are a quintessential example of strength in numbers.

Coastal zones, which include shallower seas along continental margins and estuaries, represent 8-10% of the ocean's surface yet are responsible for 20-30% of global primary production and support an estimated 90% of fisheries (Agardy et al., 2005; Pauly and Christensen, 1995). Eastern boundary upwelling regimes, such as those found in the California, Peru-Humboldt, Canary and Benguela Currents, are a relatively small yet particularly productive subset of these coastal zones. Occupying 0.3%-1% of the world oceans, these regions represent about 2% of global ocean productivity and support 35% of fisheries (Carr, 2001; FAO, 2007). In these

areas, sustained equatorward winds move alongshore of the coastal-ocean margin inducing net offshore transport of water through Ekman transport (Cosmic, 1987). This displacement of nearshore waters causes deep, cold, nutrient-rich waters to move to the sunlit surface, creating conditions conducive to relatively high rates of phytoplankton growth and productivity. Among the most productive regions in the world, phytoplankton form the foundation of these plentiful, diverse ecosystems that which numerous marine organisms, as well as humans and coastal economies, depend.

Regional-scale efforts to establish baseline metrics of phytoplankton abundance and distributions, as well as drivers of phytoplankton bloom dynamics, are necessary to better constrain how they respond to natural and anthropogenic environmental change. In ecologically and economically sensitive coastal zones this work is necessary to provide improved understanding of marine-related impacts on regional food web processes and coastal ecosystem services, as well as the impact of these zones on global climate. The work presented herein adds to this body of research by investigating phytoplankton dynamics in the coastal waters of a classic eastern boundary upwelling regime along the U.S. West Coast. Specifically, two regionally and globally relevant ecological questions are addressed: 1) what are the environmental factors governing the abundance of toxic phytoplankton and the concentration of phycotoxins in the foodweb, with a specific focus on toxin concentrations in shellfish; 2) how are phytoplankton spatially distributed in the water column of upwelling regimes along onshore and offshore gradients, and how does this impact estimates of phytoplankton productivity?

1.1. Oregon coastal harmful algal blooms

1.1.1 Background

Phytoplankton blooms are typically benign or beneficial in terms of their impact on the aquatic environment, but a small subset of blooms termed harmful algal blooms (HABs) can be deleterious. HAB events occur in coastal and freshwater ecosystems worldwide and are broadly categorized as either non-toxic or toxic. Non-toxic HABs impact marine ecosystems through physical alteration of the marine environment or physical damage to organisms that cause mass mortality events (Anderson and Garrison, 1997; Glibert et al., 2005). Toxic HAB events occur when blooms of phytoplankton species that produce phycotoxins are introduced into the marine foodweb (Anderson and Garrison, 1997; Van Dolah, 2000). This occurs when toxigenic blooms are ingested in sufficient quantities by suspension feeders such as bivalves or small fish. Subsequent biomagnification leads to increased toxin concentration in organisms with each successive trophic level. The greatest toxin concentrations can often be found in higher trophic level organisms such as marine mammals, seabirds, and large fish and can result in mass mortality events in wildlife. The toxins also pose a threat to human consumers of certain seafood and shellfish. Depending on the type of toxin and amount ingested, humans may experience a range of symptoms from mild (gastrointestinal distress) to extreme (memory loss, death).

HAB events worldwide are increasing in frequency, persistence, and spatial coverage (Anderson et al., 2008; Hallegraeff, 1993; Van Dolah, 2000). The deleterious nature of HAB activity is particularly apparent in highly productive coastal zones as they tend to have greater human population density with a strong de-

pendence on the nearby marine environment. These regions often have vibrant commercial and recreational harvest of potentially toxic shellfish. HAB events are costly to coastal economies that rely on marine ecosystem services, such as fisheries and tourism (Hoagland and Scatasta, 2006). Most coastal regions affected by toxic HABs have ongoing HAB-monitoring efforts to protect public health by reducing incidences of sickness caused by ingestion of toxins. Due to the widespread ecosystem and economic effects, HAB researchers work to characterize the frequency and distribution of these events, search for causal mechanisms, and develop forecasting systems to mitigate the impacts of HABs on economies and public health.

Chapters 2 and 3 investigate toxic HAB events in the Oregon coastal region. In this region there are two potent neurotoxins of concern that are produced by phytoplankton. Domoic acid (DA) is produced by some species of the diatom genus *Pseudo-nitzschia*. DA mimics glutamate, a primary neurotransmitter in the vertebrate brain, binding more readily to receptor sites than glutamate. This can lead to neurological dysfunction, including seizures and memory loss. Saxitoxin (STX) is produced by certain dinoflagellates, including some species of *Alexandrium*. Saxitoxin acts as a selective sodium channel blocker causing neurological dysfunction that can lead to paralysis. When present in sufficient quantities in the water column, both STX and DA accumulate in the marine food web. Human consumption of DA- or STX-contaminated shellfish can lead to Amnesic Shellfish Poisoning (ASP), also known as domoic acid poisoning (DAP), or Paralytic Shellfish Poisoning (PSP), respectively (Picot et al., 2011). Symptoms of these illnesses range from gastrointestinal distress to neurological dysfunction such as memory loss and seizures (ASP) or paralysis (PSP) and, in rare cases, death (Van Dolah, 2000). The overarching goal of chapters 2 and 3 is to describe when and where these HAB events occur in the

coastal upwelling zone off the U.S. West Coast state of Oregon and to understand the mechanisms driving these ecologically and economically deleterious events.

1.1.2 Scope of research

DA and STX HAB events occur all along the U.S. West Coast, affecting several types of wildlife (e.g. marine mammals, birds) and commercially-harvested organisms (e.g. crabs, shellfish) Lewitus et al. (2012). In Oregon, the shellfish industry is most heavily affected by DA and STX. HAB-induced restrictions imposed on commercial and recreational shellfish harvesting are costly. In the first known estimate for Oregon, Nosho et al. 1999 determined that full closures of razor clam fisheries in 1991 along the Washington and Oregon coasts resulted in a loss of $23-$28 million in combined revenue to these states. Prior to 2007, HABs along the Oregon coast had been understudied compared to California and Washington. In response to this, a collaborative research program termed MOCHA, Monitoring Oregon Coastal Harmful Algae, was funded by the National Oceanic and Atmospheric Administration as the first long-term project (5 years) to explore HAB events in this region. The MOCHA project's primary goals included collection of the scientific data necessary to describe both HAB occurrence in Oregon and the ecological mechanisms underlying the events, then to use these findings to inform future HAB monitoring.

The MOCHA project collected the first extensive time series database of the Oregon coastal region's biological, chemical, and physical variables in both the surf zone and offshore habitat over a variety of sampling scales. Chapter 2 is a synthesis of these data, providing the first synopsis of coast wide HAB occurrence and frequency. This work also includes two more in-depth case studies of the largest toxic HAB events observed during the MOCHA time frame focused on defining the en-

vironmental conditions associated with HAB events in the study region. Chapter 3 further explores ecological mechanisms through investigation of controls on shellfish DA at the climate-scale, a large time-space scale perspective relative to previous research on DA regulation. Over 20 years of toxin monitoring in Oregon reveals a robust, predictable association between DA in shellfish and climate-scale warm ocean conditions, the first evidence for climatic regulation of shellfish DA toxicity.

1.2. Remote observations of phytoplankton via Slocum glider and satellite

1.2.1 Background: Chlorophyll-a

Phytoplankton utilize an array of pigments to harvest energy from the sun to fuel photosynthesis. Chlorophyll-a (chl-a) stands out as the one universal pigment found in nearly all phytoplankton, making it a unique biomarker that serves as a proxy of bulk phytoplankton abundance. Due to the key role phytoplankton play in biogeochemical processes and the ability to measure chl-a or proxies therof relatively easily with several different methods, chl-a concentration is likely the most frequently measured biogeochemical parameter in oceanography (Jeffrey et al., 1997). Three commonly applied methods of chl-a quantification include: extraction of chl-a pigments from discrete water samples; in-water fluorometry; and satellite-based approximation of surface chl-a derived from reflectance measurements. Extraction techniques generally include filtration of a known volume of water onto a filter followed by extraction of the pigment and quantification via absorbance or fluorescence (Millie et al., 2011; Arar and Collins, 1997). These measures, sampled using water collected from the surface or other depths of interest, reflect discrete measurements

and a point in space/time in the water column. In-water fluorometers, in contrast, provide much finer time- (seconds to minutes over periods of weeks to months) and depth- (when vertically profiling,$<$ 1 meter) resolved chl-a measurements. Fluorometers emit blue light that induces excitation of chl-a molecules and then measure the resulting emission of red light (fluorescence), a signal that is distinctive to chl-a. Platforms for fluorometers are varied: from a Eulerian view of the surface collected at a static mooring location or Lagrangian view afforded by drifters, to vertical and horizontal surveys conducted by autonomous gliders (e.g. Schofield et al. (2007); Eriksen et al. (2001)), bio-argo floats (Claustre et al., 2010), or even elephant seals (Xing et al., 2012), among others. Earth-orbiting satellites equipped with visible spectral radiometers are a another major source of chl-a estimates. These platforms provide daily measures of chl-a for nearly the entire ocean, offering a consistent (as clouds allow), synoptic-scale record of chl-a. Collectively these commonly used tools provide a wealth of information on phytoplankton abundance and distribution applied to a broad range of research questions worldwide.

There is a major caveat to this apparently ideal proxy: chl-a concentration is commonly regarded as a measure of phytoplankton biomass without qualification even though the relationship between various proxies of biomass is not constant (Kruskopf and Flynn, 2005; Falkowski et al., 1985). Phytoplankton physiology changes the chl-a to carbon (chl:C), ratio according to changes in phytoplankton community composition and environmental conditions such as light (Kiefer, 1973; Álvarez et al., 2016) and nutrient (Kruskopf and Flynn, 2005) status. A second, and often related, consideration is that each instrument and protocol applied to quantify chl-a concentration comes with its own set of assumptions and limitations, providing another layer of uncertainty in chl-a concentration measurements. For example, a

protective mechanism known as non-photochemical quenching (NPQ) that protects phytoplankton cells from damage during high light conditions dampens fluorescence signal per unit chl-a (Falkowski and Kiefer, 1985). This causes an apparent decrease in chl:C during high light conditions (Sackmann et al., 2008). As another example, the accuracy of standard satellite-based chl-a products is known to be reduced in coastal regions (Werdell and Franz, 2007) because the measurement algorithms were developed in comparatively clearer, optically simpler open ocean regions where contaminants to the chl-a signal such as dissolved organic matter are less significant. These examples, among many others, demonstrate that each method quantifies chl-a from a different perspective (in terms of both protocol and time-space scales), hence carries their own differing sets of strengths, weaknesses, and assumptions. It is important that these considerations are, at minimum, acknowledged or, at best, constrained in applications seeking to constrain chl-a concentration as a proxy for phytoplankton biomass and production. In sum, researchers must ask not only questions may be investigated with chl-a data (Chapter 4), but also consider based on known sources of uncertainty what those data represent with respect to the actual abundance of phytoplankton (Appendix A).

1.2.2 Scope of research

Marine biogeochemical research, in particular the global carbon cycle, as well as ecosystem and resource management applications, depend on satellite chl-a products as a proxy for phytoplankton. Models that estimate the net primary productivity (NPP) of the world's oceans require satellite-based estimates of phytoplankton abundance (Carr et al., 2006), such as standard chl-a products (O'Reilly et al., 2000). Satellite-derived chl-a represents the average chl-a concentration within the

first optical depth (FOD), or first extinction depth of solar irradiance in the water column. Empirical models are then used to extrapolate from surface chl-a to depth-integrated chl-a within the euphotic depth, defined as the depth where sunlight is 1% of surface values. These models typically assume a constant power law relationship between surface chl-a and euphotic-depth integrated chl-a (Morel and Berthon, 1989; Morel and Maritorena, 2001). The presence of subsurface chl-a maxima associated with density features, vertical migration of motile plankton, or other processes that concentrate phytoplankton in discrete layers can violate the assumptions of a well mixed-surface layer followed by a smooth decay in chl-a with depth. In these instances satellites can miss a potentially significant fraction of chl-a and underestimate depth-integrated pigment concentrations. This is a known issue for NPP models that rely on standard surface chl-a products to estimate depth-integrated chl-a. Regional-scale evaluation of satellite chl-a proxies and modeled euphotic zone chl-a content applied to ocean NPP models is key to improving global carbon budget models.

In the last decade or so oceanography has added to its sampling toolbox an array of autonomous, vertically-profiling platforms that cover larger temporal and spatial scales than any previous *in situ* methods. These ubiquitous datasets collectively represent the largest number of water column chl-a measurements in existence (Lavigne et al., 2012). This provides a data-rich source of *in situ* ocean measures within the full euphotic zone at time-space scales ideal for pairing with satellite remote sensing data. In this dissertation, an 8 year dataset of bio-optical (chl-a, backscatter) and physical (temperature, salinity) parameters collected by routine Slocum glider deployments off the dynamic central Oregon coast were combined with shipboard extracted and satellite chl-a observations. Appendix A thoroughly

considers best practices for calibration of the gliders' bio-optical instruments, with an emphasis on necessary corrections for chl-a fluorometry. This provides the dataset necessary for chapter 4 which compares in water and satellite chl-a proxies, then tests a model of the surface chl-a to chl_{tot} relationship (Morel and Berthon, 1989) that is utilized in a widely applied model of NPP (Behrenfeld and Falkowski, 1997b). The glider dataset spans a productive, high chl-a upwelling regime along the Oregon coast to a less productive, low chl-a offshore region nearly year round. This allows the model to be tested relative to seasonal and physical variability in differing ocean regimes. The findings are then extended to in-water NPP models for the coastal Oregon waters of the productive California Current regime.

Chapter 2:
Monitoring Oregon Coastal Harmful Algae: observations and implications from a harmful algal bloom monitoring project

S. Morgaine McKibben[1], Katie S. Watkins-Brandt[1], A. Michelle Wood[2], Matthew Hunter[3], Zach Forster[4], Alyssa Hopkins[2], Xiuning Du[4], Bich-Thuy Eberhart[5], William T. Peterson[6], Angelicque E. White[1]

[1]College of Earth, Ocean and Atmospheric Sciences, Oregon State University, 104 CEOAS Administration Building, Corvallis, OR 97331, USA

[2]Institute of Ecology and Evolution, 5289 University of Oregon, Eugene, OR 97403, USA

[3]Oregon Department of Fish and Wildlife, 2001 Marine Drive, Astoria, OR 97103, USA

[4]Cooperative Institute for Marine Resources Studies, Oregon State University, Hatfield Marine Science Center, 2030 SE Marine Science Drive, Newport, OR 97365, USA

[5]Marine Biotoxins Program, Environmental and Fisheries Sciences Division, Northwest Fisheries Science Center, National Marine Fisheries Service, National Oceanic and Atmospheric Administration, 2725 Montlake Blvd. E, Seattle, WA 98112, USA

[6]National Oceanic and Atmospheric Administration, Northwest Fisheries Science Center, Hatfield Marine Science Center, 2032 S. OSU Drive, Newport, OR 97365, USA

Published in *Harmful Algae*
December 2015
Volume 50
Pages 32-44

2. MONITORING OREGON COASTAL HARMFUL ALGAE: OBSERVATIONS AND IMPLICATIONS FROM A HARMFUL ALGAL BLOOM MONITORING PROJECT

2.1. Abstract

The accumulation of domoic acid (DA) and saxitoxins (STX), phycotoxins produced by some species of *Pseudo-nitzschia* and *Alexandrium*, respectively, in coastal food webs are a focus of research on the West Coast of the United States due to the deleterious effects they have on coastal ecosystems and economies. Results are presented from the 2007-2012 Monitoring Oregon Coastal Harmful Algae (MOCHA) project, the Oregon coasts first HAB monitoring and research program. Both historical toxin databases and more detailed case-study observations of individual HAB events are compiled to provide the first detailed overview of HAB occurrence in this region. These results are also presented in the context of informing future HAB monitoring in this and other upwelling regimes affected by STX and DA. A 2009-2010 warming event was associated with the greatest HAB activity during the MOCHA project, including anomalously high sea surface temperatures and shellfish harvesting closures due to STX and DA in 2009 and 2010, respectively. In regards to HAB monitoring, it is shown that (1) razor clams are a more sensitive indicator of DA than mussels; (2) water column concentrations of particulate domoic acid greater than 10^3 ng L^{-1} can be used as a threshold for early-warning of shellfish DA toxicity and (3) approximately bi-weekly, or shorter, monitoring of *Alexandrium* in the surf zone and/or offshore can provide advance notice of STX

contamination of shellfish. Both of the latter two metrics gain added value when coupled with daily wind stress, a proxy of downwelling/relaxation events, which facilitate greater interaction between offshore blooms and shellfish.

2.2. Introduction

Globally, harmful algal blooms (HAB) are increasing in their frequency, persistence, toxicity, and regional coverage (Anderson et al., 2008; Hallegraeff, 1993; Van Dolah, 2000). Toxigenic HAB events along the West Coast of the United States are no exception and have been a topic of extensive HAB research and monitoring due to the threats they impose on coastal economies, ecosystems, and public health. Two of the major phycotoxins of interest in this region are the water-soluble amino acid domoic acid (DA), produced by some species of the diatom genus *Pseudo-nitzschia*, and a suite of heterocyclic guanidines collectively called saxitoxins (STX) that are produced by certain dinoflagellates, including some species of *Alexandrium* (Horner et al., 1997; Horner, 2001; Van Dolah, 2000). Both STX and DA can accumulate in the marine food web, potentially threatening living marine resources and public health. Human consumption of DA- or STX-contaminated shellfish in sufficient quantities can lead to Amnesic Shellfish Poisoning (ASP) or Paralytic Shellfish Poisoning (PSP), respectively (Picot et al., 2011). Symptoms of these illnesses range from gastrointestinal distress to neurological dysfunction and, in rare cases, death. (Horner et al., 1997) note that it is evident from early records, local native customs and the apparent ability of some native marine animals to distinguish toxic prey items, that PSP has been present on the West Coast for hundreds of years, perhaps longer. (Fryxell et al., 1997) found historical accounts of *Pseudo-nitzschia* on the

West Coast, including reports of *Pseudo-nitzschia* in Oregon as early as 1920. Globally, DA and ASP first became a public health concern in 1987 when an outbreak of food-related illness, including three deaths, in Prince Edward Island, Canada were traced to DA in mussels (Bates et al., 1989). On the West Coast of the United States, the first recorded DA event occurred in 1991 when cormorant and pelican deaths were traced to DA in diatoms (Buck et al., 1992). Subsequent research revealed both DA in razor clams on the West Coast of the U.S (Drum et al., 1993) and the production of DA by *Pseudo-nitzschia* strains isolated from Monterey Bay, California and Coos Bay, Oregon (Garrison et al., 1992; Villac et al., 1993).

The Oregon coast, a key transition zone in West Coast oceanography, has been understudied compared to other regions (Lewitus et al., 2012); although there have been several Master's theses on HAB species in Oregon (Cziesla, 1999; Hughes, 1997; Ohana-Richardson, 2007; Scott, 2007) and a West Coast summit on DA was held at the Oregon Institute of Marine Biology (Wood et al., 1994). In 2007 a collaborative research program termed MOCHA, Monitoring Oregon Coastal Harmful Algae, was the first long-term project (5 years) funded by the National Oceanic and Atmospheric Administration to explore HAB events in this region. The MOCHA project's primary goals included collection of the scientific data necessary to describe both HAB occurrence in Oregon and the ecological mechanisms underlying them and then to use these findings to inform future HAB monitoring.

Harvest restrictions for commercial and recreational harvest of razor clams are costly to Oregons coastal economy. In the first known estimate for Oregon, (Nosho, 1999) determined that full closures in 1991 along the Washington and Oregon coasts resulted in a loss of $23-28 million in revenue in combined revenue to these states. Due to the popularity of these fisheries, the accumulation of phycotoxins in shellfish

poses serious risks for both human health and local economies (Hoagland et al., 2002; Hoagland and Scatasta, 2006; Picot et al., 2011). As a result, the Oregon Department of Agriculture (ODA) has been routinely monitoring STX and DA concentrations in shellfish since 1979 and 1994, respectively. When thresholds of 80 μg 100g^{-1} for STX or 20 ppm for DA are exceeded, shellfish harvesting is suspended. Until the MOCHA project (2007-2012), the ODAs shellfish toxin data (Lewitus et al., 2012) were the only time-series record of HAB events in Oregon, and few data regarding the spatial or temporal variability of HAB forming species were available.

High primary productivity along the Oregon coast occurs from late spring through early fall when net northerly wind stress brings nutrient-rich waters to the surface through Ekman transport. Variability in net northerly and southerly winds occurs on the order of 3-10 days (Hickey and Banas, 2003), driving fluctuations in surface currents and water properties. Phytoplankton blooms are initiated by upwelling-favorable (northerly) winds and, as measured by in situ chlorophyll-a, vary at similar scales (McKibben et al., 2012). Relaxation of these upwelling winds can transport blooms to the shore (Shanks et al., 2014). Du and Peterson (2014) have shown that the patterns of phytoplankton community structure during upwelling season in coastal Oregon follow the classic paradigm of diatom dominance in spring/summer during the early/mid upwelling season and dinoflagellate dominance in autumn/late upwelling season, as the water column warms and stratifies. The trends in species composition (e.g. which diatoms bloom in summer), however, are unpredictable. Given that diatoms and dinoflagellates are favored under different environmental conditions (Smayda and Trainer, 2010), STX-(dinoflagellate) and DA-related (diatom) HAB events do not regularly co-occur. Prediction of specific

HAB events is a goal for coastal managers, but is not currently possible due to the high biophysical variability inherent in coastal upwelling regions (Shanks and McCulloch, 2003). Even so, long-term (years to decades) HAB datasets can be used to determine regions and seasons with the greatest probability of a HAB event; HAB-specific parameters associated with shellfish tissues should be useful as early warning proxies of future HAB events.

The 5-year MOCHA project collected the first extensive time series database of the Oregon coasts biological, chemical, and physical variables in both the surf zone and offshore habitat over a variety of sampling scales. HAB events are defined here as DA or STX levels in coastal shellfish tissue that exceed the threshold values that trigger a closure decision. In order to provide a comprehensive overview of HAB occurrence in Oregon and to inform future HAB monitoring efforts the following are presented: 1) a retrospective analysis of long-term (decades) historical shellfish toxin levels; 2) synoptic, coastwide analysis of HAB events and phytoplankton counts during the MOCHA project and 3) case studies of major HAB events that occurred during the MOCHA project, including a combined view of shipboard, surf zone, and environmental data.

2.3. Data & Methods

2.3.1 Surf zone monitoring

Coastal HAB monitoring was conducted via 1) monitoring of STX and DA levels (1979-present and 1994-present, respectively) in tissue samples from mussels and razor clams and 2) collection of surface water from the surf zone for phytoplankton cell counts (2007-2012). For the former, the ODA collects shellfish at intertidal

sites along the Oregon coast (Fig 2.1) every 2-4 weeks. Shellfish sampled include predominantly mussels *(Mytilus californianus, Mytilus edulis)* and razor clams *(Siliqua patula)*. Concentration of STX is measured using the standard mouse bioassay method (AOAC, 1990) and DA concentrations are measured using high performance liquid chromatography (HPLC) methods recommended by the Canadian Food Inspection Agencys Shellfish Sanitation Program. Detection limits for STX and DA are approximately 38 μg 100 g^{-1} and 1 part per million (ppm), respectively. Closure thresholds for STX and DA in shellfish tissue are 80 μg 100 g^{-1} and 20 ppm, respectively.

The second type of coastal HAB monitoring, phytoplankton counts in the surf zone, was conducted coastwide (Fig 2.1) from 2007-2012. These samples were collected and analyzed by the Oregon Department of Fish and Wildlife (ODFW) every 2-4 weeks for the MOCHA project. Water was collected in the surf zone using a bucket and gently swirled to provide a well-mixed sample. The water was poured into a 125 mL glass jar and fixed with 5 mL of 37% formaldehyde solution buffered with sodium acetate for a final concentration of 1.5% formalin.

Surf zone data were separated into 3 latitudinal bins: north (45°N-46.5°N), central (43°N-45°N), and south (42°N-43°N) (Fig 2.1). Bins partition the data according to distinct hydrographic features: the Columbia River Plume in the north, a retentive feature that is a source of freshwater (and buoyancy); Heceta Bank, a retentive central coast shelf feature (Fig 2.1); and Cape Blanco, a region characterized by a strong coastal jet that both transports water offshore north of Cape

---

[0]Method disseminated at the 1992 Washington Sea Grant Program, Workshop on Domoic Acid, Seattle, WA

Blanco (Fig 2.1; 43°N) but causes also retention to the south between 42-43°N (Tweddle et al., 2010; Venegas et al., 2008). Binning of surf zone samples by region also allows for comparison of data to offshore shipboard sampling.

2.3.2 Shipboard sampling

The central Oregon coast was routinely sampled aboard the R/V Elakha on cruises of 8-12 hour duration from 2007-2012. Cruises covered either the Newport Hydrographic (NH) line only (44.65°N; Fig 2.1) year-round at bi-weekly to monthly intervals, or surveyed six hydrographic lines including the NH-line (Fig 2.1) every 4-6 weeks between March and October. During the latter, up to 28 stations were sampled between 44.2°N to 45°N at isobaths from 20-100 meters (m) deep. The number of stations sampled per cruise and cruises per year varied according to weather conditions and ship availability. Regional surveys also occurred once or twice per year aboard larger research vessels. Data from four of these surveys are included: an August 10-18, 2009 Pacific Coast Ocean Observing System (PaCOOS) cruise aboard the R/V McArthur II; an August 29-September 10 Center for Coastal Margin Observation (CMOP) cruise aboard the R/V New Horizon; a May 24-June 4 2010 PaCOOS cruise aboard the R/V Miller Freeman; and a May 21-May 26 CMOP cruise aboard the R/V Wecoma. Broadly, these cruises covered on- and off-shelf locations off the Oregon, California, and Washington coasts. Data include surface water samples of total phytoplankton cell counts and community composition, as well as coincident concentrations of particulate and dissolved DA (pDA and dDA, respectively).

2.3.3 Shipboard particulate and dissolved domoic acid

Several methods are available for measuring pDA and dDA, including high performance liquid chromatography (HPLC) and various ELISA methods. During the 2003-2006 NOAA's Oceans and Human Health (OHH) project between the University of Oregon and Oregon State University it was decided the indirect competitive enzyme-linked assay kit (PNW-ELISA) already in use by Washington researchers would be used for the MOCHA project. The similarity in methods ensured that data between Oregon and Washington could be compared directly.

For particulate DA (pDA), 1 liter of seawater was filtered onto a 0.45 μm 47 mm diameter nitrocellulose membrane filter (Millipore HAWP04700), which was folded and wrapped in foil. Dissolved DA (dDA) was measured by filtering seawater through a 25 mm 0.45 /mum nitrocellulose membrane filter (Millipore HAWP02500) into a cryovial. Filters and cryovials were frozen and stored at -80°C for weeks up to 26 months prior to DA analysis. Both pDA and dDA in unknown samples were quantified using an indirect competitive enzyme-linked assay (PNW-ELISA) developed at the NOAA/Northwest Fisheries Science Center (Eberhart et al., 2012). Briefly, pDA samples were prepared by placing a filter into a centrifuge tube containing 4 mL of deionized water. The filter was then ground using a metal spatula and sonicated for 2 hours, with vortexing after every hour. Samples were then stored at 4°C overnight to settle any filter paper. Samples for dDA required 10 fold dilution in deionized-distilled water prior to analysis to eliminate sample matrix. Diluted dDA or pDA samples were then distributed into a 96 well plate for ELISA analysis (Eberhart et al., 2012). Note the differences in units for DA levels in coastal shellfish tissue discussed in section 2.3.1 (ppm) and shipboard pDA and dDA samples

(ng L^{-1}). These units were not converted to a common unit to emphasize the two different DA data types and sources.

Cell counts of *Pseudo-nitzschia* that were collected in 2010 were linearly regressed against coincident pDA and dDA for two time frames: all 2010 shipboard data; and May 2010 only, when a DA event was observed. These data were $\log_{10}$ transformed and reduced to only non-zero values from on-shelf (0-200 meter depth) locations between 42°-46.5°N. Count data were subdivided into four categories: total *Pseudo-nitzschia*as well as three size-delineated subclasses (see section 2.3.4).

2.3.4 Phytoplankton cell enumeration

For both shipboard and surf zone cell counts, preserved whole water samples were concentrated prior to counting by chilling samples at 4C overnight and allowing all plankton to settle in the 125 mL jars in which they were collected. Details are described in White et al. (2014). Briefly, samples were concentrated 10 fold, settled on a Palmer-Maloney slide, and then counted using a compound microscope at 200x magnification (20x objective, 10x ocular). The limit of detection for this method is <1000 cells L^{-1}. All diatoms and dinoflagellates were identified to the genus level using Tomas (1997). Counts of *Pseudo-nitzschia* spp. were further subdivided into three categories based on size and morphology: wide (4-8 microns wide); medium (2-4 microns wide); and thin (<2 microns wide). While these size categories are not intended to substitute for species-level identification using cleaned material and/or scanning electron microscopy, three species clusters can be attributed to the categories above: wide, *P. australis, P. fraudulenta, P. heimii*; medium, *P. pungens and P. multiseries*; and thin, *P. delicatissima and P. pseudo-delicatissima* (Trainer and Suddleson, 2005).

2.3.5 Wind stress and seasonal upwelling

Seasonality in this region is defined by a productive spring/summer upwelling season, with net movement of water offshore through Ekman transport. During fall/winter a more turbulent downwelling season is defined by strong southerly (from the south) wind stress and net movement of water towards the shore. Daily net northerly and southerly wind stress was calculated from wind speed and direction data from NOAA station NWP03 in Newport, OR (Fig 2.1) using the methods of Large and Pond (1981).

The cumulative upwelling index (CUI) is a measure of wind stress energy input into coastal waters during upwelling season. The annual CUI is calculated by integrating the daily wind stress observed at Newport, Oregon from January 1st. The first day of the year when integrated wind stress is negative defines day one of both the CUI and upwelling season. The negative value of the CUI is a directional indicator of northerly wind stress and offshore (westward) movement of water due to Ekman transport. A shift to cumulative positive wind stress signifies the end of the annual CUI and day one of downwelling season. Data were obtained from http://damp.coas.oregonstate.edu/windstress/index.html.

2.3.6 Satellite sea surface temperature anomaly

Daily Level-3 (L3) 4-kilometer (km) Moderate Resolution Imaging Spectroradiometer (MODIS) nighttime SST (nSST) standard products (processing version R2012.1) were downloaded for each year that had complete MODIS coverage (20032012) from http://oceancolor.gsfc.nasa.gov/cms. Daily climatology was calculated by composite-averaging imagery for each day of the year (day 1365) from 2003 to 2012, resulting in 365 images that describe the average nSST observed over

a 9-year period. This daily climatology was then subtracted from the corresponding daily L3 nSST product in 2009 and 2010 to yield a daily anomaly product. A Hovmller map was then compiled by averaging 48 km (12 pixels), the approximate average width of the continental shelf along the Oregon coast, due west of the coast for each day of the year and each pixel of latitude from 42°N to 46.5°N. Seasonally, satellite coverage is best and potential bias due to cloud cover is least during upwelling season (McKibben et al., 2012).

2.4. Results

Retrospective shellfish toxin analysis

Coastwide, more mussels than razor clams are sampled for monitoring of STX and DA. For all shellfish and toxin types, the north coast is the most and the south is the least sampled (Table 2.1). Central coast mussel sampling is also relatively high. Razor clams are sampled less frequently than mussels and the number of samples collected decreases from north to south coast regions (Table 2.1).

Levels of STX are more pronounced in mussel versus razor clam tissue; depending on the region, mussel tissue exceeded STX closure levels in 49-108 instances whereas high STX was less frequently observed in razor clams with 0-115 closures (Table 2.1). 107 of the 115 instances in the north were due to sustained high STX values in razor clams during a single event that spanned late 1992-1994 (ODA unpublished data). Aside from this event, STX in mussels surpassed closure levels 8 times in the north. The maximum STX concentrations in mussels were 10-58% greater than in razor clams (Table 2.1). Conversely, DA levels are higher in in razor clam versus mussel tissue: coastwide, 5 mussel samples had DA levels above closure

threshold while 27-107 razor clam samples surpassed threshold (Table 2.1). Maximum DA levels in razor clams were 10-42% higher than maximum DA in mussels (Table 2.1).

Out of the 35-year record of STX levels in shellfish, 20 (57%), 7 (2%), and 14 (40%) of the years had at least one STX sample above closure threshold at north, central, and south coast regions respectively (Table 2.1). In the 35-year record, from June through November coastwide, 201 total mussel samples had STX levels above closure and 11 in December through May (Fig 2.1 b-d). Out of the 22-year record of DA levels in shellfish, 10 (50%), 6 (30%), and 6 (30%) of the years had at least one DA sample above closure threshold at north, central, and south coast regions respectively (Table 2.1). In the 22-year record, from April through November coastwide, 295 total razor clam samples had STX levels above closure and 42 in December through March (Fig 2.1 b-d).

HAB events during MOCHA monitoring time frame

Between 2007 and 2012, STX levels in shellfish tissue samples annually exceeded the closure threshold of 80 μg 100 g^{-1} (Fig 2.2). Elevated STX was most prevalent in 2008 (27/271, i.e. 27 of 271 total samples for the year were above closure threshold) and 2009 (37/390) with samples above closure level 6 and 7 months out of each year, respectively (Fig 2.2 a). From a coastwide perspective, surf zone concentrations of *Alexandrium* spp. corresponded to STX levels in shellfish (Fig 2.2a,b), although not at a statistically significant level (t-test, $p > 0.05$). In contrast, 6 samples of 163 total exceeded the DA closure threshold during just 4 months of the 5-year study period (Fig 2.2 c), and changes in total *Pseudo-nitzschia* spp. were not synchronous with DA (Fig 2.2 c,d).

North coast *Alexandrium* counts (Fig 2.2 b) ranged from <1000 to 23,000 cells L-1 while central and south coast *Alexandrium* spp. had a lower range, from <1000 to 3000 cells L-1 (Fig 2.2 b). Counts of *Alexandrium* were typically below the limit of detection (Fig 2.2 b). In contrast, total *Pseudo-nitzschia* spp. showed marked seasonality, with one to three separate count maxima of 10^5-10^6 cells L^{-1} occurring each year during upwelling season (Fig 2.2 d). Successional patterns of the *Pseudo-nitzschia* subgroups varied considerably from year-to-year, showing no consistent pattern; there was also no clear successional pattern when the time series was separated by region (not shown).

Based on cell count maxima, toxin maxima, and closure frequency, the greatest HAB activity during 2007-2012 occurred in 2009 and 2010 (Fig 2.2). During the first event shellfish harvesting was closed from August through December of 2009 along the entire Oregon coast. Concentrations of *Alexandrium* spp. in the surf zone (23,000 cells L^{-1}, 8 August; Fig 2.2 b) and STX levels (948 g 100 g^{-1}, 1 September; Fig 2.2 a) both reached their highest levels observed during the study period. This event also yielded the third-highest STX value observed since 1979. The second HAB event occurred in mid-2010 when central Oregon coast shellfish harvesting was closed due to elevated DA up to 55 ppm in shellfish tissue (Fig 2.2 c). This was the only DA-related HAB event during the MOCHA study period. These two events were selected for case studies to further elucidate the environmental forcing of these HAB events.

2009-2010 Physical conditions

As indicated by the PDO and a strong El Niño event, the eastern Pacific Ocean was anomalously warm from August 2009 through May 2010 (Fig 2.3). This basin-

scale warming is also observed in local SST observations, which were warmer than average from August 2009 through mid-June 2010 (Fig 2.3 a). Positive temperature anomalies were greatest in August and September 2009, up to +4-5°C, and persisted through spring 2010 (Fig 2.3 a). Negative, or cool favorable, conditions returned in June 2010.

The 2009 upwelling season began on 14 May 2009 (Fig 2.3 b; average is 29 April +/- 24 days) and ended on 12 October 2009. Five downwelling/relaxation events occurred during this upwelling season (Fig 2.3 b). In 2010, upwelling season was delayed, and began on 10 June, one standard deviation later than the mean (30 April). During 2010, two extended upwelling phases in late July and August 2010 alternated with three major relaxation events (Fig 2.3 b). The 2010 upwelling season was 54 days shorter than in 2009, but upwelling wind stress was stronger and more persistent.

2009 STX Event

In 2009, STX concentrations in shellfish first surpassed the closure threshold in late June, late July, and late October at north, central, and south coast regions, respectively (Fig 2.4 a,b,c). North coast surf zone *Alexandrium* spp. counts reached their maximum value for the year (23,000 cells L^{-1}, 8 August; Fig 2.4 a) before the maximum STX value (948 g 100 g^{-1}, 1 September; Fig 2.4 a) for the region. Central coast surf zone *Alexandrium* spp. counts remained low, reaching a maximum of 1,000 cells L^{-1} once each in May, July, and September (Fig 2.4 b). Offshore central coast *Alexandrium* spp. counts increased from May through September 2009, reaching a maximum of 47,000 cells L^{-1} (10 September, Fig 2.4 b). Surf zone STX in this region surpassed closure levels in July through September, with a maximum of 532

g 100 g^{-1} (15 September, Fig 2.4 b). South coast *Alexandrium* spp. surf zone counts were low, reaching high values of 5,000 cells L^{-1} once in June and 1,000 cells L^{-1} in August and September (Fig 2.4 c). South coast STX exceeded the closure threshold in late October and early November, with a high of 757 g 100 g^{-1} (22 October, Fig 2.4 c). In August the ODA closed mussel harvesting over the full Oregon coast. In September all bays and estuaries were closed to the harvest of scallops, oysters, razor clams, and bay clams. Bay clam harvesting was reopened in mid-October, mussels in late December, and razor clams in January of 2010.

Surf zone STX and *Alexandrium* spp. maxima at the north and central coasts in August and September (Fig 2.4 a,b) coincided with regional-scale sampling efforts during two 2009 cruises (10-18 August, Fig 2.5 a; 29 August 3 September and 9-10 September, Figs 2.5b,c). Shipboard sampling occurred during a downwelling phase coincident with periods of high SST (August and September, Figs 2.3 c, 2.5 a-c). During these sampling efforts, surface *Alexandrium* spp cell concentrations reached maxima of 56,000 cells L^{-1} with the highest concentrations (up to 10^4 cells L^{-1}) north of roughly 45°N (Fig 2.5 a,b) off the Oregon and Washington coasts.

2010 DA Event

From May through September 2010, *Pseudo-nitzschia* spp. was commonly present coastwide in surf zone water samples at concentrations up to 10^5, and occasionally up to 10^6, cells L^{-1} (Fig 2.6). Central coast DA levels in shellfish tissue surpassed the closure threshold (20 ppm) from June through August, reaching a maximum of 55 ppm (28 June). In central coast surf zone counts (Fig 2.6 b), the wide, medium, and thin subclasses dominated (comprised >50%) the *Pseudo-nitzschia* community 70%, 19%, and 10% of the time, respectively (n=67); coast-

wide, the wide subclass was dominant prior to closures in June (Fig 2.2 d). From June through late October 2010 the ODA closed razor clam harvesting from Cape Meares to Bandon, OR (see Fig 2.1 for locations). By late August 2010, DA returned to sub-closure levels; DA remained sub-closure in the north and south coasts throughout 2010 (Fig 2.6 a,c).

Three day cruises (Fig 2.7 a,d) and two larger-scale cruises (Fig 2.7 b,e and 2.7 c,f) provided snapshots of the offshore spatial distribution of surface pDA and dDA just prior to the DA-related shellfish harvesting closures in mid and late June (Fig 2.6 b). In early May, surface pDA levels were mostly low (10^1 ng L^{-1}, Fig 2.7 a) with dDA being comparatively elevated (up to 10^2 ng L^{-1}, Fig 2.7 d). The highest pDA and dDA values were recorded south of 45°N after mid-May 2010 (Fig 2.7 b,c,e,f), reaching maximum values of 40,400 ng L^{-1} and 10,300 ng L^{-1}, respectively. In May through June, central coast shipboard total *Pseudo-nitzschia* spp. counts typically ranged from 10^4 to 10^5 cells L^{-1}; 2010 shipboard counts surpassed 10^6 in September four times, with 3,000,000 cells L^{-1} being the highest value (9 September). In May 2010, the only month offshore pDA and dDA were greater than 10^3 ng L^{-1}, a significant relationship was seen between total *Pseudo-nitzschia* and the wide and thin subclasses versus both pDA and dDA (Table 2). When all of the 2010 shipboard data were considered, there were no significant relationships between total *Pseudo-nitzschia* or any of the size subclasses and pDA or dDA (Table 2).

2.5. Discussion

2.5.1 Retrospective analysis of STX and DA levels in shellfish

Historical shellfish toxin levels were analyzed with respect to two questions: 1) when and where are HAB events most likely to occur, i.e. what is the seasonal, interannual, and regional variability in toxin sampling and concentrations; and 2) are mussels versus razor clams better indicators of STX or DA events? The north coast was both more heavily sampled and had the highest occurrence of DA and STX events from year to year compared to other regions. This region is also where the greatest commercial and recreational shellfish harvesting occurs. Even though it is sampled less often, the south coast also had relatively frequent STX events while the central coast had relatively few. Overall, STX events are most likely to occur later in the year from June through November. The most DA events occur from April through November, which encompasses all of upwelling season (generally mid-April through mid-October). Due to the slow depuration rate of razor clams (discussed below), when present DA is found during more months of the year that STX as DA levels remain high for several months after an event has ended.

Levels of STX and DA differ over time in mussel versus shellfish tissues at similar locations. Mussels are more heavily sampled coastwide than razor clams as they are considered the sentinel indicator species for the Oregon coasts STX and DA events due to their far greater abundances and less labor- and skill-intensive harvesting methods. This assumption holds when analyzing mussel tissue for STX; however, if only mussel tissue were sampled, most DA events would be missed entirely due to the low DA levels in mussel tissue. Similarly, razor clams were shown to be poor indicators of STX events relative to mussels, with STX levels in

razor clams rarely passing closure threshold levels.

Depuration of phycotoxins in shellfish can be modulated by a range of factors, leading to variability in DA or STX observations according to shellfish species tested. These factors include, but are not limited to: storage location of toxin in organism, organisms response to toxin, environmental factors, and size or age of the shellfish sampled (Mons et al., 1998; Van Egmond et al., 2004). In mussels, toxins accumulate in the digestive glands and are rapidly depurated (Novaczek et al., 1992). Relative to other shellfish, mussels accumulate STX faster than they other toxins (Mons et al., 1998). Mussels eliminate STX, as well as other toxins, relatively quickly (Costa et al., 2009; Mons et al., 1998). A study by Stewart et al. (1998) found bacterial metabolization as a potential mechanism of further DA elimination in blue mussels. Together these factors may explain the high STX, but much lower DA, values in mussels. In contrast, razor clams accumulate DA into body tissues such as the foot and mantle, slowing depuration rates (Wekell et al., 1994). Razor clams are among the slowest at depurating DA compared to other shellfish (Blanco et al., 2002). This combination of factors means that both intense blooms and low, persistent levels of toxin-producing *Pseudo-nitzschia* in the water can induce high DA levels in razor clams (Van Egmond et al., 2004). Due to these differences, and likely others as well, razor clams and mussels record the same DA and STX events differently over time, with mussels being more sensitive to STX events and razor clams to DA events.

2.5.2 2007-2012: HAB events during the MOCHA project

Coastal toxin and phytoplankton counts were combined to provide a synoptic overview of HAB events during the MOCHA project (Fig 2.2). Following on these findings, an event-scale analysis of the most significant STX and DA events during

MOCHA was conducted (Figs 2.3-2.7). The MOCHA projects coastal and shipboard HAB observations were combined with coincident proxies of wind and SST to yield detailed view of HAB formation, offshore extent, and movement onshore. Using these rich datasets, the following questions were investigated: 1) how informative are HAB cell counts at the coast as a proxy of HAB events; 2) what was the spatial extent of these HAB events offshore; 3) what can be learned regarding HAB initiation and movement from pairing time series wind and SST proxies with HAB observations?

2.5.3 2009 Case study: STX event

Phytoplankton of the genus *Alexandrium* are the only STX-producing dinoflagellates known to occur regularly in the Oregon coastal regime. Like other dinoflagellates, *Alexandrium* spp. tend to bloom during the late upwelling season when waters warm in response to weakening of upwelling-favorable winds and stratification of the water column (Du and Peterson, 2014). Previous work relating remote sensing data with the ODA STX record has also shown that STX events occur most frequently during upwelling events at the end of the summer off of Oregon (Tweddle et al., 2010). Regular annual closures of shellfish harvests are recorded in Oregon due to STX contamination; these closures vary in their spatial extent and persistence. In 2009 and 2010, a strong El Niño event occurred and the Pacific Decadal Oscillation (PDO) shifted to positive, or warm, values. Local SST was anomalously warm, up to +4-5°C (Fig 2.3 a). A strong downwelling/relaxation event in early-mid September 2009 (Fig 2.3 b) and a peak in central coast STX levels in shellfish (Fig 2.4 b) coincided with the highest SST values observed along the Oregon coast, including the central coast, in 2009-2010 (Fig 2.3 a). This combination of events suggests

onshore transport of warmer, and apparently HAB-rich, waters. Offshore counts for the central coast became elevated throughout the summer and fall, peaking coincident with the regions highest STX levels in shellfish for 2009 (Fig 2.4 b). During this warm phase in the fall of 2009, just as winds became downwelling-favorable and the water column presumably became more stratified, intense dinoflagellate blooms formed. In 2009, STX closures coincided with historical highs in *Alexandrium* cell concentrations, as well as the first recorded occurrence of seabird mortality due to the dinoflagellate Akashiwo sanguinea (Du et al., 2011; Phillips et al., 2011; White et al., 2014) in this region. The STX closures were not limited to the Oregon coast. Elevated STX levels up to 191 g L^{-1} were also recorded in Washington State in September 2009 (A. Odell, Olympic Region HAB Monitoring program, personal communication) and in California from mid-August through mid-October, with an early September high of 916 g L^{-1} Anomalously high, latitudinally extensive SST driven by large-scale climactic forcing are hypothesized to have promoted this STX event (Fig 2.3 a). The optimal temperature for vegetative growth of *Alexandrium* spp. ranges from to 15-20°C, depending on the species and environment (Anderson, 1998; Laabir et al., 2011; Laanaia et al., 2013), hence warming may simply have led to an increase in net growth rates. This is not to say that the complexities of *Alexandrium* blooms in this dynamic coastal regime can be constrained by a single forcing term. The coupling between physical forcing (e.g. circulation and transport, water column stratification, temperature, salinity), behavior (e.g. migration), and physiological adaptation to these conditions ultimately regulates cell abundance and toxicity (Anderson, 1998). While these observations are limited, it appears as if the combination of high temperatures, low winds (relaxation events), and water column stratification promote regular *Alexandrium* blooms in this region towards the end

of upwelling season. The 2009 warming event presumably amplified these effects, leading to anomalously high SST and record high levels of both *Alexandrium* and STX compared to the other years in the study period.

Cell counts of *Alexandrium* equal to and above 1,000 cells L^{-1} generally coincide with STX closures (Fig 2.2 a,b). This temporal coherence is largely driven by samples collected in the northern region (Table 1, Figs 2.2 b, 4). In 2009, 92% of the northern region STX samples that exceeded closure levels (n=24 of 26, Fig 2.4 a, circles) corresponded within a two week window to *Alexandrium* cell counts at or above 1,000 cells L^{-1}. In the central region, offshore *Alexandrium* counts exceeded 1,000 cells L^{-1} during all STX closures (July-September; Fig 2.4 b). Surf zone counts, however, were consistently below this threshold, suggesting a lack of onshore transport to the surf zone of *Alexandrium* from offshore waters. There were only three closure-level STX samples in the south, and no cell count data were available for comparison during these events. In all regions, particularly for offshore data collected in the central region, there were instances when cell counts exceeded a threshold of 1,000 cells L^{-1} and no STX events were detected within a 2-week window (e.g. false positives).

While surf zone cell count thresholds in the north were an indicator of shellfish toxicity in the region, this was not the case in the central or southern regions. At the central coast, surf zone counts remained low while offshore counts, and ultimately STX, continually increased. This lack of coherence between cell counts and the absolute concentration of STX in shellfish tissue is not unexpected given the variability in toxin accumulation and depuration rates in shellfish, inherent patchiness of phytoplankton populations, and temporal and spatial offsets between the collection of surf zone shellfish tissue and cell count samples. Despite these

caveats, *Alexandrium* cell counts >1,000 cells L^{-1} are found to be effective predictors of STX contamination of shellfish in the north. This strong relationship in the north may be due to the combination of greater sampling frequency and/or greater retention in the north (described below), which may have increased the probability of capturing the short-lived blooms.

Along-shelf variability in local circulation patterns may also explain the regional variability in both the 5-year (Fig 2.2 a,b) and 2009 STX records (Fig 2.4). The highest *Alexandrium* concentrations observed in 2009 were on the shelf north of 45.5°N (Fig 2.5), near the influence of the Columbia River. Under upwelling conditions, the Columbia River normally acts as a strong barrier to cross-shelf transport (Banas et al., 2009; Giddings et al., 2014). Conversely, during the transition to downwelling favorable winds, the predominant flow of surface currents is northward and onshore, pushing the Columbia River plume along the Washington coast and bloom retention. Under these conditions, cells generated in local, productive hot spots like Heceta Bank (44°N; Fig 2.1) may be transported onshore. Heceta Bank has been identified as a local incubator for phytoplankton growth due to the fact that it is a region of high nutrient supply and retentive circulation (Hickey and Banas, 2003; Trainer et al., 2001). Giddings et al. (2014) have used a particle tracking approach to show that particles produced in Heceta Bank would rapidly be transported north rapidly, with beachings occurring from the site of origin to north of the Oregon border in less than two weeks. Our surf zone and offshore cell counts are consistent with the hypothesis that *Alexandrium* concentrations during downwelling/relaxation events are elevated at latitudes north of Heceta Bank. Additional characterization of the seasonal patterns of phytoplankton community structure in Heceta Bank is necessary to evaluate whether this region acts as an incubator for

Alexandrium blooms at certain times of the year.

2.5.4 2010 Case Study: DA event

During the five-year MOCHA study, a single DA closure event was observed in the summer of 2010. While this event was not particularly toxic or prolonged relative to past DA events in the region, it was the only DA-related shellfish closure after a four-year closure hiatus. It was also the only DA event captured by both on- and offshore monitoring during MOCHA. This event coincided with the beginning of a delayed upwelling season that immediately followed, and was likely delayed by, a basin-scale warming event. Anomalously high SST and strong downwelling-favorable winds persisted late into 2010, from winter 2009 into mid-2010. Reversal to a cool phase conducive to cooler, upwelling favorable coincided with the beginning of a delayed upwelling season in June 2010. Elevated pDA and dDA levels offshore of the central and southern Oregon coast corresponded to closures at the central coast three weeks later, after strong upwelling winds relaxed during early upwelling season. The relaxation event, and subsequent onshore flow, would have allowed interaction between the toxigenic bloom and shellfish in the surf zone.

Surf zone observations show that when shellfish DA became elevated in June, the wide subclass frequently comprised the majority of the *Pseudo-nitzschia* community in 2010, both before and after the closure event. Total *Pseudo-nitzschia* counts were abundant throughout the upwelling season. As such, there is no predictive relationship between DA in shellfish and total counts or subclasses of *Pseudo-nitzschia* . This finding may reflect the same issues due to regional variability in sampling frequency and hydrography discussed in 4.2.2 above for relating *Alexandrium* counts to STX, as well as the fact that toxigenic species of *Pseudo-nitzschia* do not always

produce DA (e.g. Lelong et al. (2012); Trainer et al. (2012)). It is also consistent with other studies in the region that note that *Pseudo-nitzschia* abundance does not always correspond to DA events (Giddings et al., 2014).

By restricting our analyses to May 2010 only, the only time pDA and dDA values exceeded 10^3 ng L^{-1}, hence spanned the broadest range (10^{-1} - 10^4 ng L^{-1}), significant positive relationships were found between pDA or dDA and both wide and thin subclasses, as well as total *Pseudo-nitzschia* (Table 2). The wide cell type had the most significant relationship with pDA and was present in more samples than other classes. In May 2010, wide subclass abundances ranged 10^3 - 10^5 cells L^{-1} while the thin and medium ranged 10^3 - 10^4 cells L^{-1}. This morphotype also dominated *Pseudo-nitzschia* community structure in the surf zone samples collected during the early upwelling season, prior to the high DA levels in shellfish. These trends suggest the wide subclass was potentially responsible for the May-June 2010 DA event and shellfish closures, however the thin subclass and total *Pseudo-nitzschia* also had significant relationships with pDA and dDA in offshore waters. In Washington State, *P. australis* and *P. pseudodelicatissima* have been identified as the major toxigenic problem species (Trainer and Suddleson, 2005). These species would be expected to fall into the wide and thin morphologies assessed here and either, or both, could have been responsible for the 2010 DA event although this would need to be confirmed by more formal methods of species identification.

The co-occurrence of toxigenic and non-toxigenic *Pseudo-nitzschia* species makes it impossible to determine the threat of shellfish contamination from total cell counts alone. For this reason, investigators have either identified cells to the species level, grouped cells according to size and morphology, or directly measured pDA. Previous studies have found positive relationships between abundances

of toxigenic species of *Pseudo-nitzschia* and water column DA (e.g. Bargu et al. (2012); Busse et al. (2006); Trainer and Hickey (2002)) and determined the presence of particular toxigenic species of *Pseudo-nitzschia* to be a potentially robust early indicator of coastal DA toxicity (Trainer et al., 2001). These studies identified *Pseudo-nitzschia* to the species level, whereas this work instead tested the predictive ability of morphologically-grouped *Pseudo-nitzschia* cells, a practice adopted from resource management practices in Washington state (Trainer and Suddleson, 2005).

Nearly all pDA and dDA samples collected offshore during the 5 year study period yielded values below 10^3 ng L^{-1}. The only exception was in May 2010 when pDA and dDA values both exceeded 10^3 ng L^{-1} (Fig 2.7). The possibility exists that the overall very low trends in our pDA and dDA data may be due in part to DA degradation during storage prior to sample analysis (Lane and Kudela, 2007). Even so, it is notable from our observations is that during the 5-year monitoring period the only high pDA and dDA values ($>10^3$ ng L^{-1}) observed in shipboard data (May 2010) occurred three weeks before the only DA-related shellfish harvesting closure in Oregon (June 2010). Based on these observations, an alert threshold value of 10^3 ng L^{-1} pDA is proposed as an early warning of shellfish toxicity in the Pacific Northwest region.

2.5.5 Monitoring Implications

Concentrations of STX and DA in shellfish are currently the only information used to guide management of shellfish harvests in Oregon. Ideally, resource managers and recreational and commercial harvesters could use earlier warning of HAB events to avoid human ingestion of contaminated shellfish or wastage of already-harvested shellfish. Monitoring observations reveal regions and seasons with the

greatest likelihood of HAB events, as well as potential event-scale early warning metrics of HAB events.

North coast *Alexandrium* cell counts, where surf zone sampling efforts were greatest, closely track STX levels in shellfish. Accordingly, approximately bi-weekly cell counts are proposed as a low-cost, rapid, and effective means of early warning for potential shellfish closures due to STX. The concentration of total *Pseudo-nitzchia* cells and morphological subgroups were not correlated to either pDA, dDA, or concentrations of DA in shellfish tissue offshore or in the surf zone when the full dataset was evaluated. Based on shipboard data from May 2010 and the timing of subsequent DA closures in the surf zone, screening the intertidal zone for pDA levels exceeding a threshold of 10^3 ng L^{-1} during the upwelling season should provide early warning of shellfish contamination.

The north and south coast regions are most likely to have STX events from June through November. During the upwelling season DA events are most likely, but DA may persist in razor clams throughout the year. The north coast, and to a lesser extent the south coast, have the greatest occurrence of STX events. The south coast is comparatively under-sampled for STX in mussels, potentially contributing northern bias in these results. Relative to central or south coasts, the north coast also has the greatest occurrence of DA events. The decrease in razor clam sampling from north to south reflects their natural abundance along the coast. Over 90% of the razor clam population and harvesting effort occurs in the northernmost 18 miles of the Oregon coast (ODFW, 2000). South of this area, abundances are episodic and unpredictable due to infrequent recruitment success.

Mussels are currently considered the sentinel indicator of STX and DA events, but here mussels are shown to be a poor indicator of DA events. Razor clams

represent the bulk of the commercial and recreational shellfish harvesting revenue in Oregon and also accumulate greater levels of DA that remain in edible parts of the clam for longer amounts of time compared to mussels. As such, ideally, razor clams instead of mussels should be considered sentinel indicators of DA events in this region and sampling increased; however this is not logistically feasible. Razor clams exist in numbers far lower than mussels and require greater skill and labor to harvest than mussels, which reside much higher in the intertidal at much greater and more consistent abundances. Nevertheless, knowledge that razor clams are more sensitive to DA events is critical to any DA monitoring or management program and evaluation of resulting data by researchers or managers.

The regional-scale survey cruises in 2009 and 2010 that fortuitously coincided with the regions major HAB events at the time reveal snapshots of both the STX and DA events and their regional-scale extent. The STX bloom spanned both the Washington and Oregon coasts and the DA event spanned the Oregon and California coasts. Due to the time and cost involved in oceanic data collection, shipboard views of HAB events of this scale are rare; however, they remind us that HAB events are often beyond the scope of data collection of most research projects, which are usually limited to a specific area of a specific coastline. As mentioned in previous work (Lewitus et al., 2012), these observations underscore the need for more regional-scale HAB research efforts to explore the potential causes of these events and how they move over time.

In this region and others, the inherent ecological and biogeochemical complexity complicate prediction of specific HAB events. Nonetheless, this work has identified a number of terms related to HAB formation that can be utilized as precursors of an increased likelihood of HAB events: cell counts of HAB-forming dinoflagellates,

pDA, and downwelling/relaxation events that facilitate onshore transport of HAB species or toxins detected offshore via ship or automated mooring. Additionally, coincident MOCHA research has found warm phases of the PDO to be a reliable proxy of DA events (McKibben et al., 2017). All of these measurements should be included in any STX- or DA-monitoring program aimed at early detection in the California Current regime. In order to more completely grasp the dynamics of HAB ecology in the region, further research into the following outstanding questions is warranted: (1) progress needs to be made to understand the conditions under which *Pseudo-nitzschia* become toxic and (2) identification the regions and conditions that foster *Alexandrium* blooms (i.e. pelagic or benthic cyst beds). Addressing these concerns will lead to more capable HAB monitoring programs in the region.

Acknowledgements. This study was supported by National Oceanic and Atmospheric Administration (NOAA) grant NA07NOS4780195 from the Monitoring and Event Response for Harmful Algal Blooms (MERHAB) program and NA08NES4400013 from the Cooperative Institute for Oceanographic Satellite Studies and NSF OCE-0424602 from the Coastal Margin Observation and Prediction project. This is MERHAB publication number 188. Thank you to Vera Trainer for DA ELISA kits, as well training for both DA sample processing and analysis. Thank you to Mary Silver, Raphe Kudela, and members of the Caron Laboratory for advice and assistance in planning our approach to toxin analysis, and to members of the ORHAB community in Washington state, especially Rita Horner, for input on sampling and counting methods to use for surf zone sampling of phytoplankton. Thank you to the Oregon Department of Agricultures Food Safety and Animal Health Program for shellfish toxin data. Thank you to Stephen Pierce for wind stress and cumulative upwelling

index data. The statements, findings, conclusions, and recommendations are those of the author(s) and do not necessarily reflect the views of the National Oceanic and Atmospheric Administration or the Department of Commerce.

TABLES

	N mussel samples		N razor clam samples		N Samples above closure threshold (% of total) Mussels		N Samples above closure threshold (% of total) Razor clams		Maximum STX (μg 100g^{-1})		Maximum DA (ppm)		Interannual Closure Frequency (n years)	
	STX	DA	STX	DA	STX	DA	STX	DA	Mussels	Razor Clams	Mussels	Razor Clams	STX	DA
North	1928	1117	959	894	108 (6%)	2 (0.2%)	115 (12%)	107 (12%)	3983	415	128	308	57% (20)	45% (10)
Central	3066	1650	340	427	49 (2%)	3 (0.25%)	2 (0.01%)	122 (29%)	3308	200	53	287	20% (7)	27% (6)
South	987	994	62	68	55 (6%)	0 (0%)	0 (0%)	27 (50%)	2520	43	13	120	40% (14)	27% (6)

TABLE 2.1: Statistical values for coastal shellfish toxin records.

Columns 1-2 represent the total number of mussel samples collected throughout the entire saxitoxin (STX; 1958-2014) and domoic acid (DA; 1992-2014) coastal shellfish toxin monitoring datasets. Columns 3-4 represent the same totals, except for razor clams only. Columns 5-8 display the total number of samples collected that surpassed the closure threshold values of 80μg 100g^{-1} for STX and 20ppm for DA. Values in parenthesis are the percent of samples above closure threshold relative to total samples collected (Columns 1-4). Columns 9-12 show the maximum toxin value detected for STX and DA records, separated by shellfish species. Columns 13-14 show the interannual closure frequency, or total number of years in the STX and DA records that had at least one sample above closure threshold (number in parenthesis) relative to the total number of years in the record (35 for STX, 22 for DA). All data are binned by region, with rows 1-3 corresponding with the north, central, and south coastal regions (Fig 2.1 a).

	$\log_{10}$(Wide) *P. fraudulenta* *P. australis*			log10(Medium) *P. multiseries* *P. pungens*			$\log_{10}$(Thin) *P. pseudodelicatissima* *P. delicatissima*			$\log_{10}$(Total *Pseudo-nitzschia*)		
	n	r^2	p	n	r^2	p	n	r^2	p	n	r^2	p
	May 2010											
$\log_{10}$(pDA)	**28**	**0.65**	**<0.0001**	11	0.25	0.12	**18**	**0.46**	**0.0021**	**41**	**0.63**	**<0.0001**
$\log_{10}$(dDA)	**25**	**0.37**	**0.0013**	10	0.16	0.24	**15**	**0.46**	**0.0052**	**34**	**0.40**	**<0.0001**
	All of 2010											
$\log_{10}$(pDA)	112	0.0094	0.31	73	0.0073	0.47	66	0.00006	0.85	153	0.014	0.15
$\log_{10}$(dDA)	64	0.00018	0.92	32	0.21	0.008	34	0.023	0.39	80	0.000001	0.99

TABLE 2.2: Shipboard *Pseudo-nitzschia* counts versus particulate and dissolved domoic acid (pDA and dDA) values.

Cell counts are reported for total *Pseudo-nitzschia* , as well as for the wide, medium, and thin size classes. P-values are reported to the 95% confidence interval. Bolded rows are significant relationships.

FIGURES

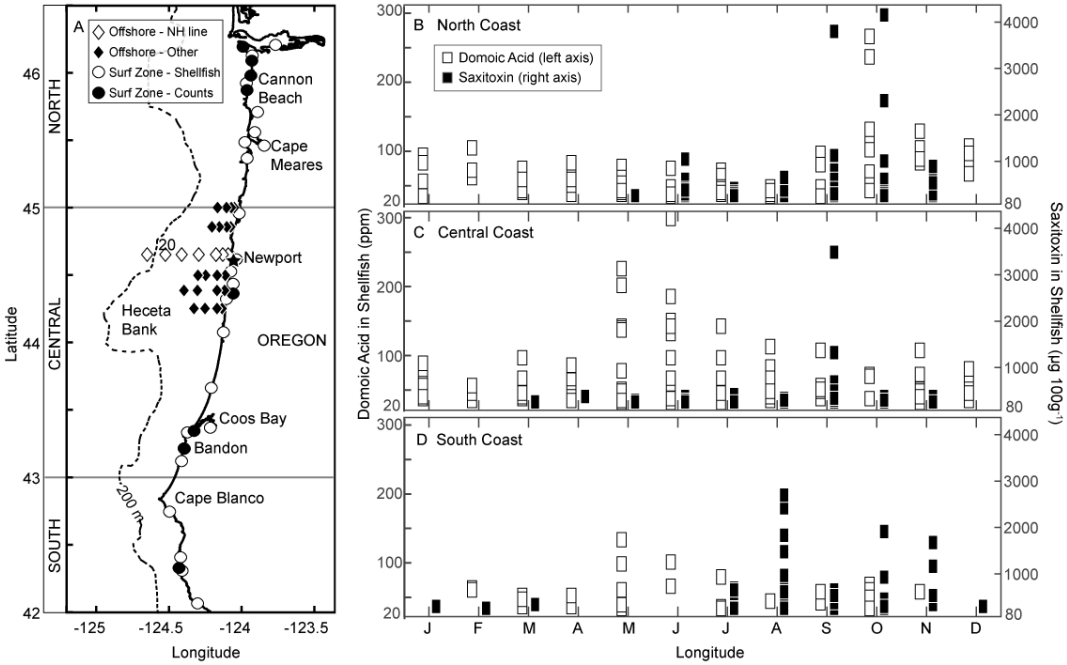

FIGURE 2.1: Area of study and monthly toxin maxima

a) Area of study, region to the right of solid black line is land (Oregon). Dashed line shows the continental shelf break at the 200-meter isobath. Diamond symbols show offshore locations sampled aboard research vessels. White diamonds highlight the Newport Hydrographic (NH) line at 44.65°N. Wind data were collected at Newport, Oregon (star symbol). Circles on coast represent surf zone sampling locations for shellfish DA and STX (white) or *Alexandrium* and *Pseudo-nitzschia* cell counts (black). Surf zone data are binned into north (45°N-46.5°N), central (43°N-45°N), and south (42°N-43°N) regions. Figure 1b-d show monthly STX (black squares, right axis) and DA (white squares, left axis) values from shellfish for b) north, c) central, and d) south coast locations defined in Figure 1 a. Only values above the 80 μg 100g^{-1} and 20 ppm harvesting closure thresholds for STX and DA, respectively, are shown, i.e. y axes start at closure thresholds.

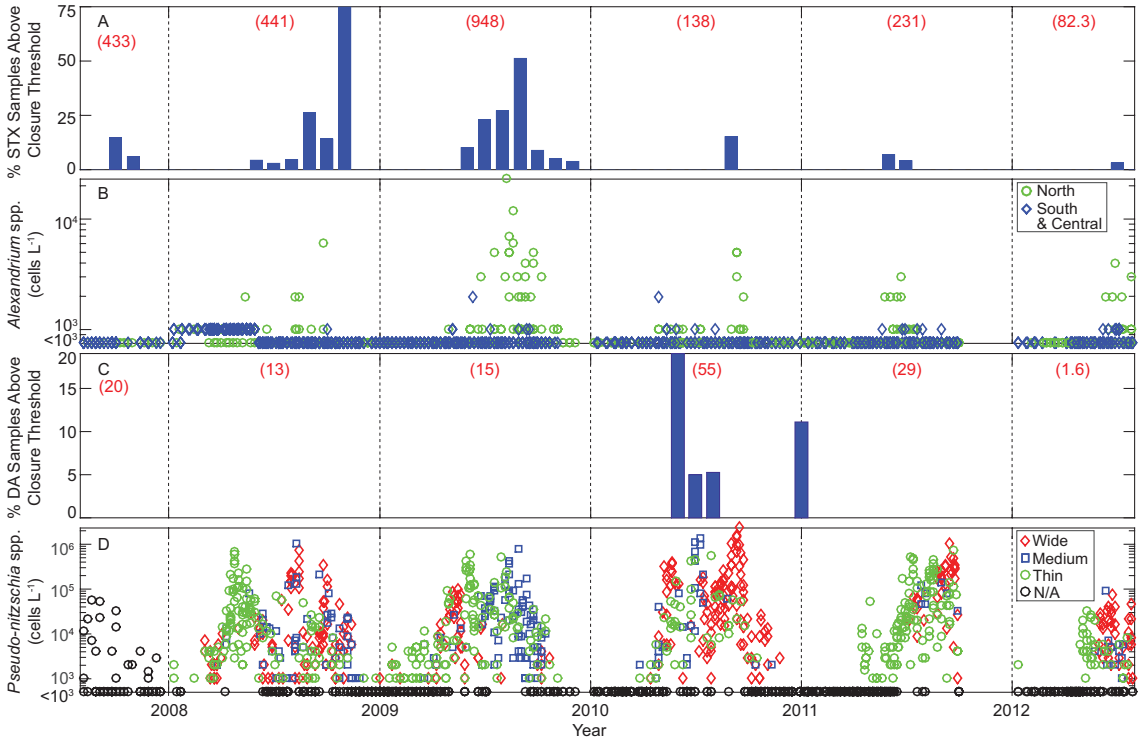

FIGURE 2.2: Shellfish toxin levels and coastal cell counts for August 1, 2007 – July 31, 2012.

Shellfish toxin and cell count data from surf zone locations (Fig 2.1, circles) during the Monitoring Oregon Coastal Harmful Algae (MOCHA) project, August 1, 2007 through July 31, 2012. a) and c) show the coastwide percentage of shellfish samples collected each month that surpassed closure levels of 80 μg 100g^{-1} and 20 ppm for saxitoxin and domoic acid, respectively. Maximum toxin value reached for each year indicated by red numbers in parenthesis. b) Surf zone cell counts for *Alexandrium* spp. at north (green circle) and central and south (blue diamond) regions. d) Surf zone *Pseudo-nitzschia* spp. counts colored to show whether the wide (red diamond), medium (green circle), or thin (blue square) subclass comprised >50% of the total *Pseudo-nitzschia* community. Black circles are data collected prior to 2008, or counts below detectable limits, that did not include distinction of subclasses.

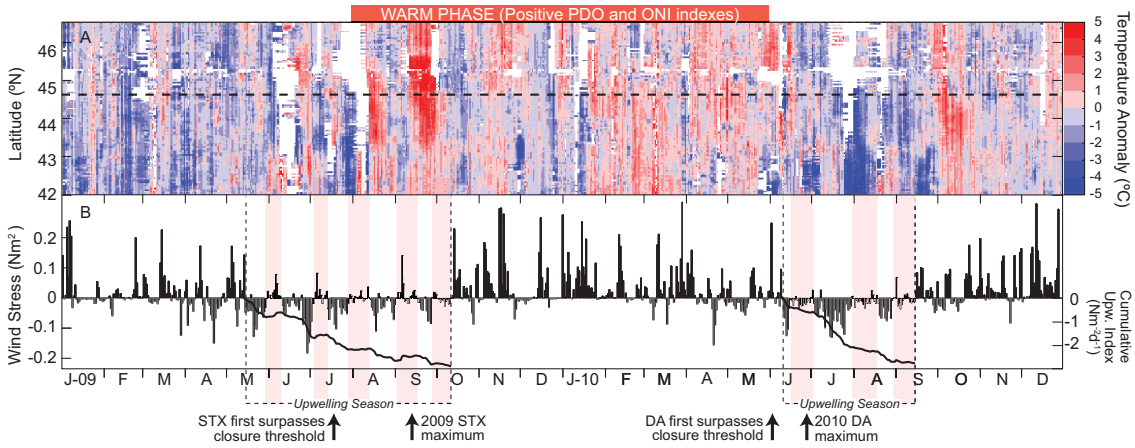

FIGURE 2.3: 2009-2010 Oregon coast physical conditions.

a) Coastwide sea surface temperature (SST) anomaly (MODIS nighttime SST) for the Oregon (OR) coastline (42-46.5°N). Dashed line shows latitude of the NH hydrographic line (Fig 2.1). b) Positive (downwelling-favorable) and negative (upwelling-favorable) wind stress conditions at Newport, Oregon. Right axis on panel (b) and black lines represent the cumulative upwelling index (CUI), a measure of net-upwelling favorable conditions. Consistently negative CUI indicates stronger, more persistent upwelling and net transport of waters offshore. Values that remain steady or become positive represent weakening or reversal in upwelling conditions. Dashed vertical lines indicate the start dates of up- and downwelling seasons as determined by the beginning and end of the CUI. Timing of the basin-scale warming event highlighted by red bar at top. Arrows below x-axis correspond to peaks in toxin levels in central coast shellfish (Figs 2.4 b and 2.6 b).

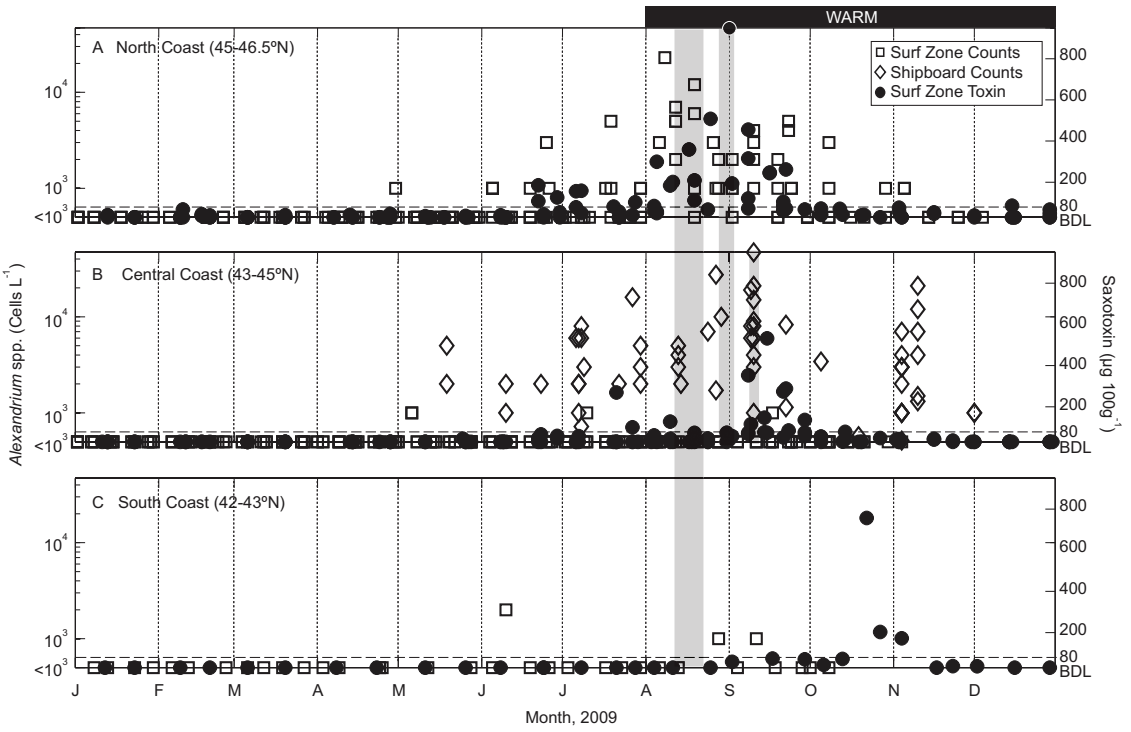

FIGURE 2.4: Intertidal concentrations of saxitoxin in shellfish and *Alexandrium* cells in 2009.

2009 concentrations of saxitoxin (STX) in intertidal, or surf zone, shellfish (circles, right y-axis) and abundance of surf zone *Alexandrium* spp. (squares, left y-axis) for a) north (45°N-46.5°N), b) central (43°N-45°N), and c) south (42°N-43°N) coast sampling locations (Fig 2.1). Horizontal dashed line indicates the 80 μg 100 g^{-1} threshold for shellfish harvesting closure. Diamonds (panel b only) indicate central coast offshore *Alexandrium* spp. obtained during research cruises. Grey shaded regions show coincidence in time and space with offshore sampling efforts featured in Fig 2.5. Warming event highlighted by black bar at the top. All y-axes are set to the minimum and maximum cell count or STX values for 2009; below detectible levels (BDL) is the minimum for STX levels (right axes).

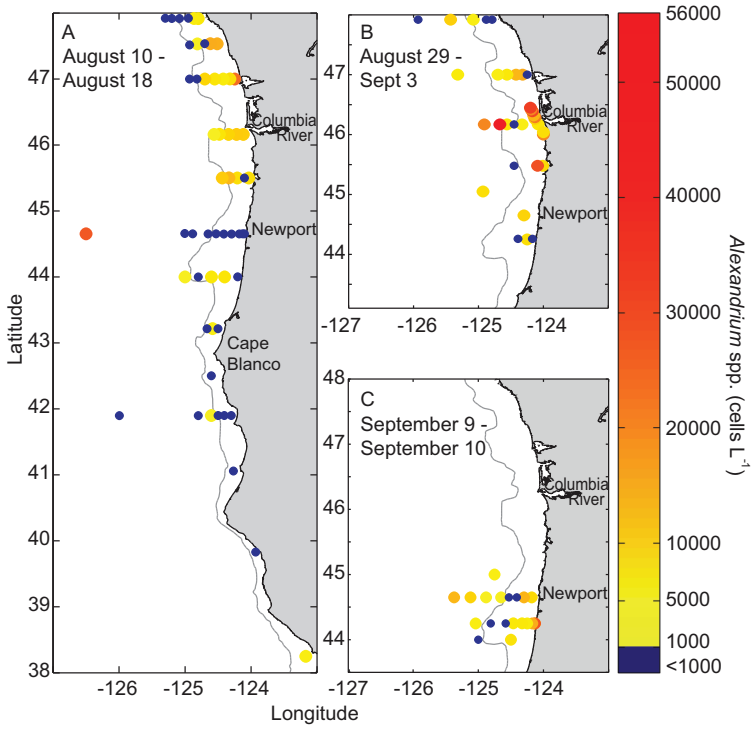

FIGURE 2.5: Surface *Alexandrium* spp. counts in August and September 2009

Total *Alexandrium* spp. counts at the surface (plots a-c) obtained during regional-scale sampling cruises that coincided with the saxitoxin closure events in 2009 (see grey vertical bars on Fig 2.4). The first cruise covered a) northern California to Washington from August 10-18, 2009. The second cruise covered b) the central Oregon coast north to Washington from August 29-September 3, 2009 and then the c) central Oregon coast on September 9-10, 2009. Grey line is the 200-meter isobath. Colors represent the total number of *Alexandrium* spp. (cells L^{-1}); smaller blue dots are indicative of counts below detectible levels (<1000 cells L^{-1}). Color axis is set to minimum (<1000 cells L^{-1}) and maximum (56,000 cells L^{-1}) for these cruises.

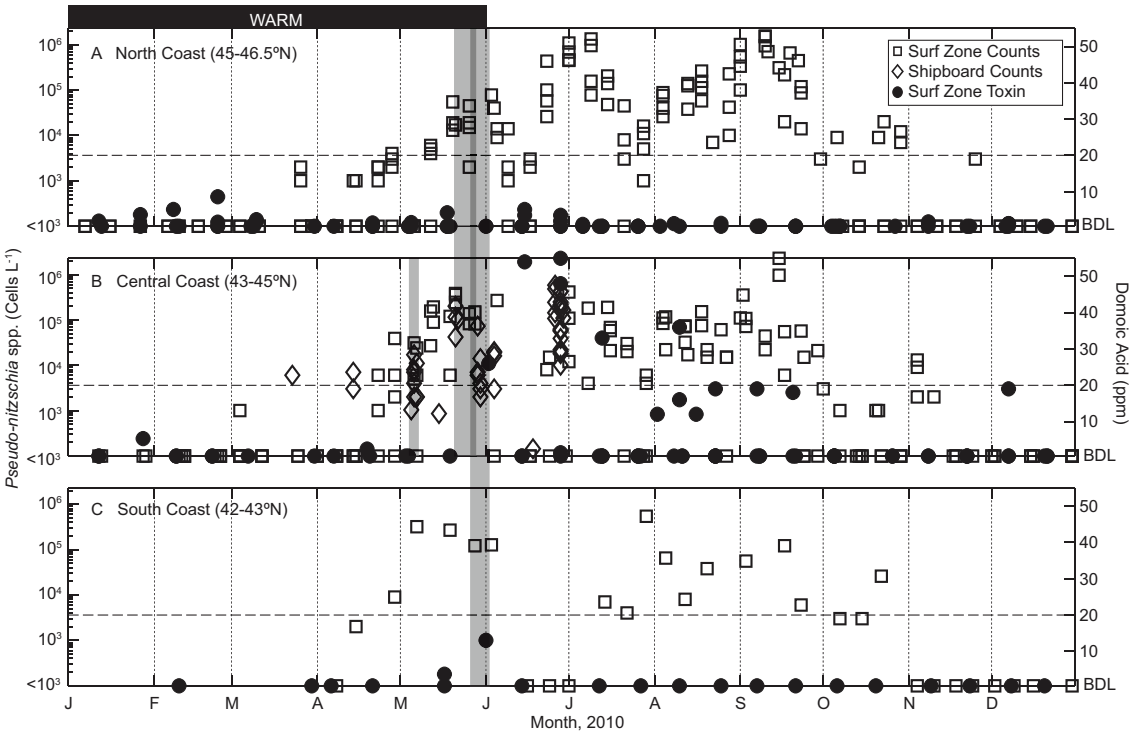

FIGURE 2.6: Intertidal concentrations of domoic acid in shellfish and *Pseudo-nitzschia* cells in 2010.

2010 concentrations of domoic acid (DA) in intertidal, or surf zone, shellfish tissue (circles, right y-axis) and surf zone *Pseudo-nitzschia* spp. abundance (squares, left y-axis) for a) north (45°N-46.5°N), b) central (43°N-45°N), and c) south (42°N-43°N) coast sampling locations (Fig 2.1). Horizontal grey line indicates the 20 ppm threshold for shellfish harvesting closure. Diamonds (panel b only) indicate offshore central coast *Pseudo-nitzschia* spp. counts obtained during research cruises. Grey shaded regions show coincidence in time and space with offshore sampling efforts featured in Fig 2.7. Warming event highlighted by black bar at the top. Y-axes are set to the minimum and maximum cell count or DA values for 2010; below detectible levels (BDL) is the minimum value for DA (right axes).

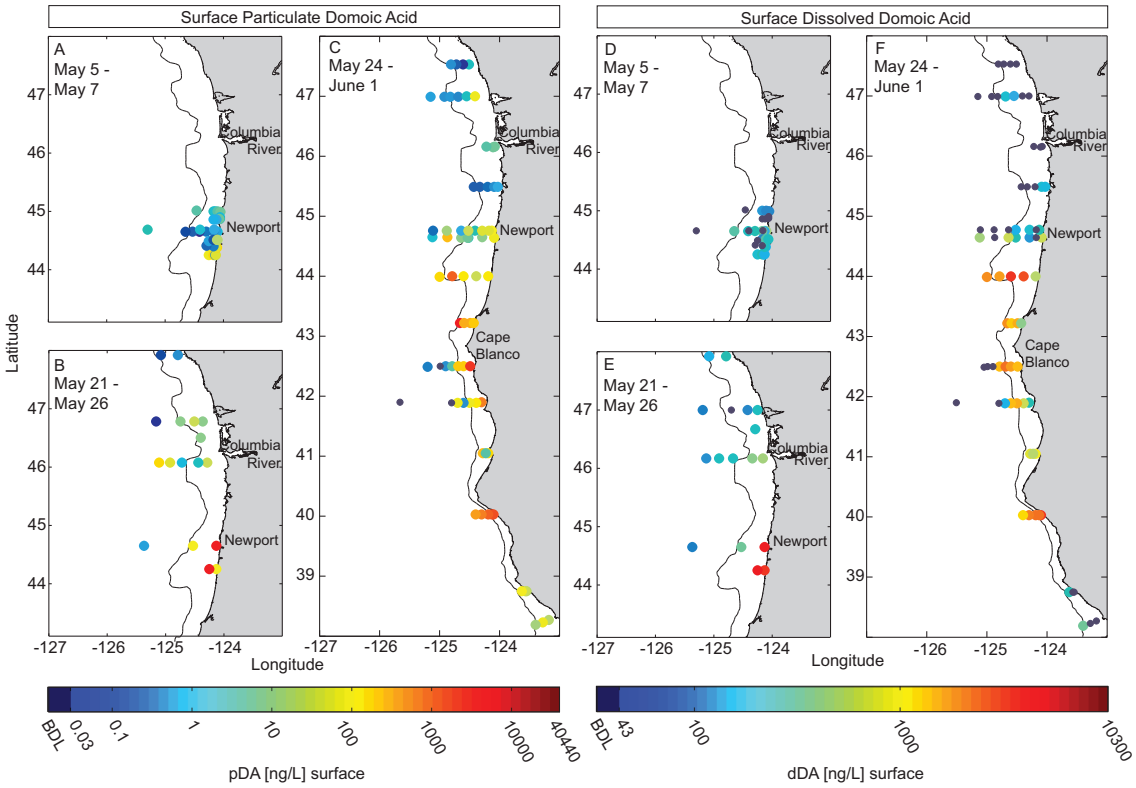

FIGURE 2.7: Surface particulate and dissolved domoic acid concentrations in May 2010

Surface particulate (panels a-c) and dissolved (panels d-f) domoic acid (pDA and dDA, respectively) concentrations obtained during sampling cruises just before the coastwide domoic acid (DA) induced shellfish closures in 2010 (see grey bars on Figure 2.6). Panels a) and d) include three separate day-long cruise efforts at the central coast (May 5: NH-line only; May 6: 3 southern lines; May 7: 3 NH-line and 2 northern lines; see diamonds on Fig 2.1 for station locations). Regional-scale cruises span b, e) the central Oregon coast north to Washington from May 21-26, 2010, and c, f) northern California to Washington from May 24 - June 1, 2010. Colors indicate the concentration of pDA or dDA at a particular sampling location; smaller blue dots are indicative of DA below detectible levels. Color axis set to minimum (below detectible levels, or BDL) and maximum values observed during these cruises. Grey line is the 200-meter isobath.

Chapter 3:
Climatic regulation of the neurotoxin domoic acid

S. Morgaine McKibben[1], William T. Peterson[2], A. Michelle Wood[3], Matthew Hunter[4], Vera Trainer[5], Angelicque E. White[1]

[1]College of Earth, Ocean and Atmospheric Sciences, Oregon State University, 104 CEOAS Administration Building, Corvallis, OR 97331, USA

[2]National Oceanic and Atmospheric Administration, Northwest Fisheries Science Center, Hatfield Marine Science Center, 2032 S. OSU Drive, Newport, OR 97365, USA

[3]Institute of Ecology and Evolution, 5289 University of Oregon, Eugene, OR 97403, USA

[4]Oregon Department of Fish and Wildlife, 2001 Marine Drive, Astoria, OR 97103, USA

[5]CORRECT Marine Biotoxins Program, Environmental and Fisheries Sciences Division, Northwest Fisheries Science Center, National Marine Fisheries Service, National Oceanic and Atmospheric Administration, 2725 Montlake Blvd. E, Seattle, WA 98112, USA

Published in *Proceedings of the National Academy of Sciences*
January 2017
Volume 112. No. 2
Pages 239-244

3. CLIMATIC REGULATION OF THE NEUROTOXIN DOMOIC ACID

3.1. Abstract

Domoic acid is a potent neurotoxin produced by certain marine microalgae that can accumulate in the foodweb, posing a health threat to human seafood consumers and wildlife in coastal regions worldwide. Evidence of climatic regulation of domoic acid in shellfish over the past 20 years in the Northern California Current regime is shown. The timing of elevated domoic acid is strongly related to warm phases of the Pacific Decadal Oscillation and the Oceanic Niño Index, an indicator of El Niño events. Ocean conditions in the northeast Pacific that are associated with warm phases of these indices, including changes in prevailing currents and advection of anomalously warm water masses onto the continental shelf, are hypothesized to contribute to increases in this toxin. We present an applied domoic acid risk assessment model for the U.S. West Coast based on combined climatic and local variables. Evidence of regional- to basin-scale controls on domoic acid has not previously been presented. Our findings have implications in coastal zones worldwide that are affected by this toxin and are particularly relevant given the increased frequency of anomalously warm ocean conditions.

3.2. Introduction

The Pacific Decadal Oscillation (PDO) and El Niño Southern Oscillation (ENSO) are recurring patterns of climate variability centered over the northeastern

(NE) and equatorial Pacific, respectively, that fluctuate at scales of years (ENSO) to decades (PDO) (McPhaden, 2002; Mantua, 2015). Distinct, yet also related, these patterns can amplify or dampen each other through atmospheric teleconnection (McPhaden, 2002; Gershunov and Barnett, 1998). In the NE Pacific they induce similar spatial patterns of sea surface temperature anomalies during positive (warm) and negative (cool) phases (Mantua, 2002). Low-frequency physical variability attributed to the PDO and ENSO modulates large shifts in NE Pacific water temperature, ocean currents, and foodweb dynamics that can persist for months to years (Chavez et al., 2003; Mantua, 2015; Huyer et al., 2002). Shifts in NE Pacific plankton communities occur as well (Hooff and Peterson, 2006; Fisher et al., 2015; Batchelder et al., 2013; Yamada et al., 2015; Martinez et al., 2009; Du et al., 2015); however, climate impacts on phytoplankton ecology in this region are relatively underexplored, largely due to a lack of phytoplankton data at sufficient scales.

Decadal, regional-scale monitoring of domoic acid (DA) in shellfish can be used to investigate climate-scale impacts on phytoplankton ecology. The neurotoxin DA is produced by some species of the diatom genus *Pseudo-nitzschia*. It enters marine foodwebs when suspension feeders such as shellfish, copepods, and anchovies ingest toxic *Pseudo-nitzschia* cells. Consumption of these organisms by humans can lead to a serious neurological disorder named Domoic Acid Poisoning (DAP), also termed Amnesic Shellfish Poisoning. DAP symptoms range from gastrointestinal disturbance to seizures, memory loss, or, rarely, death (Bates et al., 1998; Mos, 2001).

DA was first identified as a public health threat in 1987 (Wright et al., 1989). Toxin-producing *Pseudo-nitzschia spp.* and DA have since been identified worldwide with the greatest prevalence in, and most deleterious impacts on, productive eastern

boundary upwelling systems (Trainer et al., 2012). Laboratory experiments have found multiple factors that can up- or down-regulate cellular DA synthesis, but there is no consensus regarding whether any one factor or combination of factors lead to predictable DA production *in situ* (Lelong et al., 2012; Trainer et al., 2012). DA regulation has primarily been investigated using field observations of discrete bloom events and laboratory-based experiments (Lelong et al., 2012). With some exceptions (e.g. Barron et al. (2010)) the majority of these studies are based on temporally short or spatially small datasets relative to climate-scale indexes. To protect public health, DA in shellfish has been monitored along the U.S. West Coast since 1991 (Lewitus et al., 2012). These records are now long enough to investigate DA regulation at the temporal-spatial scales associated with NE Pacific climate events that have occurred in recent decades, such as El Niño events, PDO transitions, and the 2013-2015 NE Pacific Warm anomaly (McCabe et al., 2016; Bond et al., 2015).

Our research expands on observations of climate-scale regulation of plankton in the Oregon (OR) coastal region of the NE Pacific (e.g. Batchelder et al. (2013); Yamada et al. (2015); Fisher et al. (2015); Shanks et al. (2014)). The presence/absence of unique copepod communities is strongly correlated with the PDO (Hooff and Peterson, 2006; Peterson and Keister, 2003) and El Niño events (Fisher et al., 2015). Copepods are a robust indicator of water mass transport to the continental shelf off of OR and the strength of the Northern California Current (NCC) (Keister et al., 2011; Batchelder et al., 2013; Bi et al., 2011), a strong seasonal current along the U.S. West Coast. We investigate the relationship between low-frequency climate signals and 20 years of DA levels in OR razor clams, then apply these findings to test whether DA levels in Washington (WA) and California (CA) shellfish are also

related to warm regimes.

3.3. Methods

3.3.1 Basin-scale indices of warm/cool ocean conditions

The Pacific Decadal Oscillation (PDO) is an index of climate variability in the Pacific Ocean defined as the leading principal component of monthly sea surface temperature (SST) variability poleward of 20°N (data source: `http://jisao.washington.edu/pdo/PDO.latest`). The Oceanic Niño Index (ONI) is a monthly-scale proxy of the El Niño Southern Oscillation (ENSO). It is a 3-month running mean of the SST anomaly in the Niño 3.4 region (5°N-5°S, 120°-170°W). An El Niño (La Niña) is defined as occurring when 5 consecutive, 3-month running means of SST anomaly values are >0.5°C (<-0.5°C) (data source: `http://www.cpc.ncep.noaa.gov/products/analysis\_monitoring/ensostuff/ensoyears.shtml`). A threshold of ± 1°C separates moderate to strong El Niño (warm) events from weak ones. Both indexes were acquired for 1991-2015.

3.3.2 Local (OR) domoic acid values and indices of warm ocean conditions

DA levels in OR razor clams (*Siliqua patula*) have been monitored coastwide by the OR Department of Agriculture every 2-4 weeks from 1992-2015 (McKibben et al., 2015; Lewitus et al., 2012). These data were binned to coastwide monthly DA maxima. The closure threshold for shellfish harvesting is DA in shellfish tissue ≥20 parts per million (ppm). Depuration of DA by razor clams can take months to a year (Trainer et al., 2009; Adams et al., 2000; Wekell et al., 1994), complicating efforts

to define discrete "DA events." To aid in deconvolving events, two metrics were defined: 1) "DA event onset," or the beginning of an event, conservatively defined as the first date that DA values surpassed 20 ppm with no prior incidences of DA above 20 ppm in the previous 12 months; 2) "annual DA maxima," or the maximum DA value above 20ppm reached each year. This captures DA events that can occur during prolonged depuration and also describes when the most toxic values occur each year. If a DA maximum occurred in January or February then decreased, it was assumed to represent toxin depuration and omitted; if a peak (defined as at least 3 months of an upward trend in monthly DA above 20ppm) occurred later that year yet was less than this depuration-based maxima, it was assigned as the annual maxima.

Two copepod community metrics were derived from roughly fortnightly zooplankton sampling at 44.65°N, 124.30°W, 5 nautical miles (nm) offshore (west) of Newport, OR, from 1996-2015: the annual date of the 'biological spring transition' and the monthly copepod species richness (CSR) anomaly. The former is a seasonal proxy, the first day the copepod community transitioned from warm-water (southern/offshore) species assemblages typical of winter to cold-water (northern) summer assemblages (Peterson and Keister, 2003) each year as determined by a two-tiered cluster analysis (McCune et al., 2002). This transition indexes the date when a biological signal can be detected as increased production of phytoplankton, increased biomass of zooplankton, or change in species composition of copepods associated with the change in coastal circulation patterns (data source: `http://www.cbr.washington.edu/status/trans`). The second copepod metric, the CSR anomaly, represents monthly anomalies in the number of copepod species present over time. It was calculated by subtracting the average number of species

present per month from the climatological average (1996-2015) for that month. More species are indicative of warmer water masses.

Average alongshore current measurements for March-April were calculated from acoustic doppler current profiler deployments at 44.65°N, 124.31°W, 10 nm offshore of Newport or high-frequency radar current mapping observations from shore (Yamada et al., 2015).

Central OR coast water temperature: SST data were collected 0.6 meters below the surface by National Data Buoy Center mooring station 46050 near 44.65°N, 124.53°W, 20 nm offshore of Newport. A monthly SST anomaly index was calculated as the difference between monthly average SST and the 1992-2015 climatological mean for each month. Annual mean water temperatures for December through March were also obtained for Yaquina Bay, an estuary in Newport (Yamada et al., 2015).

Seasonal upwelling: The OR coastal region is an eastern boundary upwelling regime, with an annual upwelling season (April-October) characterized by net northerly winds and offshore currents that lead to increased nutrients and phytoplankton biomass. Downwelling season (November-March) is typified by net southerly winds, onshore movement of water, and low biomass. The cumulative upwelling index (CUI) describes the annual dates that these seasons begin, based on the cumulative northerly wind stress observed at Newport each year (source: `http://damp.coas.oregonstate.edu/windstress/index.html`; see McKibben et al. (2015) for methods).

3.3.3 Cross-correlation and regression analyses

Cross-correlation was conducted for 1996-2015 (MATLAB code at `https://github.com/smmckib/crosscor`); any gaps in sampling data were interpolated. March PDO and ONI values were regressed against annual-scale physical and biological parameters. March was chosen because it is representative of the conditions leading into upwelling season.

3.3.4 West Coast risk assessment

A risk-analysis model was developed for the West Coast to evaluate whether parameters associated with elevated DA in OR also applied to elevated DA in WA and CA shellfish, to the north and south of OR. Our goal was to develop a basic, applied model that can be easily created and interpreted by both scientists and non-scientists. We selected publicly available parameters and an additive method to evaluate risk, allowing others to utilize the model without the need for specialized datasets or statistical tools.

Model parameters: In WA, DA sampling of razor clams occurred every 2 (September-May) or 4 weeks (June-August) from 1991-2015 (source: WA Department of Fish and Wildlife; `http://wdfw.wa.gov/fishing/shellfish/razorclams/domoic_levels.html`). DA levels in CA shellfish from 2000-2015 were available as weekly maxima detected at various sites (source: CA Dept of Public Health, Marine Biotoxin Monitoring Reports, `http://www.cdph.ca.gov/HealthInfo/environhealth/water/Pages/Shellfishreports.aspx`). If values were reported as a discrete range they were converted to continuous values: 1 to <20ppm=10ppm; ≥20ppm=50ppm. CA data included mussels (63%), razor clams (17%), oysters (14%), and other shellfish (6%, e.g. scallops). DA analyses were performed only when blooms of *Pseudo-*

nitzschia were detected. Liquid chromatography with ultraviolet absorbance detection was used to determine DA levels in WA (Quilliam et al., 1995) and CA (Dhoot et al., 1992) shellfish tissue. DA data were binned into monthly maxima and annual maxima (see above) over 8 latitude bins based on hydrography and sampling frequency: southern CA (32°N-34°N); south central CA (34°N-36°N); central CA (36°N-39°N); northern CA (39°N-42°N); southern OR (42°N-44°N); central OR (44°N-45°N); northern OR (45°N-46.3°N); and WA (46.3°N-48°N).

Upwelling: Monthly average coastal upwelling indexes were obtained from the Pacific Fisheries Environmental Laboratory (PFEL) for 32°N-48°N latitude. These data are based on geostrophic winds derived from monthly mean surface atmospheric pressure fields (source: `https://www.pfeg.noaa.gov/products/PFEL/modeled/indices/upwelling/upwelling.html`). Negative values represent the intensity of large-scale, wind-induced coastal upwelling. Data were linearly interpolated from provided increments of 3° latitude to 1°.

SST anomaly: Daily SST values were obtained from the NOAA Environmental Research Division's Data Access Program for the West Coast (32°N to 48°N) from 1991-2015. The "Daily Optimum Interpolation, Advanced Very High Resolution Radiometer Only, Version 2, Final + Preliminary SST" product generated by the National Oceanographic and Atmospheric Administration (NOAA) National Climatic Data Center and disseminated by the NOAA Environmental Research Division's Data Access Program `http://coastwatch.pfeg.noaa.gov/erddap/griddap/ncdcOisst2Agg.html` is a blend of *in situ* and satellite SST observations combined on a 0.25° spatial grid (Banzon et al., 2016). Daily data were binned to monthly average values, then a monthly climatology (based on 1991-2015 monthly averages) was subtracted from each month. The resulting monthly SST

anomaly products were binned to a mean across 1° (north-south) by 0.5° (east-west, the closest 2 pixels to the coast). This yielded a monthly SST anomaly metric along the coast at 1° of latitude for 32°N to 48°N.

Risk assessment model: Positive PDO, ONI, and SST anomaly, and upwelling conditions were assigned as proxies of DA risk. These data were compiled for 1991-2015 between 32°N to 48°N at 1° increments. The PDO, ONI, and SST anomaly data were first reduced to include only values >0 (warm). Each parameter was then divided by its maximum value during 1991-2015, scaling all to a common range (0 to 1). The maximum ONI value observed each winter was also determined. If the value was ≥1 (moderate-strong El Niño), then the maximum was propagated to each month of the following upwelling season. If upwelling conditions were present (negative value), then the four scaled variables (PDO, ONI, SST anomaly, and the maximum prior winter ONI) were summed to yield a monthly indicator of risk for elevated DA.

Model evaluation: Risk values were compared to "DA events," defined for model assessment as the annual DA maxima from each of the 8 latitudinal bins. The annual maximum risk value and the risk value during the month the DA event occurred were both regressed against the annual DA maxima for each bin. Model predictions of the frequency of "expected" DA events relative to the "observed" frequency were tallied. If risk values for any latitude were positive for 3 consecutive months in any given year per bin, that year was expected to experience closure levels of DA. Relationships between upwelling and DA events were quantified separately from risk assessment: 1) the sum of the PDO+ONI in March of the corresponding year was regressed against annual DA maxima; and 2) the number of annual maxima occurring during upwelling season through one month following the season were

tallied. The 2 southern CA bins were omitted as upwelling favorable conditions span much, or all, of the year.

3.4. Results

Warm PDO phases occur between 1996-1998, 2002-2006, 2009-2010 and January 2014-15 (Fig 3.1A). The ONI and PDO are highly correlated with zero lag (Table 3.1). Moderate to strong El Niño and La Niña events coincide with warm to cool transitions of the PDO, respectively (Fig 3.1A). The local SST anomaly (Fig 3.1B) is highly correlated with PDO and ONI at zero lag, with a slightly stronger relationship to the PDO (Table SI1).

In OR, six DA events occurred between 1996 and 2016 (Fig 3.1): 1996, 1998-1999, 2001, 2002-2006, 2010, 2014-2015. All were preceded by or coincident with positive PDO values and three were preceded by or coincident with positive ONI values. The shift to a positive CSR anomaly (Fig 3.1C,D), lags warm shifts in the physical indices (Fig 3.1A,B) by 0-9 months (Table SI1). During warm phases, the annual spring biological transition date occurs average to later than average and occurs earlier than average in cool phases (Fig 3.1D). DA maxima in 2003-2005 suggest events happened each year during the prolonged 2002-2006 event.

The onset of DA events and the annual DA maxima typically occur in association with upwelling season (Fig 3.1D,E). Event onset in 1996, 1998, 2010, and 2015 and annual DA maxima in 1996, 2001, 2010, and 2004-2006 occurred during upwelling season. Event onset in 2002 and 2014 and annual maxima in 1998, 2002, 2014, and 2015 occurred near the end of, or the month after, upwelling season. The 2001 event was not associated with upwelling season; maxima in 1999 and 2006 were

likely depuration.

At annual scales, nearly all physical and biological parameters were significantly, positively correlated with March PDO and ONI values: higher estuarine water temperature; more positive CSR and SST anomalies; weaker southward alongshore currents; later biological transition date; and a higher annual maximum DA (Table SI2). Most parameters had a stronger statistical relationship with the PDO than the ONI (Table SI2). Exceptions were CSR and DA values, which were about equally related to the March PDO and March ONI. Maximum annual DA is also significantly and positively correlated to these proxies of warm conditions, with the exception of direction of alongshore currents (Table SI2).

The sum of the March PDO and ONI is a stronger predictor of warm biological and physical conditions than either index alone (Fig SI1, Table S2). The exception is average alongshore currents, which were only significantly related to the March PDO. For all regressions, the 5 highest annual DA values corresponded to the warmest conditions (Fig SI1). The year 2002 consistently fell lower than predicted by these regressions (Fig SI1); DA was the fifth highest on record, but PDO and ONI conditions were cool to neutral in March. The 2002 DA maximum occurred in October, largely coincident with an abrupt late-year shift in all indexes to warm conditions during the onset of an El Niño event.

Risk model output and monthly DA values show latitudinal variability in DA, event risk, and upwelling phenology in OR and WA (Fig 2) and CA (Fig SI2). False positives range from 0% to 50% (Table SI3). The model did not predict the high DA levels observed in 2001 in WA, northern and central OR (Fig 2), or in 2011 in southern California (Fig SI2). Regressions of annual maximum DA with both model values (annual maximum and value during month of DA onset), as well

as the March PDO+ONI value show significant, positive correlations (Table SI4). Statistical outliers (2007 & 2011 in southern CA, 1992 in southern OR) were not included in these regressions. Comparison of Fig 2 and Fig SI1 also show differential expression of DA in routinely sampled OR and WA razor clams (Fig 2) compared to event-based sampling of predominately mussels in CA (Fig SI1).

3.5. Discussion

Our observations indicate that OR DA events occur during warm ocean regimes due to conditions that favor advection of anomalously warm water masses from southern or offshore locations onto the continental shelf. In warm years, the following are seen: (1) the spring biological transition date, indicative of the seasonal transition of the NCC to southward flow, is later; (2) alongshore currents tend to be weaker in association with warm PDO values; (3) estuarine and offshore water temperatures are elevated; (4) the copepod species richness anomaly is positive, showing a planktonic regime shift to copepod species of a predominantly offshore/southern origin; (5) DA levels in OR coast razor clams surpass closure threshold values.

A series of associations, from basin- to regional-scale, explain DA transport and elevated levels in shellfish. The DA events along the OR coast are a result of low frequency variability in climate-scale forcing modulated by local conditions (upwelling season). The PDO and ONI indicate when the NE Pacific may experience warm conditions, and local factors such as copepod community composition and offshore and estuarine water temperatures collectively describe whether warm water masses and their endemic plankton communities have reached the nearshore zone of the OR continental shelf waters. The phenology of upwelling season and the spring

biological transition modulate when conditions are most favorable to phytoplankton blooms and which plankton communities are present, respectively. Warm conditions leading into upwelling season (PDO+ONI in March) are indicators of the annual magnitude of DA toxicity and spring transition date. Seasonal termination of upwelling winds in late-summer/autumn may coincide with the onset (2002, 2014) or annual maxima (1998, 2015) of DA events. Shorter-term wind relaxation/reversal events (weeks) transport toxic blooms to the intertidal zone where they are ingested by shellfish (McKibben et al., 2015; Shanks et al., 2014) and may be responsible for the annual DA maxima observed during warm-phase upwelling seasons. Two categories of potential mechanisms behind these relationships in the context of our observations and relevant literature are discussed below.

1) Changes in water masses, circulation during warm regimes

Evidence linking basin-scale physical changes in ocean circulation to plankton is well-constrained in the OR coastal region. The planktonic copepod community off the central OR coast is a robust indicator of PDO- and ONI-related shifts in the source waters that feed the NCC (Hooff and Peterson, 2006; Peterson and Keister, 2003; Fisher et al., 2015). Negative (cool) PDO phases favor the influx of cooler waters into the NCC from the north, delivering zooplankton assemblages to coastal OR that are dominated by larger, lipid-rich subarctic copepods with lower species richness. In contrast, positive (warm) PDO phases favor poleward transport and onshore intrusion of subtropical oceanic waters (Keister et al., 2011), so smaller, lipid-poor subtropical copepod communities with higher species richness are dominant. Climate-scale warm ocean conditions are also conducive to the transport, and successful recruitment, of planktonic European green crab larvae *(Carcinus maenas)*

into OR estuaries. This invasive species is found in low numbers during cool regimes, however, annual recruitment success is greatly increased when the PDO is positive, SST is warmer, and the biological spring transition is later (Yamada et al., 2015). Annual DA maxima in OR razor clams are significantly and positively correlated with annual green crab recruitment strength in OR (Yamada et al., Table 2) from 1998-2014 (r^2=0.49, $p<0.002$), suggesting similar conditions may lead to both crab success and elevated DA in razor clams. For example, crab success was increased by both onshore transport and nearshore retention of the larvae in OR estuaries (Yamada et al., 2015). Assuming the presence of a toxigenic bloom, this would also promote elevated DA in shellfish through bloom transport into, and prolonged retention within, the intertidal and subtidal zones where phytoplankton are ingested by the shellfish. In sum, warm water copepod communities, green crab recruitment success, and DA in shellfish are all positively correlated with warm regimes. These seemingly disparate factors share one thing in common: a dependence on organisms that are meroplankton (crab larvae) or holoplankton, hence are indicators of water mass transport during oscillations between warm and cool regimes.

2) Cellular-level drivers of DA production

There at least two potential hypotheses to connect physical conditions during warm regimes, *Pseudo-nitzschia* communities, cellular DA production, and elevated DA in OR razor clams: 1) warm water *Pseudo-nitzschia* assemblages that are more likely to produce DA are advected into the region from offshore or southern waters due to circulation changes during warm phases; 2) environmental conditions during warm phases lead to up-regulation of DA synthesis in resident populations. These need not be mutually exclusive explanations. The 2002 and 2014 DA events support

the former hypothesis; they occurred during years with initially cool ocean conditions that abruptly shifted to warm conditions as, or just after, the annual transition from up- to downwelling season. In 2002, both elevated DA and warm conditions persisted through 2006, along with the warm PDO. In 2014 the DA event began coincident with the arrival of the NE Pacific Warm Anomaly on the OR coast. This strongly positive temperature anomaly, the greatest observed in the region since the 1980s, was identified in the Gulf of Alaska during the winter of 2013-2014 (Bond et al., 2015) and expanded to much of the NE Pacific by 2015. In mid 2014 the warm anomaly was held offshore of OR by upwelling-favorable winds (Pierce et al., 2016). Downwelling season initiated in mid September; winds reversed, the warm waters moved shoreward, and central OR coast SST rose 8°C over a period of just 31 hours (Pierce et al., 2016). This same month, the 2014 DA event began and the SST and CSR anomalies became positive (Fig 3.1).

In contrast, the 1998 and 2010 DA events and CSR lagged strong, coincident warm-to-cool transitions in the PDO and ONI (Fig 3.1). These events support the hypothesis that up-regulation of DA, and/or enhanced growth of toxigenic *Pseudo-nitzschia*, are favored during the transition from warm to cool-regimes, among others. Warm ocean regimes potentially affect *Pseudo-nitzschia* species abundance and toxicity in an array of ways, from cellular and metabolic processes that are sensitive to elevated temperatures to larger-scale changes in phenology, water column structure, and circulation patterns (Wells et al., 2015; Trainer et al., 2009). The linkages between DA production and environmental factors such as macronutrients, trace metals, temperature, and salinity are also complex and variable (Trainer et al., 2012). It is likely the case that no one single environmental variable is a strong predictor of DA (Trainer et al., 2009), hence a mechanistic explanation behind cellular-

level DA production and elevated DA in shellfish during warm ocean regimes is outside the scope of this study given the data we have. Even so, our findings frame future work investigating DA production by *Pseudo-nitzschia* in the context of conditions associated with warm regimes. For example, monitoring changes in species composition over time to investigate whether distinctive "warm" *Pseudo-nitzschia* assemblages indeed co-occur with copepod community shifts. More data are also needed to evaluate how regional-scale controls (stratification, nutrients, etc.) change during warm-ocean regimes and potentially increase *in situ* DA production.

3.5.1 Broad-scale implications

Positive climatic indexes and local SST anomaly, as well as upwelling conditions, were found to be indicators of OR DA events; whether these indicators applied to DA events along the broader NCC was subsequently tested using a risk assessment model for the U.S. West Coast. False positives in the model were up to 50% and as low as 0%. The higher values are due, at least in part, to the the long-term depuration and resulting conservative definition of a "DA event." This potentially skewed false positive calculations high. For example, false positives were greatest in WA: in 2009 a peak in DA occurred, but it was below the 20ppm threshold and not considered a "DA event" for that year (Fig 3.3); and in 2007, DA levels increased for the first several months but were sub-threshold. There were also annual maxima not detected by the model in 2001 from WA to central OR. In OR, this event occurred in association with a short, positive shift in the PDO and CSR (Fig 3.1); however, it was during the downwelling season, hence not detected by the model. A maximum was also missed in southern California in 2011 (Fig 3.4). The rationale for this omission is unclear, but may be related to local-scale regulation of DA

events (discussed below). Even with these exceptions, the model has a significant success rate and absolute risk values were strongly correlated to measured monthly and annual DA (Table 3.2).

3.5.2 Extreme warming events

When warm PDO conditions and El Niño events coincide their positive SST anomalies are approximately additive (McPhaden, 2002); coincidence of El Niño and warm PDO conditions typically yield the most classic signatures of an El Niño event in North America (Mantua, 2002; Gershunov and Barnett, 1998; McCabe and Dettinger, 1999). As such, concurrently positive PDO and ONI indices lead to periods of more extreme warming in the NE Pacific relative to when one or the other is positive. Our OR results support this, the summed March PDO+ONI value was typically more significantly related to environmental indicators of warm ocean conditions than either index alone; the greater the March PDO+ONI, the warmer the conditions, and the greater the DA levels.

If basin-scale warming events regulate DA events in OR, it follows that DA levels may be elevated by these events in nearby CA and WA as well. Our results (Figs 3.3, 3.4; Tables 3.3-3.4) and previous work collectively indicate that extreme warm phases (positive PDO concurrent with a strong to moderate El Niño) promote DA events along the the West Coast that span 2-3 contiguous states. Since 1991, 5 extensive warming events have occurred: 1991-1992, 1997-1998, 2002-2003, 2009-2010, and 2015-present. DA surpassed 20 ppm in shellfish in 2-3 contiguous states during time frames associated with all of these warm phases: late 1991-1992 (WA,

OR, and CA[1]); 1998-1999 (WA and OR); 2002-2003 (WA, OR, and CA); 2010 (OR and CA); and 2015 (WA, OR, and CA). The most latitudinally extensive DA events initiated when the highest risk values occurred (values >1). The 1991, 1998, and 2010 events were described as the most "exceptional and widespread" West Coast occurrences of DA between 1991-2010 (Lewitus et al., 2012). In OR and WA the 1991-1992, 1998-1999, and 2002-2003 events caused significant economic losses (Adams et al., 2000; Anderson, 1995; Tweddle et al., 2010; Lewitus et al., 2012) due to closures of razor clam and Dungeness crab (WA only) fisheries. In 2010 shellfish closures occurred in OR and CA (Figs. 3.3, 3.4) and DA reached record highs in CA mussels and lobster (Lewitus et al., 2012), and high DA was detected in coastal waters from at least central CA north to central OR (McKibben et al., 2015). In 2015, extensive NE Pacific warming coincided with an unprecedented, record-setting DA event from CA to WA (Du et al., 2016; McCabe et al., 2016).

Variability among DA events in WA, OR, and CA is also evident. Maximum DA in CA mussel tissue is higher (610 ppm) than in OR or WA razor clams (295 ppm) (Lewitus et al., 2012) and DA has exceeded 20 ppm in CA shellfish and other seafood species (sardines, anchovies) (Lewitus et al., 2012) nearly every year since 2000. Documented cases of DA in marine birds and mammals predominantly occur in CA (Lelong et al., 2012). These differences in CA relative to OR or WA may be due to differing distributions of planktivorous shellfish and finfish affected by DA, differing sampling methods and frequencies, and/or greater incidence of toxigenic *Pseudo-nitzschia*. If the latter is indeed a factor, it suggests the potential

---

[1]Lewitus et al. show DA over 20ppm in late 1991, but these data were not available on the California Department of Health's website for this study.

for 'seeding' populations moving northward during warm ocean regimes. Several retentive areas (e.g. Heceta Bank and the Juan de Fuca Eddy) are conducive to phytoplankton bloom initiation, including toxigenic *Pseudo-nitzschia* (Trainer et al., 2001; Pitcher et al., 2010; Trainer et al., 2010). Northward advection during warm regimes may be a source of toxic blooms to these regions. Also, latitudinal variability among the 3 states depends on a number of sub-climate-scale processes. This may explain inaccuracies in the risk assessment model. For example, 2010 a DA event did not occur in N. OR or WA, but did further to the south, yet the model was positive for the entire region. The Columbia River Plume may have halted furher northward advection of the toxigenic bloom (Banas et al., 2009). These processes will be important to consider in future regional-scale model application.

3.5.3 Conclusions

We present evidence for climate-scale regulation of shellfish DA the NCC. Even with the large potential for differences among WA, OR, and CA , our observations reveal a common relationship: the warmer the ocean conditions, the more likely DA is to surpass alert thresholds during upwelling season, and the more toxic and/or more widespread a DA event has the potential to become. The risk parameters presented in this work as indicative of elevated DA in shellfish (positive PDO, ONI, and local SST anomaly values, and upwelling conditions) can be applied to future examination of relationships between warm regimes and DA along the West Coast, as well as other eastern boundary currents worldwide. If these warm ocean regimes become more persistent due to global warming, as some hypothesize, West Coast DA events may also increase in persistence and frequency.

ACKNOWLEDGEMENTS: This study was supported by National Oceanic and Atmospheric Administration (NOAA) grant NA07NOS4780195 from the Monitoring and Event Response for Harmful Algal Blooms (MERHAB) program to Angelicque White, William Peterson, Michelle Wood, and Matt Hunter. This is MERHAB publication no. 190. Additional support was provided by the Sloan Foundation to Angelicque White. We thank Dr. Stephen Pierce for the upwelling data and Dan Ayres for providing the WA shellfish data. The statements, findings, conclusions, and recommendations are those of the author(s) and do not necessarily reflect the views of the NOAA or the Department of Commerce.

TABLES

	r* (lag, months)	Lag Range, in months (range of r values)	n**	Description
	x = Pacific Decadal Oscillation (PDO)			
y = Oceanic Niño Index (ONI)	0.59 (0)	-4 to +3 (0.52-0.59)	231	ONI typically lags PDO by 0 months with a range of -4 to +3 months
y = Sea Surface Temperature (SST) Anomaly	0.54 (0)	-1 to +1 (0.45-0.54)	231	SST anomaly typically lags PDO by 0 months with a range of -1 to +1 months
y = Copepod Species Richness (CSR) Anomaly	0.48 (+4)	0 to +9 (0.39-0.48)	231	CSR typically lags PDO by 4 months with a range of 0 to 9 months
y = Monthly Maximum Domoic Acid (DA)	0.38 (+6)	+2 to +10 (0.28-0.38)	231	DA typically lags PDO by 6 months with a range of 2 to 10 months
	x = Oceanic Niño Index (ONI)			
y = Sea Surface Temperature (SST) Anomaly	0.39 (0)	-3 to +5 (0.30-0.39)	231	SST anomaly typically lags ONI by 0 months with a range of -3 to +5 months
y = Copepod Species Richness (CSR) Anomaly	0.54 (6)	+3 to +8 (0.45-0.54)	231	CSR typically lags ONI by 6 months with a range of 3 to 8 months
y = Monthly Maximum Domoic Acid (DA)	0.45 (9)	+7 to +14 (0.35-0.45)	231	DA typically lags ONI by 9 months with a range of 7 to 14 months

TABLE 3.1: Cross-correlation results for monthly time series and Pacific Decadal Oscillation (PDO) and Oceanic Niño Index (ONI).

Column 1 shows the maximum correlation value (r_{max}) and the corresponding lag in months (in parentheses). Variables were also significantly related across a range of r; this range (Column 2) spans r_{max} to r_{max}-1 and the associated lag is in parenthesis. Column 3 shows the n values of the time series. Column 4 gives a brief description of the results shown in each row.

**r is the cross correlation value*

***n is the number of values in cross correlation analysis*

	Summed March PDO[1]+ONI[2]	March PDO	March ONI	Maximum Annual Domoic Acid (ppm)
Mean Yaquina Estuary Water Temperature, Dec-March (°C) n=17	**0.81 (p<0.0001)**	**0.69 (p<0.0001)**	**0.63 (p<0.0001)**	**0.68 (p<0.0001)**
Sea Surface Temperature Anomaly, March (°C) n=20	**0.66 (p<0.0001)**	**0.67 (p<0.0001)**	**0.37 (p=0.0047)**	**0.27 (p=0.0196)**
Copepod Species Richness Anomaly, March n=19	**0.51 (p=0.0006)**	**0.43 (p=0.0022)**	**0.42 (p=0.0025)**	**0.23 (p=0.0379)**
Mean Alongshore Currents, March-April (cm s^{-1}) n=15	0.22 (p=0.0771)	**0.29 (p=0.0376)**	0.070 (p=0.3422)	0.22 (p=0.0758)
Annual Spring Biological Transition Day (Year-day) n=20	**0.70 (p<0.0001)**	**0.65 (p<0.0001)**	**0.47 (p=0.0009)**	**0.53 (p=0.0003)**
Maximum Annual Domoic Acid in Razor Clams (ppm) n=20	**0.63 (p<0.0001)**	**0.50 (p=0.0005)**	**0.54 (p=0.0002)**	n/a

TABLE 3.2: Annual linear regression results for March Pacific Decadal Oscillation (PDO) and Oceanic Niño Index (ONI) values.

March PDO and ONI (x values, columns) versus physical and biological parameters (y values, rows) reported as r squared values with the corresponding significance level in parenthesis. All y values were measured near the central Oregon coast, except for DA values in razor clams, which were measured coastwide. Bold values are significant at a 95% confidence interval or better.

[1] *Pacific Decadal Oscillation*
[2] *Oceanic Niño Index*

	WA	N. OR	C. OR	S. OR	N. CA	C. CA	S. Cent CA	S. CA
"Actual" number of DA maxima captured[1]	10	8	8	8	5	6	6	10
"Expected" number of DA maxima[2]	19	19	20	20	12	13	13	13
Number "Expected" during "Undersampled" years[3]	0	3	8	10	7	3	5	2
Adjusted number of "Expected" events[4]	19	16	12	10	5	10	8	11
Approximate number of false positives[5]	9	8	4	2	0	4	2	1
Percent false positives[6]	**47%**	**50%**	**33%**	**30%**	**0%**	**40%**	**25%**	**9%**
DA maxima occurring during a month with elevated risk, i.e. warm, upwelling-favorable conditions	6	3	5	4	4	5	NaN	NaN
DA maxima occuring during the 1 month following upwelling season	1	2	1	3	1	0	NaN	NaN
Total number of upwelling-associated annual DA maxima[7]	7	5	6	7	5	5	NaN	NaN
Percent of DA maxima during warm upwelling season conditions[8]	**37%**	**31%**	**50%**	**70%**	**100%**	**50%**	NaN	NaN
Total number of months with a sample	291	231	145	98	57	129	129	142
Total number possible months	300	300	300	300	192	192	192	192

TABLE 3.3: Evaluative metrics of domoic acid (DA) risk model performance.

Rows 1-6 report calculations for estimates of false positives for each bin of DA data. Bins include Washington (WA); Northern, Central, and Southern Oregon (N.,C., & S. OR, respectively, see Fig 3.3); and Northern, Central, South-Central, and Southern California (N., C., S.C., & S. CA, respectively, see Fig 3.4). Rows 7-10 report calculations for the percentage of annual maxima that coincided with upwelling season. Upwelling-related values for S. and S.C. CA were not calculated due to the nearly year-round upwelling season that occurs there.

[1]Number of annual DA maxima values exceeding 20 parts per million (ppm) in bin
[2]Positive risk values for $\geq$3 consecutive months at any latitude in bin
[3]Number of "Expected" years that were "Undersampled," i.e. had less than 6 months with at least one DA sample in the bin
[4]Number of "Expected" years minus "Undersampled" years
[5]"Actual" minus "Expected" minus "Undersampled" years
[6]Number of false positives divided by adjusted number of "Expected" years x 100
[7]Sum of the number of annual DA maxima that occurred during elevated risk (i.e. upwelling-favorable conditions) and those that occurred one month after upwelling season terminated, i.e. during the annual transition from upwelling to downwelling-favorable conditions.
[8]Sum of the total number of upwelling associated maxima divided by adjusted number of "Expected" years x 100

	x=log10(Annual DA Maximum)		
	States Included	r^2 (p value)	N
y1=Model value coincident with annual maximum	WA & OR	0.38 (p<0.0053)	19
	CA	0.26 (p<0.012)	23
	WA, OR & CA	0.28 (p<0.00027)	42
y2=Annual maximum value of risk model	WA & OR	0.30 (p<0.0023)	28
	CA	0.35 (p<0.0018)	25
	WA, OR & CA	0.28 (p<0.000011	53
y3=March PDO[1]+ONI[2]	WA & OR	0.31 (p<0.0013)	30
	CA	0.33 (p<0.0029)	25
	WA, OR & CA	0.27 (p<0.000042)	55

TABLE 3.4: Linear regression results between annual metrics of domoic acid (DA) events (y values, rows) and $\log_{10}$(annual maximum DA values) (x value).

Data reported by state groupings (column 2) according to r^2 and p values (column 3) and number of data points (column 4). All values are significant at a 99% confidence interval or better.

[1] *Pacific Decadal Oscillation*
[2] *Oceanic Niño Index*

FIGURES

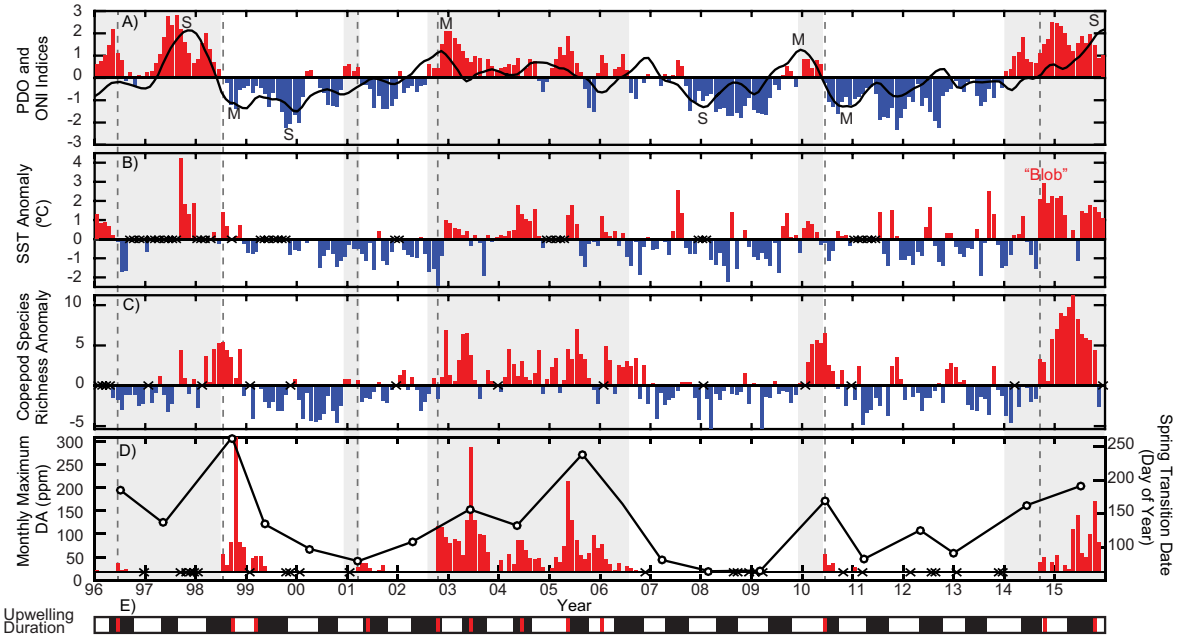

FIGURE 3.1: Warm and cool ocean regimes, local sea surface temperature anomaly and biological response.

(A) Pacific Decadal Oscillation (PDO, vertical bars) and Oceanic Niño Index (ONI, black line) indices; strong (S) to moderate (M) El Niño ($\geq$1) and La Niña ($\leq$-1) events are labeled. (B) Sea surface temperature anomaly 20 nautical miles (nm) off central Oregon (OR). (C) The copepod species richness anomaly 5 nm off central OR. (D) Monthly OR coast maximum domoic acid (DA) levels in razor clams (vertical bars); horizontal black line is the 20 parts per million (ppm) closure threshold, data below omitted. Black line (D) shows the spring biological transition date (right y-axis). Black boxes (E) indicate the duration of upwelling season each year; timing of annual DA maxima in relationship to upwelling in red. Grey shaded regions are warm regimes based on the PDO. Onset of six major DA events shown by dashed vertical lines. The September 2014 arrival of the NE Pacific Warm Anomaly (colloquially termed "The Blob") to the OR coastal region labeled on (B). "X" symbol indicates no data for that month (B-D).

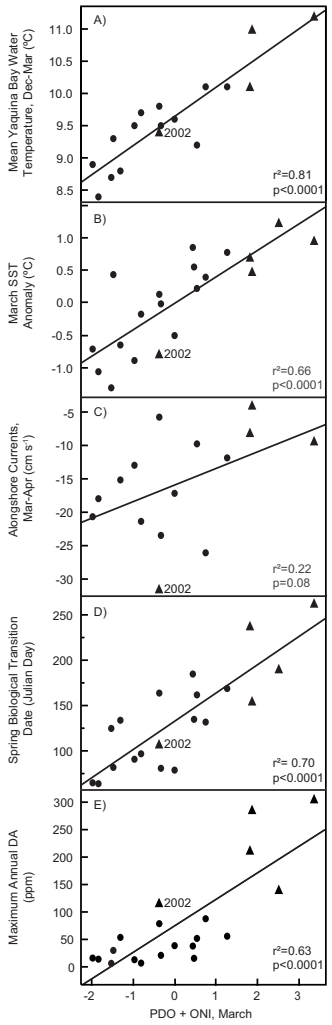

FIGURE 3.2: Climate indexes in March and Oregon coast parameters

Regressions of sum of the Pacific Decadal Oscillation (PDO) and Oceanic Nino Index (ONI) for March (x-axis) and 5 Oregon (OR) coast parameters. (A) average water temperature in the Yaquina estuary during winter, (B) March sea surface temperature anomaly 20 nautical miles offshore, (C) average alongshore currents for March-April (more negative means stronger southward flow), (D) the spring biological transition date, and (E) the annual maximum domoic acid (DA) concentration in razor clams for the OR coast. Triangles indicate the 5 highest annual DA values on record. The year 2002 is marked on each plot; this year saw the fifth highest DA on record, but is associated with cooler ocean conditions than predicted by these plots. Statistical results in Table 3.2.

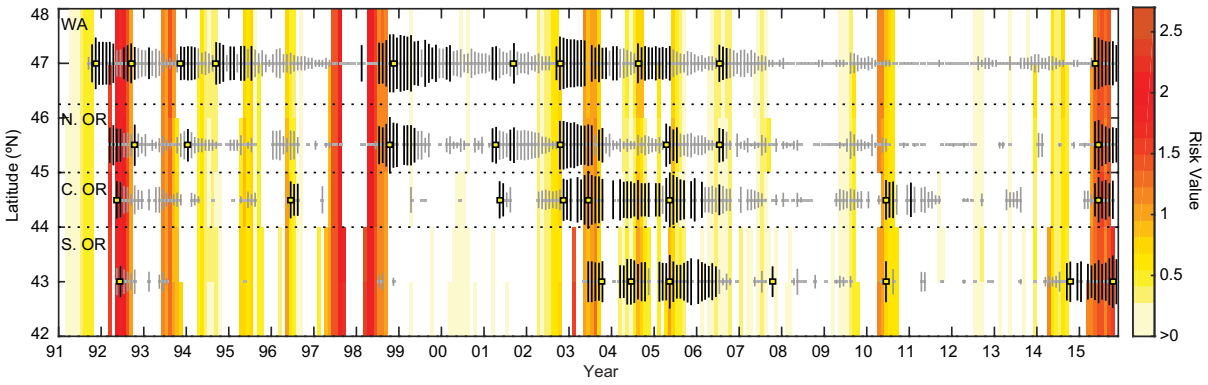

FIGURE 3.3: Domoic acid risk analysis for Oregon and Washington

Domoic acid (DA) risk analysis model output (yellow to red) and domoic acid (DA) levels in Oregon (OR) and Washington (WA) razor clams (vertical bars) from 1992-2015. Model values indicate increased risk of elevated DA based on proxies of warm ocean parameters; model values are only calculated during upwelling season when concentrations of phytoplankton are likely to be greatest each year. White regions indicate elevated DA is least likely as the model equals zero and/or it is downwelling season. From top to bottom, monthly maximum DA values (vertical bars) are latitudinally-binned as follows: WA (46.3°N-48°N), northern OR (45°N-46.3°N), central OR (44°N-45°N), and southern OR (42°N-44°N). Bar length is proportional to the monthly maximum DA value. Color indicates DA $\geq$20 parts per million (ppm, black lines), from 1 to <20ppm (grey lines), or not detected (grey squares). An absence of points indicates no DA data available. Annual DA maxima used in model evaluation are highlighted with yellow squares. Results of model evaluation are shown in Table 3.3-3.4. See also Fig 3.4 for CA risk analysis.

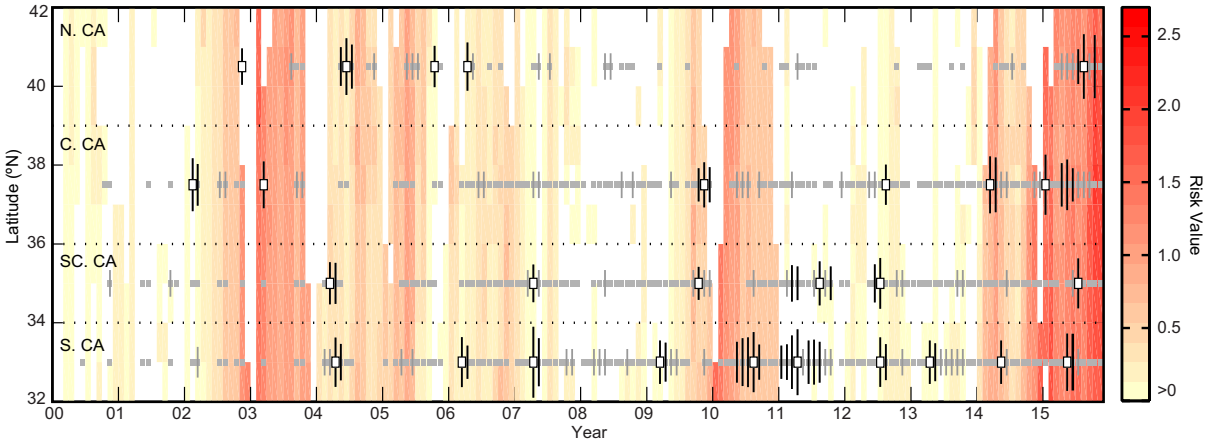

FIGURE 3.4: Domoic acid risk analysis for California

Domoic acid (DA) risk analysis model output (yellow to red) and domoic acid (DA) levels in California (CA) shellfish (vertical bars) from 2000-2015. Model values indicate increased risk of elevated DA based on proxies of warm ocean parameters; model values are only calculated during upwelling season when concentrations of phytoplankton are likely to be greatest each year. White regions indicate elevated DA is least likely (the model equals zero and/or it is downwelling season). From top to bottom, monthly maximum DA values (vertical bars) are latitudinally-binned as follows: northern CA (39°N-42°N), central CA (36°N-39°N), southern CA (34N-36N), and far southern CA (32°N-34°N). Bar length is proportional to the monthly maximum DA value. Color indicates DA $\geq$ 20 parts per million (black lines), between 1 and <20ppm (grey lines), or not detected (grey squares). An absence of points indicates no DA data available. Annual DA maxima used in model evaluation are highlighted with yellow squares. Results of model evaluation are shown in Tables 3.3-3.4. When comparing to Fig 3.3, risk analysis for Oregon (OR) and Washington (WA), note the shorter x-axis here. Also CA DA levels are concentrations from predominantly mussels. Sampling periods differ from OR and WA: in CA samples are event-based, i.e. taken only when blooms of *Pseudo-nitzschia* are observed.

Chapter 4:
Glider-based investigation of the relationship between *in situ* surface, satellite, and euphotic column-integrated chlorophyll-a in a coastal regime

S. Morgaine McKibben[1], Angelicque E. White[1]

[1]College of Earth, Ocean and Atmospheric Sciences, Oregon State University, 104 CEOAS Administration Building, Corvallis, OR 97331, USA

4. GLIDER-BASED INVESTIGATION OF THE RELATIONSHIP BETWEEN *IN SITU* SURFACE, SATELLITE, AND EUPHOTIC DEPTH-INTEGRATED CHLOROPHYLL-A IN A COASTAL REGIME

4.1. Introduction

Phytoplankton are a sentinel class of organisms in the marine environment. As primary producers they draw carbon dioxide out of the atmosphere and convert it into organic matter that sustains the marine food web, making them indicators of both the biological productivity of that system and the amount of carbon it assimilates over time. Chlorophyll-a (chl-a) concentration is a commonly applied proxy of phytoplankton abundance, hence serves as a foundation for constraining ecosystem and climatic processes. Ocean color sensors, such as the Moderate-resolution Imaging Spectraradiometer aboard the spacecraft Aqua (MODIS-Aqua), measure satellite chl-a (chl-a$_{sat}$) over nearly the full ocean domain on a daily basis. Primary productivity (PP) models that quantify the ocean's role in the global carbon cycle rely on the synoptic coverage of phytoplankton abundance and distribution afforded satellite-based sensors.

Daily, global-scale measures of chl-a are unprecedented relative to any other sampling method, yet the coverage of chl-a$_{sat}$ below the surface is limited. Each pixel of chl-a$_{sat}$ is a chl-a concentration value averaged across a 1 kilometer (km) by 1 km cube that spans the surface downward to the first optical depth (FOD, typically a few meters or less in coastal regions). Light levels in the water column are sufficient for photosynthesis within the euphotic zone, which extends from the sunlit

ocean surface to the euphotic depth (Z_{eu}, depth where light has attenuated to 1% of surface values)(Kirk, 1994). The euphotic zone extends below the FOD (Gordon and McCluney, 1975; Morel and Berthon, 1989); photosynthesizing phytoplankton below the FOD are not detected by remote sensing reflectance.

Depth-generalized, also called depth-integrated, oceanic PP models address this shortfall with models that relate surface chl-a to total, depth-integrated chl-a within the euphotic zone (chl-a_{tot}) (Behrenfeld and Falkowski, 1997a; Carr et al., 2006). For example, the widely-applied Vertically Generalized Primary Productivity model (VGPM, Behrenfeld and Falkowski (1997b)) uses an empirically-derived model developed by Morel and Berthon (1989) to determine Z_{eu} and chl-a_{tot} from chl-a_{sat}. This model was developed in open ocean waters using vertical profiles of discrete shipboard chl-a concentrations. Years later the model was confirmed with a new open ocean database of chl-a profiles that used updated, more accurate pigment extraction methods (Uitz et al. (2006)). More recently, Frolov et al. (2012) tested the relationship in a coastal upwelling regime based on both discrete vertical profiles of chl-a concentration and continuous profiles collected via a fluorometer on an autonomous underwater vehicle. They found that the premise behind the Morel model, that chl-a_{tot} can be predicted from surface chl-a, held in a coastal upwelling regime with surface chl-a values an order of magnitude higher than the regions the model had been developed and previously tested in.

In this work, 8 years of routine Slocum glider surveys off the central Oregon coast are applied to further investigate the relationship between surface chl-a and chl-a_{tot} in this region and the implications for satellite-based PP estimates. This dataset spans the high chl-a nearshore zone of a coastal upwelling regime to a low-chl-a regime about 100 kilometers offshore and also experiences strong influence

from freshwater input. These features afford the unique opportunity relative to past work to test the Morel model in hydrographically distinct regions with respect to seasonality and freshwater influence.

Oregon's coastal waters reside in the northern portion of the California Current and are characterized by seasonal upwelling interspersed with short-term, wind-driven up- and downwelling events that lead to high frequency biological variability on the order of days (McKibben et al., 2012; Henson and Thomas, 2007a,b). Annually up 70% of the coastal ocean domain in this region is obscured by cloud cover (McKibben et al., 2012) limiting current satellite characterizations of chl-a in the region to mesoscale patterns (10s to 100s of km) of surface variability at time scales greater than 8 to 30 days (Venegas et al., 2008; Thomas et al., 2009). Influxes of particulate-rich waters from the Columbia River Plume (CRP) in summer (Hickey et al., 2005) and smaller coastal rivers in winter (Wetz et al., 2006), introduce high concentrations of colored dissolved organic matter (CDOM) and particulate matter into surface waters that reduce the accuracy of the globally-parameterized (O'Reilly et al., 2000) chl-a$_{sat}$ product (Siegel et al., 2005; Werdell and Franz, 2007; Bailey and Werdell, 2006).

Regional development of methods to couple satellite and *in situ* data in ways that maximize the descriptive power of each is one of the crucial next steps in oceanographic research and is essential to more accurately quantifying how phytoplankton affect the carbon cycle and respond to climate change. Vertical profiles collected by autonomous Slocum gliders complement chl-a$_{sat}$ as they continuously, irrespective of cloud cover, collect long-term (weeks to months) physical and biological parameters in the upper 200 meters of the water column. This project applies 8 years of Slocum glider data, as well 11 years of discrete shipboard chl-a measure-

ments, to evaluate chl_{sat} in the region through the following research objectives: 1) Assessment of the globally-parameterized chl_{sat} product compared with *in-situ* metrics of chl-a obtained by gliders and research vessels; 2) Determination of whether a predictive relationship oberved by Morel and Berthon (1989) between surface chl-a and chl-a_{tot} holds in this region and 3) how the relationship varies according freshwater, seasonal (up- and down-welling seasons), and regional (nearshore to offshore) influence; and 4) a first order assessment of the effects of the vertical generalization inherent in the Morel and Berthon (1989) model to estimates of NPP relative to vertically resolved estimates.

4.2. Methods

4.2.1 Slocum Gliders and Area of Study

Slocum gliders are autonomous underwater vehicles that utilize variable buoyancy to sample waters in a vertical sawtooth pattern. Two Slocum gliders transected the Newport Hydrographic Line (NH line) off the central Oregon coast (Fig. 4.1) approximately every 1-6 weeks year round from 2006-2014 (data for 2008 were not available for this study). The NH line begins 1 nautical mile (nm) offshore of the central Oregon coast at 44.65°W and extends due west across the continental shelf, past the shelf break (200 meter isobath) to deeper offshore waters (Fig. 4.1). Surface (horizontal) resolution of glider transects was roughly 100 to 800 meters from the nearshore to offshore zones, respectively. Subsurface (vertical) resolution was less than one meter. Surface resolution achieved and route traveled along the NH-line were a function of the depth of the area being surveyed (shallower regions had greater surface resolution) and interaction with strong ocean currents, which

sometimes pulled the glider off course of the east-west NH-line transect (Fig. 4.1). Gliders descended to a maximum depth of 200 meters (beyond the shelf-break only), and deployments were roughly 1-3 weeks long.

4.2.2 Data sets

Glider data

Bio-optical parameters: Each glider was equipped with a WET Labs ECO Puck Triplet that included the following sensors: chl-a fluorescence (excitation 470 nm/ emission 695 nm), CDOM fluorescence (excitation 370 nm/ emission 460 nm), and scattering (660 nm); CDOM was not used for this study. For all 3 optical sensors, the raw signal was processed with a 5 point median filter followed by a 7 point mean filter to reduce noise. Optical data that lacked coincident pressure or pitch values were omitted, this typically occurred just prior to or immediately after glider communication operations at the surface (i.e. not during dives).

A dark signal offset and scale factor were used to calibrate the raw optical data (see also Appendix A). For each deployment and sensor, the minimum of the "reduced" dataset (Appendix A) was defined as the dark offset and subtracted from the raw data to zero the signal. Factory-provided scale factors were used to convert the dark-corrected chl-a fluorescence values to chl-a concentration (mg m^{-3}). For dark-corrected scattering data, factory-provided scale factors with a revised centroid angle of 124 degrees (Sullivan et al., 2012) were applied, yielding the total volume scattering function ($\beta(\theta,\lambda)$). The seawater VSF ($\beta_{sw}(\theta,\lambda)$) at a wavelength of 660 nm according to Zhang et al. (2009) was subtracted from $\beta(\theta,\lambda)$, yielding the VSF due to particles ($\beta_p(\theta,\lambda)$). $\beta_p(\theta,\lambda)$ was converted to integrated particulate backscattering (b_{bp}) using equation 4.1 where χ=1.076 (Sullivan et al., 2012).

$$b_{bp}(\theta, \lambda) = 2\pi\chi\beta_{\mathrm{p}}(\theta, \lambda) \tag{4.1}$$

Salinity: Conductivity, temperature, and pressure data were collected at 0.5 Hz. Conductivity and temperature data were cleaned by removing spikes. Salinity was estimated from conductivity and temperature by applying a thermal lag correction as described by Garau et al. (2011).

Gridding: All glider deployments were gridded to 0.5 kilometer (km, horizontal) x 1 meter (vertical) bins. Each vertical slice of gridded data (1 km by the depth of profile, in 1 meter bins) was considered an individual vertical profile with a unique longitude, latitude, and time of collection determined from the surface bin of each profile.

Profile Parameters: A set of parameters was calculated for each vertical profile of glider data; parameters and methods are summarized in table 4.1. 1) The glider-based surface proxy of chl-a (chl-a$_{glider}$) is the surface bin of each profile of glider chl-a, from 0 to 1 meter. 2) The depth of the chl-a max (Z$_{chlmax}$) was the depth where the chl-a value in each glider profile was greatest. 3) Fresh vs. salty profiles: The Columbia River Plume is a known source of freshwater to the region in the summer (Hickey et al., 2005), altering water column structure and optical properties along the NH-line (Saldías et al., 2016). In consideration of this, vertical profiles were categorized as "fresh" or "salty" if any values in the upper 10 meters were less than 32 PSU (i.e. fresh water was present) or greater than or equal to 32 PSU, respectively. 4) Euphotic depth-integrated chl-a (chl$_{tot}$) was derived from chl-a$_{glider}$ according to Morel and Berthon (1989). 5) The euphotic depth (Z$_{eu}$) was calculated from a power law relationship described in Morel and Maritorena

(2001) that is a function of chl-a$_{tot}$. 6) The first optical depth (Z$_{fod}$) was calculated from Z$_{eu}$ according to (Morel and Berthon, 1989) using equation 4.2. 7) A density threshold of 0.03 kg m^3 with a reference depth of 10 meters was applied to define the the mixed layer depth for all profiles.

$$Z_{fod} = \frac{Zeu}{4.6} \tag{4.2}$$

NPQ correction: The dark-corrected scattering signal was divided by the dark-corrected fluorescence signal (scattering:chl-a) for all gridded vertical profiles in the glider dataset. Non-photochemical quenching (NPQ), a photoprotective mechanism that causes reduced chl-a fluorescence, will cause an increase in this relationship during daylight hours that deepens with greater sunlight intensity and shoals with less. Assuming phytoplankton cells are the dominant scattering medium, the scattering:chl-a signal would be linearly related. An in-lab dilution series, conducted with the ECO Puck in the glider platform as described in Cetinić et al. (2009), except using a dark-adapted diatom monoculture, found significant linear relationship between scattering:chl-a with a ratio of 0.85 (Appendix A). The value of this ratio varies somewhat *in situ* due to the complexity of in water conditions (riverine particulates, differing phytoplankton communities, etc), but the relationship of increased scattering:chl-a persists with daytime sunlight. As a result, when using in-water fluorometers to measure chl-a, there is a daily pattern of reduced chl-a in the upper water column from NPQ dampening of chl-a fluorescence (an example in Sackmann et al. (2008)) which increases the scattering:chl ratio during daylight hours.

Based on this assumption, for each profile of scattering:chl-a the quenching depth (Z$_{quench}$) is defined as the first depth bin above the depth of Z$_{chlmax}$ where

where the "baseline" scattering:chl-a value begins to increase. The "baseline" value is defined as the scattering:chl-a value at Z_{chlmax}, i.e. at this depth assumptions include low to no quenching and that phytoplankton are the dominant scattering particle. The chl-a value at Z_{quench} is then propagated to the surface, yielding a NPQ-corrected profile; however, if the mixed layer depth was less than Z_{chlmax}, then chl-a value at the MLD was propagated to the surface. This step conserved subsurface chl-a features that occurred with riverine influence. This process was repeated for all daytime chl-a profiles. See table 4.1 for summary.

Shipboard Chlorophyll-a

Routine *in situ* measurements of chl-a concentration were collected at the ocean surface during approximately bi-weekly surveys of up to seven stations along the NH-line (Fig. 4.1). Chl-a concentration in discrete surface water samples (chl-a_{ship}) was determined through extracted fluorometric analysis (Arar and Collins, 1997). The approximately 2500 chl-a samples span 2002-2013 and were collected year-round as weather permitted.

Satellite Data

Level-2 (L2) MODIS-Aqua standard chl-a_{sat} (OC3M, O'Reilly et al. (2000)) and k_{d490} (the diffuse attenuation coefficient at 490 nanometers) products were acquired from the Ocean Biology Processing Group (http://oceancolor.gsfc.nasa.gov) and processed to Level-3 (L3) gridded imagery at 1 km resolution for 2006-2014. L3 files remained in individual swaths, i.e. were not daily-averaged, to maintain specific times of satellite over pass. See McKibben et al. (2012) for data masking (flagging) criteria applied. Satellite-based FOD (in meters) was calculated using the formula:

$Z_{FODsat}=1/k_{d490}$.

Satellite to *In Situ* Match-ups

L3 swath chl-a_{sat} pixels were matched within a +/− 0.5 km and +/− 3 hour time window of each chl-a_{glider} and chl-a_{ship} value. Chl-a_{sat} values 2 standard deviations above or below the geometric mean were removed. This eliminated satellite chl-a values on the order of 10^2mg L^{-1}, a range not observed in this region via shipboard measures of pigment concentration (e.g. Nechad et al. (2015) and chl-a_{ship} in this study).

Seasonality

Seasonality in this region is defined by a productive spring/summer upwelling season, with net northerly (towards the south) winds that induce movement of water offshore through Ekman transport (Cosmic, 1987). During fall/winter a more turbulent downwelling season is defined by strong southerly (towards the north) wind stress and net movement of water towards the shore. Daily net northerly and southerly wind stress was calculated from wind speed and direction data from NOAA station NWP03 in Newport, Oregon (Fig 4.1) using the methods of Large & Pond (1981). From these values, dates of seasonal transitions were determined by the cumulative upwelling index (CUI), a measure of wind stress energy input into coastal waters during upwelling season. The annual CUI is calculated by integrating the cumulative wind stress each day from January 1st. The first day of the year when integrated wind stress is negative (northerly) defines day one of both the CUI and upwelling season. A shift to cumulative positive (southerly) wind stress signifies the end of the annual CUI and day one of downwelling season. Data were obtained

from http://damp.coas.oregonstate.edu/windstress/index.html.

Photosynthetically available radiation

A LI-COR pyranometer was used to measure global solar radiation-the combination of direct and diffuse solar radiation-in the 400 to 1100 nm range. Values were taken every 10 minutes and expressed in watts per square meter (W m^{-2}). The data were multiplied by 2.15 according to Britton and Dodd (1976) to convert the global solar radiation to surface photosynthetically active radiation (PAR, μmol $m^{-2}s^{-1}$) for clear-sky irradiance.

4.2.3 Analyses of *in situ* and satellite data

Temporal and spatial coverage, seasonality:

All chl-a_{glider} and Z_{FODsat} values were plotted in time versus latitude space to demonstrate the temporal and spatial coverage of the datasets; Z_{FODsat} points are also representative of the number of matchup instances between chl_{glider} and satellite overpasses. Wind stress, a measure of seasonality, was included to elucidate seasonality in the variables.

Data Bins:

All data for regressions and probability distributions were binned according to region (Fig. 4.1) and season. Strong currents can pull the glider from the idealized NH-line trajectory (Fig. 4.1b). As a result, north-south bounds were set to 44.55°N and 44.75°N; this range was chosen because it captures 90% of the glider dataset. Points outside of this range were omitted. East-west bounds were determined according to hydrography along the NH-line: nearshore (124.47°W-124.03°W), shelf-

break (124.83°W-124.47°W), and offshore (125.2°W-124.83°W) regions (Fig. 4.1).

Regressions and probability distributions:

Chl-a$_{glider}$ was linearly regressed against chl-a$_{\mathrm{sat}}$ using least squares regression; correlation coefficients, p-value, slope-intercept equation, and N values for each regression were reported. Probability distributions were plotted for all 3 surface chl-a datasets (chl-a$_{glider}$, chl-a$_{ship}$, chl$_{\mathrm{sat}}$) to compare the dynamic ranges and biases of the chl-a proxies. For all glider chl-a profiles, chl-a$_{tot}$ was plotted versus chl-a$_{glider}$, with salty and fresh profiles evaluated separately. Points were colored according to the corresponding profile's ratio of Z_{chlmax}:Z_{FOD}, a proxy of the depth of the chl-a max relative to the portion of the upper water column detected via satellite. Correlation coefficients, p-value, slope-intercept equation, and N values for each regression were reported. This was repeated for all glider chl-a profiles categorized as salty. All regressions and frequency distributions were binned by season (upwelling/downwelling) and region (nearshore, shelf-break, offshore), with the exception of chl-a$_{sat}$ versus chl-a$_{ship}$; not enough matchups were present for binning. Instead a single regression was conducted for year round nearshore values, the region best represented by the dataset.

Primary Productivity

A depth-resolved primary productivity model (Equation 4.3) developed by Jacox et al. (2015) was applied to the glider dataset. This model is based on the VGPM (Behrenfeld and Falkowski (1997b)), with vertically-generalizing factors removed, and an empirical relationship between *in-situ* carbon fixation rates collected in coastal California and derived *in-situ* $\mathrm{PAR_z}$.

$$PP_z = 2.9 \cdot chl_z \cdot d_{irr} \cdot \frac{PAR_z}{PAR_z + 2.6} \tag{4.3}$$

For each profile of glider chl-a, the variables needed to calculate primary productivity at a given depth (PP_z) are glider chl-a (chl_z) and PAR (PAR_z) at that depth, as well as the time in hours it took to complete the profile (defined as the time of the final chl-a reading in a profile minus time of initial). For depth-resolved PP_z at depth z, chl_z equals the chl-a value at that depth.

As there was no PAR sensor on the glider platform, solar irradiance values from a nearby mooring (at hydrographic station NH-10, Fig 4.1) were converted to surface PAR and used to derive water column PAR. Due to this constraint, only glider profiles from the nearshore bin near the mooring were included; NH-10 is nearly in the middle of this region. The mooring PAR value coincident in time with the glider profile was defined as surface PAR and used to calculate PAR_z for each depth bin, starting at the surface and proceeding downward according to Equation 4.4). The diffuse attenuation coefficient, k_z, at that depth (Equation 4.5) is dependent on chl_{totz}, the trapezoidally-integrated chl-a value from the surface to depth z.

$$PAR_z = PAR_{z-1} \cdot e^{-k \cdot z} \tag{4.4}$$

$$k_z = 0.04 + 0.0088 \cdot chl_{totz} + 0.054 \cdot chl_{totz}^{0.67} \tag{4.5}$$

As a first order approximation of depth-averaged primary productivity to compare to the vertically-resolved estimates, chl_z and k_z in equation 4.3 were set equal to constant values. Chl_z was set equal to mean glider chl-a from the surface to Z_{eu}. K_z was derived from the Beer Lambert Power Law as a function of Z_{eu} (Table 4.1).

Resulting PP_z values for each profile were vertically-integrated using trapezoidal integration. PP_z, mooring-derived PAR, vertically-integrated PP_z, chl_z, Z_{FOD}, and Z_{eu} for each profile were plotted together for comparison.

4.3. Results & Discussion

4.3.1 Satellite and glider data in space and time

Characterization of the spatial and temporal coverage of the chl-a_{glider} and Z_{FODsat} provides an accounting of seasonal and regional trends, as well as gaps in coverage among the datasets. Winds and chl-a_{glider} show the seasonal relationship between phytoplankton and the annual up- and downwelling seasons; chl-a is highest during upwelling season in the nearshore and may extend to the offshore environment during the peak of upwelling season (Fig. 4.2a). Z_{FODsat} ranges from 0 to 23 meters, and is 15 meters or less 90% of the time (Fig. 4.2c). Z_{FODsat} generally increases with distance offshore and lower chl-a values. On average, glider coverage is slightly greater during upwelling (62%) compared to downwelling (46%) season. This is because rough ocean conditions due to strong winds (Fig. 4.2a) often limited the opportunity for shipboard glider deployments during downwelling season. Also satellite coverage is lowest during downwelling season when cloud cover is the most persistent (McKibben et al., 2015). Annual mean spatial coverage of chl-a_{sat} is 30% percent in the nearshore zone and declines in the offshore direction to about 15 to 20% beyond the shelf break (McKibben et al., 2015). Due to this relatively low satellite coverage in the region and the somewhat stringent matchup criteria, just 3.9% and 2.9% of the surface glider chl-a values had coincident satellite data during up- and down-welling seasons, respectively (Fig 4.2c).

4.3.2 Comparison of surface chl-a proxies

Regression analysis and probability distributions of satellite and *in situ* chl-a proxies describe relative differences in surface chl-a according to season and region. Chl_{ship} is known to vary widely according to a number of factors including incident irradiance, nutrient status, and community composition (Kruskopf and Flynn, 2005; Roesler and Barnard, 2013) although, in the absence of other *in situ* metrics of chl-a against which to compare chl_{sat} and chl_{glider}, it will be considered an approximation of actual in-water chl-a in these analyses. There were 201 nearshore chl_{sat} and chl_{ship} matchups, with 162 and 39 during up- and downwelling seasons, respectively (Fig. 4.3). The significant fit of the nearshore chl_{sat} and chl_{ship} values shows a bias towards elevated chl_{sat} at lower concentrations (below 1 mg m^{-3}), although the datapoints are relatively few in that range (Fig. 4.3). At higher values, the regression model is closer to 1:1, but scatter in chl_{sat} tends to be higher relative to chl_{ship}. Surface glider values tended to be higher than chl-a_{sat}; scatter is greatest, and r^2 values lower, in the mid to nearshore zones (Fig. 4.4). The large bias in these observations is, at least in part, due to the relationship between chl-a_{sat} and the scale factor used to calibrate the chl-a fluorescence signal (Appendix A), plus biases that chl_{sat} signal exhibits (Fig. 4.3).

All surface chl-a proxies increased in maximum concentration and dynamic range closer to shore. Surface chl-a is higher, and dynamic ranges are broader, during upwelling season (Figs. 4.4 & 4.5). Chl-a_{sat} and chl-a_{glider} are biased high, and chl-a_{sat} exhibits a narrower dynamic range, in the offshore and shelf-break regions during upwelling season. (Fig. 4.5 a,b). The broad dynamic ranges among the 3 different proxies match well in the nearshore, with the exception of chl-a_{sat} values that extend

an order of magnitude higher than other proxies. Chl-a$_{ship}$ does not exceed 10^2 in this region based on long term shipboard measurements (Fig. 4.5, Nechad et al. (2015)), hence these values are assumed to be error in the satellite product caused by saturated reflectance values due to nearby clouds, land, or sediment from the Columbia River.

4.3.3 Surface chl-a and total euphotic depth integrated chl-a

The relationship between chl-a$_{tot}$ and chl-a$_{glider}$ is significantly, positively correlated across all seasons, regimes, and in salty or fresh waters (Fig. 4.6 & 4.7). Correlation is greatest in salty waters compared to fresh, and during downwelling season compared to upwelling season. The fresh, upwelling season profiles have the lowest correlation (greater scatter and lower r^2) and least linear shape (Fig. 4.6a,b,c); all trend towards higher chl$_{tot}$ due to profiles with elevated Z_{chlmax}:Z_{fod} that have a chl-max that is greater than the FOD (indicated by color of points on plot). This measure, when greater than 1, is an an approximation of profiles with Z_{chlmax} below Z_{fod}, the depth detected by chl-a$_{sat}$. Figure 4.6a has the least linear. The chl-a$_{tot}$ and chl-a$_{glider}$ relationship these in freshwater influenced, offshore profiles (Fig. 4.6a) is similar to previously reported observations in vertically stratified waters (Morel and Berthon, 1989; Uitz et al., 2006; Frolov et al., 2012). During upwelling season the Columbia River Plume indeed causes strong vertical stratification along the NH-line characterized by a fresh layer of riverine water that thickens with distance from shore, and typically with elevated high features at its base. (Saldías et al., 2016). Relationships between chl$_{glider}$ and chl$_{tot}$ for all salty profiles and all downwelling, freshwater influenced profiles had the least scatter and highest r^2 values (Fig. 4.6d,e,f & 4.7). These observations are similar to previously

reported relationships in well-mixed waters (Uitz et al., 2006; Morel and Berthon, 1989). The original premise put forth by Morel and Berthon (1989)– that surface is predictive of chl-a_{tot}– also holds true in the coastal upwelling to offshore region surveyed in this study; however, the specific values likely vary. The next, and final, step for this assessment will be comparison to the power law coefficients from previous studies and statistical analyses of the relationships found in these waters relative to previous results.

4.3.4 Primary productivity from glider

The initial results of glider-based PP are shown in Fig 4.8. The glider platforms did not include PAR sensors, so irradiance data from a nearby mooring was converted to PAR and attenuated from the surface down the water column under the assumption that chl-a was the primary source of attenuation. Solar irradiance showed expected patterns of rising and falling through the day, including random variability due to cloud cover (Fig. 4.8a). These patterns in surface irradiance were apparent in glider PP for both the depth-averaged (Fig. 4.8b,c) and depth-resolved (Fig. 4.8b) models throughout the day. For depth-averaged PP, elevated PP values often reached below the Z_{FOD} and did not extend beyond Z_{eu}. High chl-a values were frequently found below the euphotic depth; it is not apparent whether this is due to model error in determining Z_{eu}, which can have estimated error of up to 33% (Lee et al., 2007) populations of phytoplankton that have been mixed downward, out of the euphotic zone. In contrast, depth-resolved PP values attenuated at a much shallower depth, near Z_{FOD} (not shown). The depth-dependent k value caused stronger attenuation in the water column, resulting in the lower PP values for each profile compared to the depth-averaged model (Fig. 4.8b). This first-order model will be

further developed and applied to all glider profiles with available surface irradiance data to validate these initial results and determine whether they apply across the entire dataset.

Next steps: Submesoscale patterns in the horizontal (distance), sub-daily processes in time, and biophysical variability in the water column with depth all affect daily primary productivity, making the resolution offered by glider platforms a potentially useful tool for quantifying carbon assimilation by phytoplankton. Future development of accurate glider-based PP in this region will necessitate collection of *in situ* metrics of carbon assimilation, measurements that do not exist in this region in sufficient numbers to assess glider-based productivity, and ideally a the glider platform would include a PAR sensor. As such, future work with this particular glider dataset will be applied as described above, as well as to assessing the impact of averaging in space, time, and depth inherent in the standard satellite-based VGPM model. Questions addressed will include, how does PP calculated with singular, average metrics of daily chl-a and light compare to PP calculated with an actual chl-a profile and chl-a dependent light field (Fig. 4.8 is an initial example)? What are the potential impacts on daily PP measurements due to the occurrence of subsurface chl-a maxima below z_{FOD} and deviations in the surface chl-a to chl-a_{tot} ratio that were observed in this study? Collectively, the first order models presented here form a framework for future investigations of how NPP estimates differ as a function of the different time/space scales inherent to glider and satellite measurements.

A final, and not previously discussed application, will be a first approximation of winter PP. In this region nutrient inputs from coastal rivers, combined with wind relaxation events, potentially lead to downwelling season pulses of productivity

equivalent to 20% of upwelling season estimates (Wetz et al., 2006); however, downwelling season brings intensified cloud cover that limits satellite coverage (McKibben et al., 2012) and rough seas that limit *in situ* sampling efforts. Winter estimates of PP will be compared relative to those seen in upwelling season.

4.3.5 Conclusions

Due to the diversity of marine ecosystems and optical properties across the globe, regional-scale evaluation of standardized chl-a$_{sat}$ algorithms against *in situ* metrics is critical to better constraining phytoplankton abundance and distribution by extension, the ecosystem and biogeochemical processes affected by these primary producers. This is particularly true in relatively optically complex and productive, yet ecologically and economically sensitive, upwelling margins. In this work measures of glider, ship, and satellite-based chl-a proxies in both the horizontal (surface) and vertical (depth) were presented. Pigment-based extraction methods used to quantify chl-a concentration in discrete water samples of known volume, like those used for chl-a$_{ship}$, are acknowledged to vary widely with respect to phytoplankton carbon content (biomass). Until emerging methods that reduce the many known sources of variability in chl-a and biomass content are further developed and adapted for use on moorings and vertically profiling platforms, chl-a concentration remains primary metric against which other chl-a proxies are compared (e.g. Roesler and Barnard (2013); Boss et al. (2008); Werdell and Franz (2007); Nechad et al. (2015)), as was done in this study. Chl-a$_{sat}$ trends towards higher values than chl-a$_{ship}$, with values greater than 10^{-2} considered error. Surface chl-a$_{glider}$ is strongly predictive of chl-a$_{tot}$. The relationship is weakest in freshwater influenced profiles during upwelling season, presumably due to the influence of the Columbia

River Plume on water column structure and constituents. The next steps for this work include statistical evaluations of the surface to chl-a_{tot} relationships presented here and estimation of their potential impact on satellite-based PP. In addition, glider based PP will be expanded to investigate to what extent the high-resolution vertical profiles afforded by gliders can impact PP calculations compared to time- and depth-averaged models.

Acknowledgements: This work was supported by NASA Headquarters under the NASA Earth and Space Science Fellowship Program. Thank you to Kipp Shearman, Jack Barth, and Anatoli Erofeev for providing the glider data. Thank you to Zen Kurokawa and Katie Watkins-Brandt for extensive help in conducting the glider experiments. Thank you to Bill Peterson for the shipboard chl-a data. Thank you to Ian Walsh and Dan Morrissette for helpful discussion regarding the ECO Puck Sensors.

	Variable Name (unit),	Variable Abbrev.	Units	Method Descriptions
Depths:				
	Euphotic depth (m), glider	Z_{eu}	m	Morel, *et al.* 1989 (Table 2), based on surface chl-a
	Depth of chl-a maximum	$Z_{chl\text{-}a\ max}$	m	Depth at maximum chl-a value in the water column
	First optical depth, satellite-based	$Z_{fod\ sat}$	m	$Z_{fodsat} = 1/K_{d490}$, derived from Beer Lambert power law
	First optical depth, glider-based	Z_{fod}	m	$Z_{fod} = Z_{eu}/4.6$ (Morel, *et al.* 1989)
Z-integrated chl-a:				
	Euphotic-depth integrated, chl-a concentration	C_{tot}	mg m^{-2}	Trapezoidally-integrated glider chl-a profile from surface to Z_{eu}
	Euphotic-depth integrated chl-a concentration	$C_{tot\ srf}$	mg m^{-2}	C_{tot} based on surface glider chl-a only, Morel method
Surface proxies:				
	Glider surface chl-a (at 1 m)	$Chl\text{-}a_{glider}$	mg m^{-3}	Glider chl-a over in surface 1-meter bin
	MODIS chl-a concentration	$Chl\text{-}a_{sat}$	mg m^{-3}	MODIS standard chl-a product, 1 km^2 pixel
	Shipboard chl-a concentration	$Chl\text{-}a_{ship}$	mg m^{-3}	Shipboard chl-a value
Diffuse attenuation coefficient:				
	Satellite-derived k	K_{d490}	m^{-1}	MODIS standard diffuse attenuation coefficient at 490 nm product, 1 km^2 pixel
	Depth, chl-a dependent k	K_Z	m^{-1}	Depth-dependent diffuse attenuation coefficient (Parsons 1985)
	Average water column k	K_{avg}	m^{-1}	K_{avg} =-log(0.01)/Zeu, derived from Beer Lambert Power Law

TABLE 4.1: Table of Parameters

FIGURES

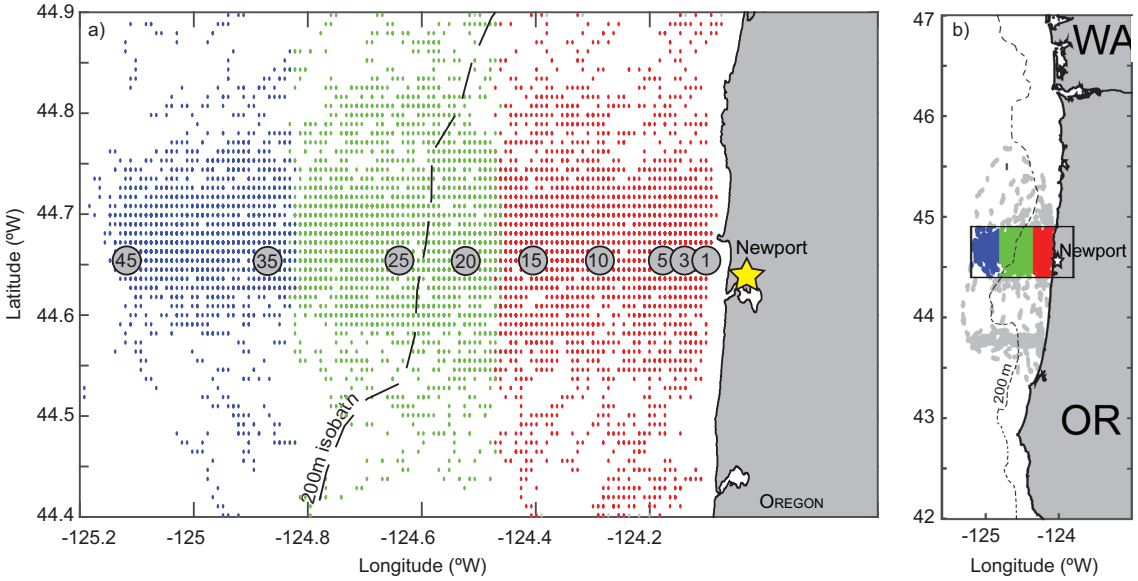

FIGURE 4.1: Area of Study

Figure 1a: Glider-satellite matchups (colored dots) along the Newport Hydrographic (NH) line (grey, numbered circles) off the Oregon coast. Numbered circles are NH-line stations, named according to nautical miles from the coast, where ship samples were taken. Colors indicate bins according to hydrography: nearshore (red), shelf-break (green), offshore (blue). Figure 1b: Study area location relative to Oregon coast; study area (black outline) captures $\tilde{9}0\%$ of the glider data collected. Grey points on panel (b) indicate glider trajectory outside of study area that occurred due to strong currents that carried the gliders away from the NH-line; these data were omitted from the study. 200 meter isobath indicated by dashed line in both panels. Star indicates Newport, Oregon.

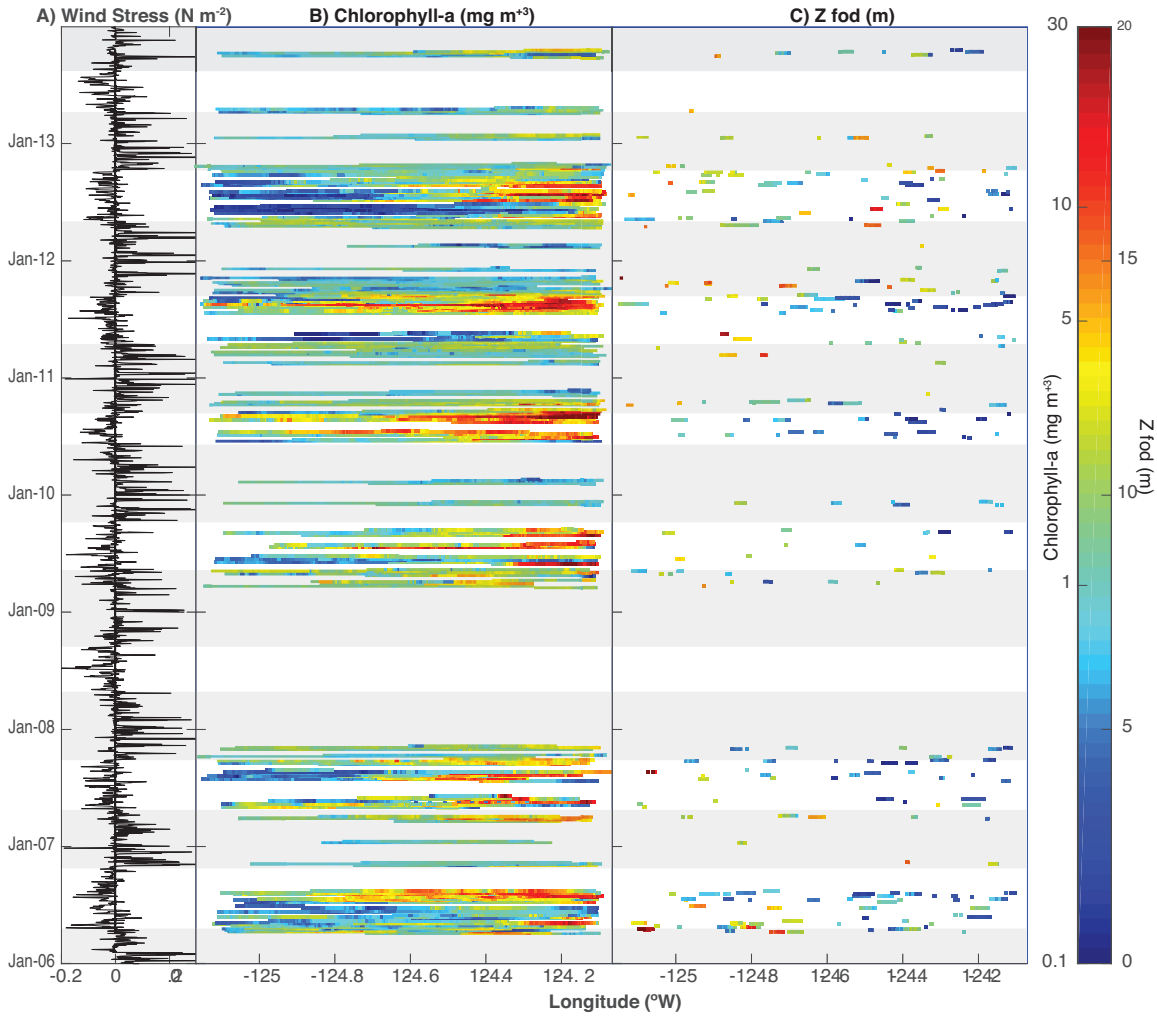

FIGURE 4.2: Temporal and spatial coverage

(A) Wind stress at Newport, Oregon. Downwelling seasons are shaded grey, upwelling seasons are white. (B) Surface glider chlorophyll-a (chl-a) values and (C) satellite-based first optical depth plotted in longitude (x axis) and time (y axis). Panel C depicts the frequency in time and longitudinal space of coincident matchups between glider and satellite data. Glider data for 2008 were not available for this study.

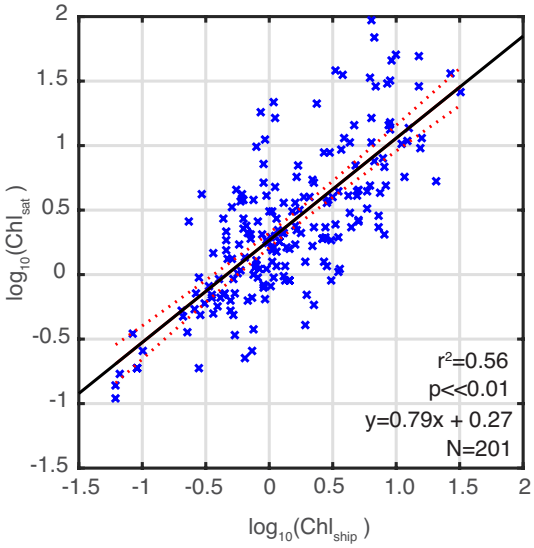

FIGURE 4.3: Satellite chl-a versus shipboard chl-a

Regression of satellite chl-a (chl_{sat}) versus shipboard surface chl-a (chl_{ship}) year-round for the nearshore region. Chl_{ship} samples were collected within +/- 0.5 kilometers and +/- 3 hours of chl_{sat}. Red lines indicate slope and dashed lines indicate 95% confidence interval.

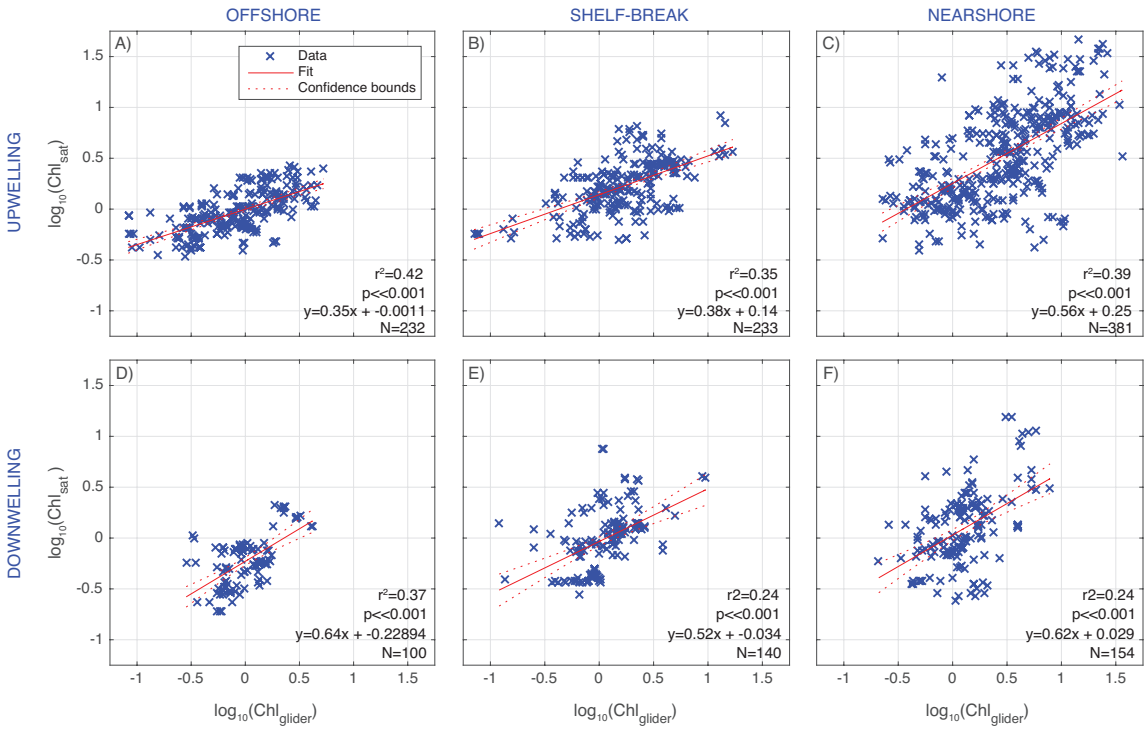

FIGURE 4.4: Glider and satellite chlorophyll-a match-ups

Comparison of 2006-2007 and 2009-2014 chlorophyll-a (chl-a) values in surface 1 meter bin of glider data (x axis) and satellite chl-a (y axis) that occurred within +/- 0.5 kilometers and +/- 3 hours of the glider chl-a measurement. Panel rows are upwelling (A-C) and downwelling (D-F) seasons. Panel columns are offshore (A, D), shelf-break (B,E), and nearshore (C,F) bins as defined in figure 4.1. Red lines indicate slope and dashed lines indicate 95% confidence interval.

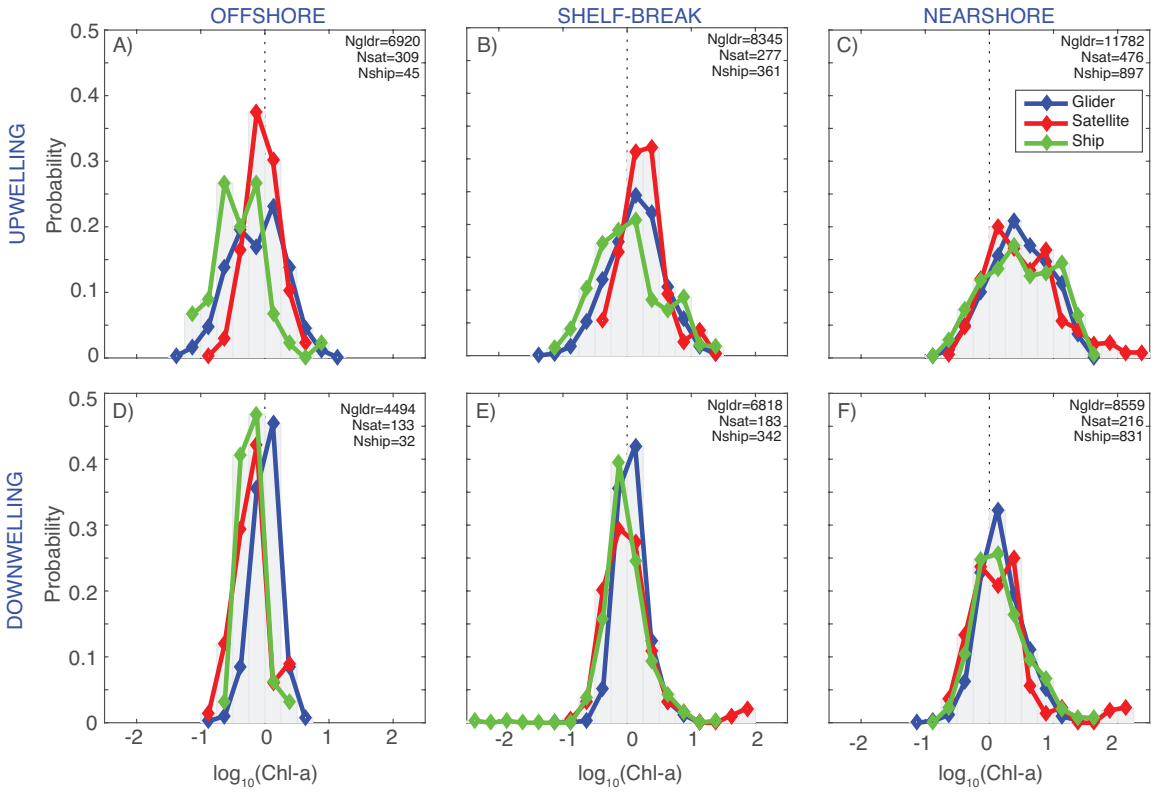

FIGURE 4.5: Probability distributions of glider, satellite, and shipboard chlorophyll-a

Probability distributions of 2006-2007 and 2009-2014 chlorophyll-a (chl-a) values in surface 1 meter bin of glider data (blue line), shipboard surface samples (green line), and MODIS chl-a satellite match-ups (red line). Panel rows are matchups during upwelling (A-C) and downwelling (D-F) seasons. Panel columns are offshore (A, D), shelf-break (B,E), and nearshore (C,F) bins as defined in figure 4.1. Vertical dashed line indicates zero, or chl-a values of 1. N values reported in the upper right corner of each panel.

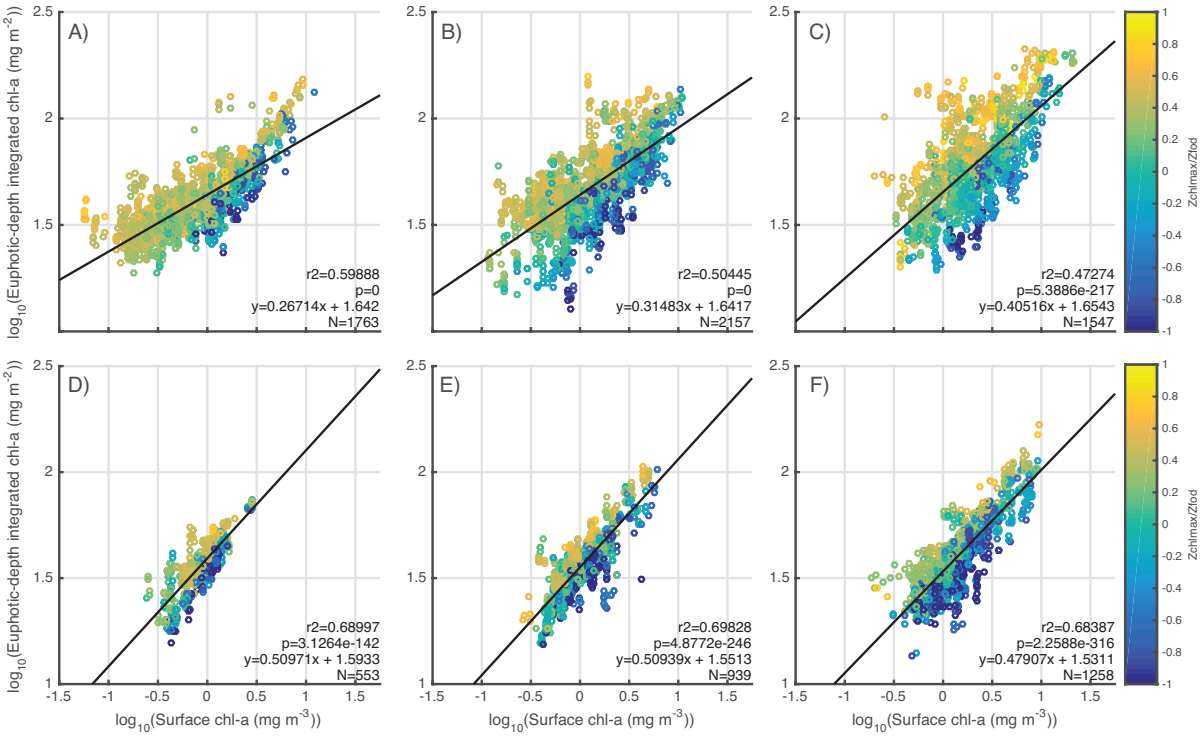

FIGURE 4.6: Surface chlorophyll-a versus euphotic depth-integrated chlorophyll-a in fresh waters

Relationship between glider surface chlorophyll-a (chl-a) and total euphotic-depth chl-a when fresh (<=32 PSU) surface waters are present in the upper 5 meters. Only night time data were used. Colorbar shows the depth of the chl-a max divided by the depth of the first optical depth (FOD); yellower colors indicate a chl-a max deeper than the FOD. Panel rows are matchups during upwelling (A-C) and downwelling (D-F) seasons. Panel columns are offshore (A, D), shelf-break (B,E), and nearshore (C,F) bins as defined in figure 4.1.

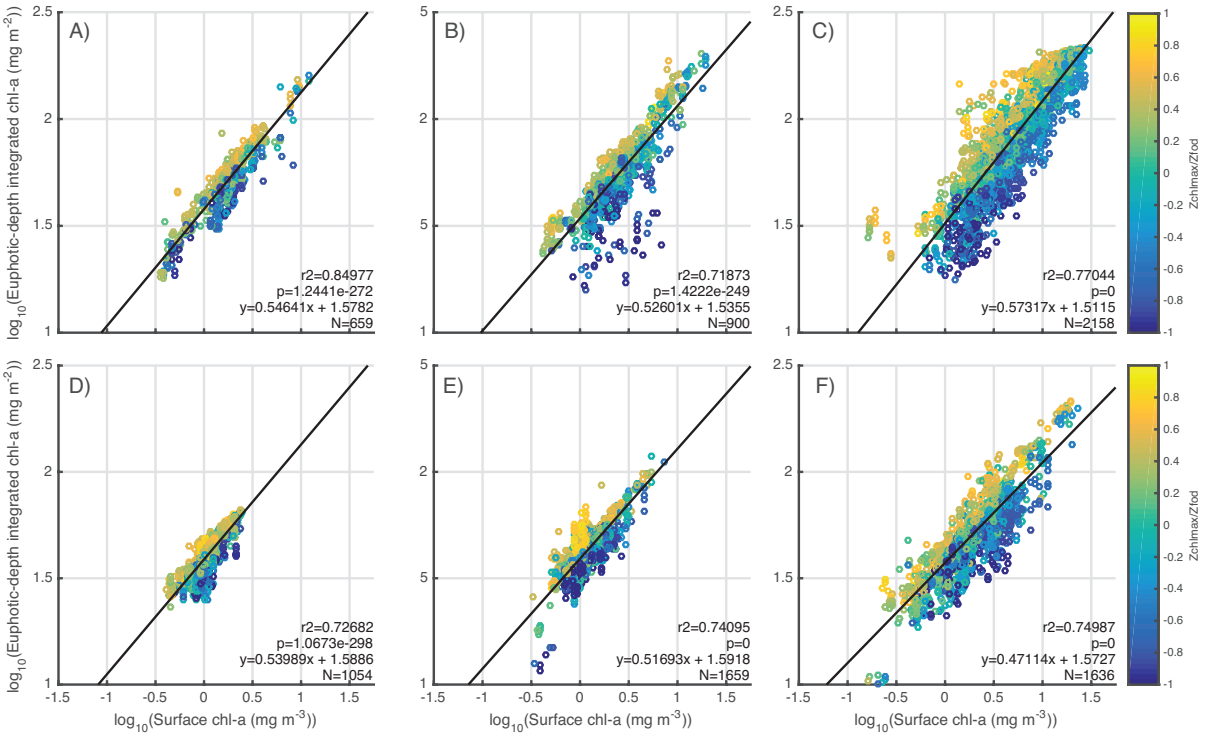

FIGURE 4.7: Surface chlorophyll-a versus euphotic depth-integrated chlorophyll-a in salty waters

Relationship between glider surface chlorophyll-a (chl-a) and total euphotic-depth chl-a when salty (>32 PSU) surface waters are present in the upper 5 meters. Only night time data were used. Colorbar shows the depth of the chl-a max divided by the depth of the first optical depth (FOD); yellower colors indicate a chl-a max deeper than the FOD. Panel rows are matchups during upwelling (A-C) and downwelling (D-F) seasons. Panel columns are offshore (A, D), shelf-break (B,E), and nearshore (C,F) bins as defined in figure 4.1.

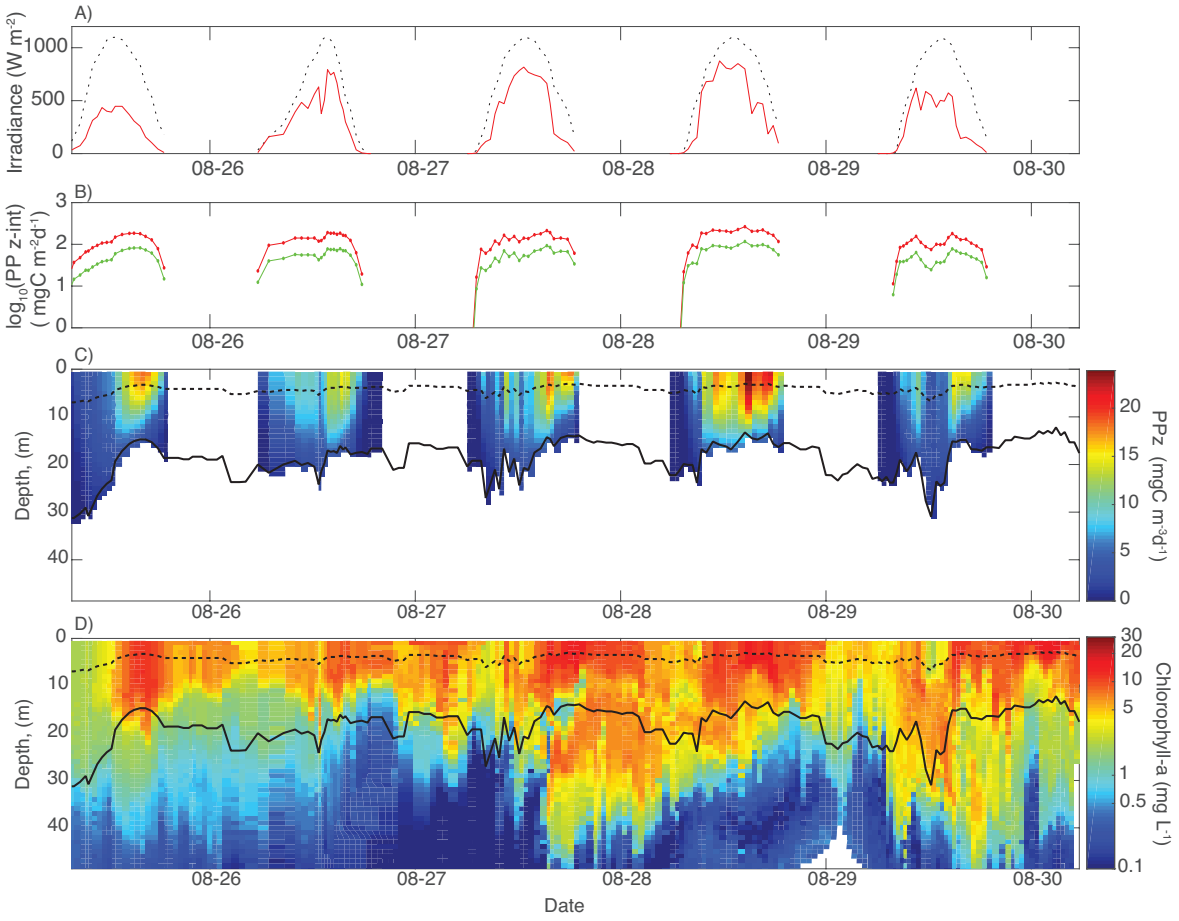

FIGURE 4.8: Glider primary productivity

(A) Modeled no-sky irradiance (black dashed line) and actual surface irradiance measured at NH-10 (red line). (B) Log 10 normalized euphotic depth-integrated primary productivity estimates based on vertical profiles in (C) for two methods: 1) depth-averaged, i.e. euphotic-depth averaged chlorophyll-a (chl-a) is derived from surface glider chl-a and a constant diffuse attenuation coefficient (k) is applied (red line); and 2) depth-resolved, i.e. actual euphotic depth integrated chl-a and chl-a dependent k, primary productivity (green line). (C) Depth-averaged primary productivity. (D) Glider chl-a profiles. Black lines in C and D indicate first optical depth (dashed) and euphotic depth (solid). All plots have a common x axis in time.

5. CONCLUSIONS

Collectively, it was the goal of this dissertation to merge various *in situ* ocean sensing technologies (via ships, surf zone sampling, moorings, gliders, and satellites) to investigate phytoplankton bloom dynamics from event to regional and climate scales along the Oregon coastal region. Chapters 2 and 3 investigated patterns in, and mechanisms underlying, Oregon coastal harmful algal blooms. Chapter 4 explored patterns in the surface (horizontal) and depth (vertical) distribution of phytoplankton based on the universal autotrophic pigment chlorophyl-a (chl-a). Together these works contributed region-specific insights into research topics of global significance. As coverage by autonomous platforms continues to expand, studies of this type– those with a highly data-rich, regional bent that contribute to globally relevant issues– are also expanding and enhancing oceanographic research through improved constraints of biogeochemical processes and marine ecosystem dynamics.

5.1. Harmful Algal Blooms in Oregon

Chapter 2 compiled decades of coastal shellfish monitoring observations and thousands of discrete samples taken at sea and in the coastal intertidal zone to present the first description of the temporal and spatial frequency of toxic HAB events in this region. In addition, case studies based on high-resolution *in-situ* coverage of two HAB events presented rare snapshots of the spatial extent of these events from a shipboard perspective; both events stretched along the coastlines of

2-3 states. Shipboard and coastal observations were combined with high-frequency measures of in-water (temperature) and atmospheric (wind stress) conditions and synoptic satellite data to yield a description of harmful algal bloom (HAB) occurrence and associated environmental conditions. Elevated HAB activity was observed in 2009-2010 and coincided with anomalously warm ocean conditions, specifically a brief change in the Pacific Decadal Oscillation to a warm phase and a coincident El Niño event. Through these analyses, key parameters came to the forefront as informative to future monitoring efforts such as wind stress, a metric for when putative blooms may move on/off shore, particulate dissolved domoic acid in surface waters, and the abundance of *Alexandrium* spp. which appear to be strongly predictive of potential saxitoxin contamination of shellfish.

The observed association between warm ocean conditions in Chapter 2 was quantitatively explored more in more detail in Chapter 3 by correlation of climate indices to regional domoic acid concentrations in shellfish over a 20-year time frame. Warm phases of the Pacific Decadal Oscillation and moderate to strong El Niño events were found to be significant predictors of domoic acid levels in shellfish, providing the first known evidence of a climate-scale control on this toxin. Via analyses of copepod community composition and other plankton indices, we were able to hypothesize that changes in ocean currents during warm phases of these climate cycles promote movement of offshore and southern waters, and their endemic plankton communities, into coastal zones. There they interact with sessile shellfish and potentially enhance toxicity. A risk assessment model was developed for the West Coast to demonstrate the practical application of these findings to forecasting elevated levels of domoic acid in Oregon and Washington, and potentially California, shellfish.

Summary, next steps: Oregon, like many other coastal regions worldwide, is negatively impacted by toxic harmful algal blooms that enter the food chain and present a threat to public health, wildlife, and the coastal economy. Until the studies contained herein (Chapters 2 and 3) and the other publications associated with the 5-year Monitoring Oregon Coastal Harmful Algae project (e.g. White et al. (2014); Du et al. (2011); Tweddle et al. (2010); Du et al. (2016)), Oregon HAB events were relatively underrepresented in the literature compared to nearby California and Washington. Results from Chapter 2 described patterns of HAB frequency and suggested improvements to HAB monitoring in this region. Chapter 3 provides the first evidence of climate-scale regulation of domoic acid and initial steps towards forecasting when domoic acid may be increased in shellfish.

Together these works build a strong foundation of data and findings for future research efforts into causal factors behind domoic acid and saxitoxin events and also raise many research questions applicable to this goal. Can particular patterns of stratification, freshwater outflow, or temperature be linked to *Alexandrium* blooms? Is there a linkage between dinoflaggellate cyst beds and HAB events in this region? Future studies should also build on the forecasting applications presented in Chapter 3 to refine and test the predictive capacity of DA events in shellfish along the West Coast. For example, do local-scale variables affect expression of the climatic warming signal along various regions of the coastline and, by extension, occurrence of DA events?

One particularly intriguing question raised by Chapter 3 is why are the *Pseudo-nitzschia* that are associated with warm water masses more likely to be toxic? Are the communities endemic to warm water from southern and offshore regions more toxic prior to arrival in this region, or are they outcompeting other coastal phyto-

plankton in low-nutrient warm waters during warm phases? These questions warrant continued long-term monitoring of the region and research efforts to investigate these important questions. Further work based on these questions has the potential to improve HAB prediction in this region, as well as others affected by these toxic HABs.

5.2. Investigation of chl-a relationships in the vertical

Due to the diversity of marine ecosystems across the globe, efforts to monitor change and model the carbon cycle cannot rely solely on global parameterizations, but must also consider regional constraints, particularly in economically and ecologically productive upwelling margins. Satellite ocean color sensors provide unprecedented synoptic coverage relative to any other oceanographic sampling technique, but limitations include relatively coarse spatial resolution (kilometers, km) for regional coastal applications, temporal resolution that is intermittently limited by cloud cover, and the fact that a significant fraction of phytoplankton biomass may be concentrated in subsurface features not captured via satellite reflectance.

Chapter 4 combined 8 years of satellite-based chl-a observations with Slocum glider and shipboard proxies of chl-a to investigate unertainty inherent to satellite-based measures of phytoplankton abundance. Building on the work of Morel (1988), Uitz et al. (2006), (Frolov et al., 2012), and others we have used chl-a fluorometry to investigate vertical and horizontal patterns of phytoplankton in terms of chl-a in a coastal ocean regime. Chapter 4 demonstrated that the premise of predictive relationships between surface chl-a and chl-a$_{tot}$, developed in the low chl-a open ocean (Morel and Berthon, 1989), holds in a productive coastal upwelling regime,

as found in (Frolov et al., 2012). Further, the quantitative values were found to vary with season and hydrography with surface values being least predictive when freshwater influence from the Columbia river plume is present during upwelling season. Next steps include statistical assessment of the surface chl-a to chl-a$_{tot}$ relationships observed and how much this variability may affect satellite based PP models. These PP models will further be to applied quantify the effects of the time and depth averaging inherent to the satellite-based vertically-generalized VGPM model.

Appendix A thoroughly considered best practices for bio-optical instrument calibration and highlighted challenges faced with calibrating the Slocum glider dataset due to instrumental limitations and regional and seasonal variability in the data. Previously presented protocols to derive dark signal offsets for the sensors, as well as correction methods for non-photochemical quenching of chl-a, were found not applicable to this particular dataset and new ones were developed instead. This section underscores the importance of evaluating which calibration and correction methods are most applicable to a particular dataset and routine calibration of bio-optical sensors.

5.3. Final remarks

The advent and ongoing evolution of autonomous ocean monitoring technology from sea and space are continually expanding our ability to monitor the ocean. Vertically-profiling platforms yield phytoplankton abundance and physical parameters beneath the waves, a realm previously only reached by relatively costly, brief visits via ship; this is a transformative evolution in research technology which provides

the sampling density of the ocean's interior necessary to better constrain oceanic biogeochemical processes. Applications of ocean observations from space continue to be improved, and advanced instruments are being developed to better image the ocean environment (e.g. PACE, GEO-CAPE). The best of two sampling worlds has been achieved through combination of direct *in situ* samples by Environmental Sample Processors (Scholin et al., 2006) and continuous environmental monitoring. These robotic in-water platforms collect and analyze discrete water samples in real time, showing promise for near real-time monitoring of HAB toxins along the West Coast and in the Great Lakes, among other applications. Advancement is also occurring through development of new approaches to existing datasets, such as measuring carbon export with underwater gliders (Briggs et al., 2011). Efforts to reduce the uncertainty in autonomously-collected chl-a measurements (Roesler and Barnard, 2013; Slade et al., 2010) are working towards a more reliable chl-a proxy. These, among numerous other examples, are both promising and timely given humanity's reliance on the sea and ever-growing population. Ongoing anthropogenic global warming, and the vast uncertainty in environmental response that it brings, add urgency to the need for continued development of ocean observing technologies that advance our understanding of oceanic processes and their response to a changing world.

BIBLIOGRAPHY

Adams, N. G., Lesoing, M., and Trainer, V. L. (2000). Environmental conditions associated with domoic acid in razor clams on the Washington coast. *Journal of Shellfish Research*, 19:1007–1015.

Agardy, T., Alder, J., Dayton, P., Curran, S., and Kitchingman, A. (2005). *Ecosystems and Human Well-Being: Current State and Trends*. Island Press, New York.

Álvarez, E., Morán, X. A. G., López-Urrutia, Á., and Nogueira, E. (2016). Size-dependent photoacclimation of the phytoplankton community in temperate shelf waters (southern Bay of Biscay). *Marine Ecology Progress Series*, 543:73–87.

Anderson, D. (1998). *Physiology and bloom dynamics of toxic* Alexandrium *species, with emphasis on life cycle transitions*, volume 41, pages 29–48. Springer, Berlin.

Anderson, D., Burkholder, J., Cochlan, W., Glibert, P., Gobler, C., Heil, C., Kudela, R., Parsons, M., Rensel, J., Townsend, D., Trainer, V., and Vargo, G. (2008). Harmful algal blooms and eutrophication: Examining linkages from selected coastal regions of the United States. *Harmful Algae*, 8:39–53.

Anderson, D. M., editor (1995). *The Ecology and Oceanography of Harmful Algal Blooms. A National Research Agenda.* Woods Hole Oceanographic Institution, Woods Hole, MA.

Anderson, D. M. and Garrison, D. J. (1997). The ecology and oceanography of harmful algal blooms.

Arar, E. J. and Collins, G. B. (1997). *Method 445.0: In vitro determination of*

chlorophyll-a and pheophytin-a in marine and freshwater algae by fluorescence. United States Environmental Protection Agency, Office of Research and Development, National Exposure Research Laboratory, Ohio.

Bailey, S. W. and Werdell, P. J. (2006). A multi-sensor approach for the on-orbit validation of ocean color satellite data products. *Remote Sensing of Environment*, 102(1-2):12–23.

Banas, N. S., MacCready, P., Hickey, B. M., Dever, E. P., and Liu, Y. (2009). A model study of tide- and wind-induced mixing in the Columbia River Estuary and plume. *Continental Shelf Research*, 29(1):278–291.

Banzon, V., Smith, T. M., Chin, T. M., Liu, C., and Hankins, W. (2016). A long-term record of blended satellite and *in situ* sea-surface temperature for climate monitoring, modeling and environmental studies. *Earth System Science Data*, 8:165–176.

Bargu, S., Goldstein, T., Roberts, K., Li, C., and Gulland, F. (2012). *Pseudo-nitzschia* blooms, domoic acid, and related California sea lion strandings in Monterey Bay, California. *Marine Mammal Science*, 28(2):237–253.

Barron, J. A., Bukry, D., and Field, D. (2010). Santa Barbara Basin diatom and silicoflagellate response to global climate anomalies during the past 2200 years. *Quaternary International: 23rd Pacific Climate Workshop (PACLIM)*, 215(12):34–44.

Batchelder, H. P., Daly, K. L., Davis, C. S., Ji, R., Ohman, M. D., Peterson, W. T., and Runge, J. A. (2013). Climate impacts on zooplankton population dynamics in coastal marine ecosystems. *Oceanography*, 26(4):34–51.

Bates, S., Bird, C. J., Freitas, A. d., Foxall, R., Gilgan, M., Hanic, L. A., Johnson, G. R., McCulloch, A., Odense, P., and Pocklington, R. (1989). Pennate diatom *Nitzschia pungens* as the primary source of domoic acid, a toxin in shellfish from eastern Prince Edward Island, Canada. *Canadian Journal of Fisheries and Aquatic Sciences*, 46(7):1203–1215.

Bates, S. S., Garrison, D. L., and Horner, R. A. (1998). *Bloom dynamics and physiology of domoic-acid-producing* Pseudo-nitzschia *species*. In: Physiological ecology of harmful algal blooms. Springer-Verlag, Heidelberg.

Behrenfeld, M. J. and Falkowski, P. G. (1997a). A consumer's guide to phytoplankton primary productivity models. *Limnology and Oceanography*, 42(7):1479–1491.

Behrenfeld, M. J. and Falkowski, P. G. (1997b). Photosynthetic rates derived from satellite-based chlorophyll concentration. *Limnology and Oceanography*, 42(1):1–20.

Bi, H., Peterson, W. T., and Strub, P. T. (2011). Transport and coastal zooplankton communities in the northern California Current system. *Geophysical Research Letters*, 38(12):L12607.

Blanco, J., Bermudez de la Puenta, M., Arevalo, F., Salgado, C., and Moroo, A. (2002). Depuration of mussels *(Mytilus galloprovincialis)* contaminated with domoic acid. *Aquating Living Resources*, 15(1):53–60.

Bond, N. A., Cronin, M. F., Freeland, H., and Mantua, N. (2015). Causes and impacts of the 2014 warm anomaly in the NE Pacific. *Geophysical Research Letters*, 42(9):3414–3420.

Boss, E., Swift, D., Taylor, L., and Brickley, P. (2008). Observations of pigment and particle distributions in the western North Atlantic from an autonomous float and ocean color satellite. *Limnology and Oceanography*, 53(5, part 2):2112–2122.

Briggs, N., Perry, M. J., Cetinic, I., Lee, C., D'Asaro, E., Gray, A. M., and Rehm, E. (2011). High-resolution observations of aggregate flux during a sub-polar North Atlantic spring bloom. *Deep Sea Research Part I: Oceanographic Research Papers*, 58(10):1031–1039.

Britton, C. M. and Dodd, J. D. (1976). Relationships of photosynthetically active radiation and shortwave irradiance. *Agricultural Meteorology*, 17(1):1–7.

Buck, K., Uttal-Cooke, L., Pilskaln, C., Roelke, D., Villac, M., Fryxell, G., Cifuentes, L., and Chavez, F. (1992). Autecology of the diatom *Pseudonitzschia Australis*, a domoic acid producer, from Monterey Bay, California. *Marine Ecology Progress Series*, 84(3):293–302.

Busse, L., Venrick, E., Antrobus, R., Miller, P., Vigilant, V., Silver, M., Mengelt, C., Mydlarz, L., and Prezelin, B. (2006). Domoic acid in phytoplankton and fish in San Diego, CA, USA. *Harmful Algae*, 5(1):91–101.

Carr, M. E. (2001). Estimation of potential productivity in Eastern Boundary Currents using remote sensing. *Deep Sea Research Part II: Topical Studies in Oceanography*.

Carr, M.-E., Friedrichs, M. A. M., Schmeltz, M., Noguchi Aita, M., Antoine, D., Arrigo, K. R., Asanuma, I., Aumont, O., Barber, R., Behrenfeld, M., Bidigare, R., Buitenhuis, E. T., Campbell, J., Ciotti, A., Dierssen, H., Dowell, M., Dunne, J., Esaias, W., Gentili, B., Gregg, W., Groom, S., Hoepffner, N., Ishizaka, J.,

Kameda, T., Le Quéré, C., Lohrenz, S., Marra, J., Mélin, F., Moore, K., Morel, A., Reddy, T. E., Ryan, J., Scardi, M., Smyth, T., Turpie, K., Tilstone, G., Waters, K., and Yamanaka, Y. (2006). A comparison of global estimates of marine primary production from ocean color. *Deep Sea Research Part II: Topical Studies in Oceanography*, 53(5-7):741–770.

Cetinić, I., Toro-Farmer, G., Ragan, M., Oberg, C., and Jones, B. H. (2009). Calibration procedure for Slocum glider deployed optical instruments. *Optics Express*, 17(18):15420–15430.

Chavez, F. P., Ryan, J., Lluch-Cota, S. E., and Niquen C, M. (2003). From Anchovies to Sardines and Back: Multidecadal Change in the Pacific Ocean. *Science*, 299(5604):217–221.

Claustre, H., Bishop, J., Boss, E., Bernard, S., Berthon, J.-F., Coatanoan, C., Johnson, K., Lotiker, A., Ulloa, O., Perry, M. J., D'Ortenzio, F., Dandon, O. H., and Uitz, J. (2010). Bio-optical profiling floats as new observational tools for biogeochemical and ecosystem studies: Potential synergies with ocean color remote sensing. *Lawrence Berkeley National Laboratory*, LBNL Paper LBNL-3108E.

Cosmic, P. I. (1987). Wind-driven ocean currents and Ekman transport. *Science*, 238:1535–1538.

Costa, P. R., Baugh, K. A., Wright, B., RaLonde, R., Nance, S. L., Tatarenkova, N., Etheridge, S. M., and Lefebvre, K. A. (2009). Comparative determination of paralytic shellfish toxins (PSTs) using five different toxin detection methods in shellfish species collected in the Aleutian Islands, Alaska. *Toxicon*, 54(3):313–320.

Cullen, J. J. and Davis, R. F. (2003). The blank can make a big difference in oceanographic measurements. *Limnology and Oceanography Bulletin*, 12(2).

Cziesla, C. A. (1999). *The transport and distribution of the toxic diatom* Pseudo-nitzschia *spp. in the Coos Bay estuary and the adjacent continental shelf*. Thesis.

Dhoot, J. S., Del Rosario, A. R., Appel, B. R., and Tamplin, B. R. (1992). An Improved HPLC Procedure for Domoic Acid Analysis in Seafood. *International Journal of Environmental Analytical Chemistry*, 53(4):261–268.

Drum, A., Siebens, T., Crecelius, E., and Elston, R. (1993). Domoic acid in the Pacific razor clam *Siliqua patula*. *Journal of Shellfish Research*, 12(2):443–450.

Du, X., Peterson, W., Fisher, J., Hunter, M., and Peterson, J. (2016). Initiation and development of a toxic and persistent *Pseudo-nitzschia* bloom off the Oregon coast in spring/summer 2015. *Public Library of Science ONE*, 11(10):1–17.

Du, X., Peterson, W., McCulloch, A., and Liu, G. (2011). An unusual bloom of the dinoflagellate *Akashiwo sanguinea* off the central Oregon, USA, coast in autumn 2009. *Harmful Algae*, 10(6):784–793.

Du, X., Peterson, W., and O'Higgins, L. (2015). Interannual variations in phytoplankton community structure in the northern California Current during the upwelling seasons of 2001-2010. *Marine Ecology Progress Series*, 519:75–87.

Du, X. and Peterson, W. T. (2014). Seasonal cycle of phytoplankton community composition in the coastal upwelling system off central Oregon in 2009. *Estuaries and Coasts*, 37(2):299–311.

Eberhart, B., Bill, B., and Trainer, V. (2012). Remote sampling of harmful algal blooms: A case study on the Washington State coast. *Harmful Algae*, 19:39–45.

Eriksen, C. C., Osse, T. J., Light, R. D., Wen, T., Lehman, T. W., Sabin, P. L., Ballard, J. W., and Chiodi, A. M. (2001). Seaglider: A long-range autonomous underwater vehicle for oceanographic research. *IEEE Journal of Oceanic Engineering*, 26(4):424–436.

Falkowski, P. and Kiefer, D. A. (1985). Chlorophyll-a fluorescence in phytoplankton: relationship to photosynthesis and biomass. *Journal of Plankton Research*, 7(5):715–731.

Falkowski, P. G., Dubinsky, Z., and Wyman, K. (1985). Growth-irradiance relationships in phytoplankton. *Limnology and Oceanography*, 30(2):311–321.

FAO (2007). The state of world fisheries and aquaculture. Rome, Italy.

Field, C. B., Behrenfeld, M. J., Randerson, J. T., and Falkowski, P. (1998). Primary Production of the Biosphere: Integrating Terrestrial and Oceanic Components. *Science*, 281(5374):237–240.

Fisher, J. L., Peterson, W. T., and Rykaczewski, R. R. (2015). The impact of El Niño events on the pelagic food chain in the northern California Current. *Global Change Biology*, 21(12):4401–4414.

Frolov, S., Ryan, J. P., and Chavez, F. P. (2012). Predicting euphotic-depth-integrated chlorophyll-a from discrete-depth and satellite-observable chlorophyll-a off central California. *Journal of Geophysical Research*, 117(C5):C05042.

Fryxell, G. A., Villac, M. C., and Shapiro, L. P. (1997). The occurrence of the toxic diatom genus *Pseudo-nitzschia (Bacillariophyceae)* on the West Coast of the USA, 1920-1996: a review. *Phycologia*, 36(6):419–437.

Garau, B., Ruiz, S., Zhang, W. G., Pascual, A., Heslop, E., Kerfoot, J., Tintoré, J., Garau, B., Ruiz, S., Zhang, W. G., Pascual, A., Heslop, E., and Tintoré, J. (2011). Thermal lag correction on slocum CTD glider data. *dx.doi.org*, 28(9):1065–1071.

Garrison, D. L., Conrad, S. M., Eilers, P. P., and Waldron, E. M. (1992). Confirmation of domoic acid production by *Pseudonitzschia australis (Bacillariophycea)* cultures. *Journal of Phycology*, 28(5):604–607.

Gershunov, A. and Barnett, T. P. (1998). Interdecadal Modulation of ENSO Teleconnections. *Bulletin of the American Meteorological Society*, 79(12):2715–2725.

Giddings, S., MacCready, P., Hickey, B., Banas, N., Davis, K., Siedlecki, S., Trainer, V., Kudela, R., Pelland, N., and Connolly, T. (2014). Hindcasts of potential harmful algal bloom transport pathways on the Pacific Northwest coast. *Journal of Geophysical Research: Oceans*, 119(4):2439–2461.

Glibert, P. M., Anderson, D. M., Gentien, P., Graneli, E., and Sellner, K. G. (2005). The global, complex phenomena of harmful algal blooms. *Oceanography*, 18(2):136–147.

Gordon, H. R. and McCluney, W. R. (1975). Estimation of the depth of sunlight penetration in the sea for remote sensing. *Applied Optics*, 14(2):413–416.

Hallegraeff, G. (1993). A review of harmful algal blooms and their apparent global increase. *Phycologia*, 32(2):79–99.

Henson, S. A. and Thomas, A. C. (2007a). Phytoplankton scales of variability in the California Current System: 1. Interannual and cross-shelf variability. *Journal of Geophysical Research: Oceans*, 112(C7):C07017.

Henson, S. A. and Thomas, A. C. (2007b). Phytoplankton scales of variability in the California Current System: 2. Latitudinal variability. *Journal of Geophysical Research: Oceans*, 112(C7):C07018.

Hickey, B., Geier, S., Kachel, N., and MacFadyen, A. (2005). A bi-directional river plume: The Columbia in summer. *Continental Shelf Research*, 25(14):1631–1656.

Hickey, B. M. and Banas, N. S. (2003). Oceanography of the U.S. Pacific Northwest Coastal Ocean and estuaries with application to coastal ecology. *Estuaries*, 26(4):1010–1031.

Hoagland, P., Anderson, D., Kaoru, Y., and White, A. (2002). The economic effects of harmful algal blooms in the United States: estimates, assessment issues, and information needs. *Estuaries*, 25(4):819–837.

Hoagland, P. and Scatasta, S. (2006). *The economic effects of harmful algal blooms*, pages 391–402. Springer, Berlin, Heidelberg.

Hooff, R. C. and Peterson, W. T. (2006). Copepod biodiversity as an indicator of changes in ocean and climate conditions of the northern California Current ecosystem. *Limnology and Oceanography*, 51(6):2607–2620.

Horner, R. (2001). *Alexandriuum and Pseudo-nitszchia:* Two of the genera responsible for harmful algal blooms on the U.S. West Coast. Report, University of Alaska Sea Grant.

Horner, R., Garrison, D., and Plumley, F. (1997). Harmful algal blooms and red tide problems on the U.S. West Coast. *Limnology and Oceanography*, 42(5):1076–1088.

Hughes, M. P. (1997). *Temporal and spatial variability of phytoplankton in coastal and estuarine habitats in Coos Bay, Oregon.* Thesis.

Huyer, A., Smith, R. L., and Fleischbein, J. (2002). The coastal ocean off Oregon and northern California during the 1997–8 El Niño. *Progress in Oceanography*, 54(1-4):311–341.

Jacox, M. G., Edwards, C. A., Kahru, M., Rudnick, D. L., and Kudela, R. M. (2015). The potential for improving remote primary productivity estimates through subsurface chlorophyll and irradiance measurement. *Deep-Sea Research Part II*, 112(c):107–116.

Jeffrey, S. W., Mantoura, R. F. C., and Wright, S. W., editors (1997). *Phytoplankton pigments in oceanography: guidelines to modern methods*, volume 10 of *Monographs on oceanographic methodology.* UNESCO Publishing, Paris.

Keister, J. E., Di Lorenzo, E., Morgan, C. A., Combes, V., and Peterson, W. T. (2011). Zooplankton species composition is linked to ocean transport in the Northern California Current. *Global Change Biology*, 17(7):2498–2511.

Kiefer, D. A. (1973). Fluorescence properties of natural phytoplankton populations. *Marine Biology*, 22(3):263–269.

Kirk, J. (1994). *Light and photosynthesis in aquatic ecosystems, Cambridge University.* Cambridge University Press, New York.

Kruskopf, M. and Flynn, K. J. (2005). Chlorophyll content and fluorescence responses cannot be used to gauge reliably phytoplankton biomass, nutrient status or growth rate. *New Phytologist*, 169(3):525–536.

Laabir, M., Jauzein, C., Genovesi, B., Masseret, E., Grzebyk, D., Cecchi, P., Vaquer, A., Perrin, Y., and Collos, Y. (2011). Influence of temperature, salinity and irradiance on the growth and cell yield of the harmful red tide dinoflagellate *Alexandrium catenella* colonizing Mediterranean waters. *Journal of Plankton Research*, 33(10):1550–1563.

Laanaia, N., Vaquer, A., Fiandrino, A., Genovesi, B., Pastoureaud, A., Cecchi, P., and Collos, Y. (2013). Wind and temperature controls on *Alexandrium* blooms (2000-2007) in Thau lagoon (Western Mediterranean). *Harmful Algae*, 28:31–36.

Lane, J. Q. and Kudela, R. (2007). Degradation of domoic acid under common storage conditions. In *Fourth Symposium on Harmful Algae in the US, Woods Hole, MA*, volume 130.

Large, W. and Pond, S. (1981). Open ocean momentum flux measurements in moderate to strong winds. *Journal of Physical Oceanography*, 11(3):324336.

Lavigne, H., D'Ortenzio, F., Claustre, H., and Poteau, A. (2012). Towards a merged satellite and *in situ* fluorescence ocean chlorophyll product. *Biogeosciences*, 9:2111–2123.

Lee, Z., Weidemann, A., Kindle, J., Arnone, R., Carder, K. L., and Davis, C. (2007). Euphotic zone depth: Its derivation and implication to ocean-color remote sensing. *Journal of Geophysical Research: Oceans*, 112(C3):C03009.

Lelong, A., Hégaret, H., Soudant, P., and Bates, S. S. (2012). *Pseudo-nitzschia (Bacillariophyceae)* species, domoic acid and amnesic shellfish poisoning: revisiting previous paradigms. *Phycologia*, 51(2):168–216.

Lewitus, A. J., Horner, R. A., Caron, D. A., Garcia-Mendoza, E., Hickey, B. M., Hunter, M., Huppert, D. D., Kudela, R. M., Langlois, G. W., Largier, J. L., Lessard, E. J., RaLonde, R., Jack Rensel, J. E., Strutton, P. G., Trainer, V. L., and Tweddle, J. F. (2012). Harmful algal blooms along the North American West Coast region: History, trends, causes, and impacts. *Harmful Algae*, 19:133–159.

Mantua, N. J. (2002). Pacific–Decadal Oscillation (PDO) . In MacCracken, M. C., Munn, T., and Perry, J. S., editors, *Encyclopedia of Global Environmental Change*, pages 592–594. Chichester.

Mantua, N. J. (2015). Shifting patterns in Pacific climate, West Coast salmon survival rates, and increased volatility in ecosystem services. *Proceedings of the National Academy of Sciences*, 112(35):10823–10824.

Martinez, E., Antoine, D., D'Ortenzio, F., and Gentili, B. (2009). Climate-Driven Basin-Scale Decadal Oscillations of Oceanic Phytoplankton. *Science*, 326(5957):1253–1256.

McCabe, G. J. and Dettinger, M. D. (1999). Decadal variations in the strength of ENSO teleconnections with precipitation in the western United States. *International Journal of Climatology*, 19(13):1399–1410.

McCabe, R. M., Hickey, B. M., Kudela, R. M., Lefebvre, K. A., Adams, N. G., Bill, B. D., Gulland, F. M. D., Thomson, R. E., Cochlan, W. P., and Trainer, V. L.

(2016). An unprecedented coastwide toxic algal bloom linked to anomalous ocean conditions. *Geophysical Research Letters*, 43(19):10,366–10,376.

McCune, B., Grace, J. B., and Urban, D. L. (2002). Analysis of ecological communities. MjM Software Design, Gleneden Beach, OR.

McKibben, S., White, A., Peterson, W., Wood, A.M. Hunter, M., and Trainer, V. (2017). Climatic regulation of the neurotoxin domoic acid. *Proceedings of the National Academy of Sciences*, 114(2):239–244.

McKibben, S. M., Strutton, P. G., Foley, D. G., Peterson, T. D., and White, A. E. (2012). Satellite-based detection and monitoring of phytoplankton blooms along the Oregon coast. *Journal of Geophysical Research: Oceans*, 117(C12).

McKibben, S. M., Watkins-Brandt, K. S., Wood, A. M., Hunter, M., Forster, Z., Hopkins, A., Du, X., Eberhart, B.-T., Peterson, W. T., and White, A. E. (2015). Monitoring Oregon Coastal Harmful Algae: Observations and implications of a harmful algal bloom-monitoring project. *Harmful Algae*, 50:32–44.

McPhaden, M. J. (2002). El Niño and La Niña: Causes and Global Consequences. In MacCracken, M. C., Perry, J. S., and Munn, T., editors, *Encyclopedia of Global Environmental Change*, pages 353–370.

Millie, D. F., Paerl, H. W., and Hurley, J. P. (2011). Microalgal pigment asessments using high-performance liquid chromatography: a synopsis of organismal and ecological applications. *Canadian Journal of Fisheries and Aquatic Sciences*, 50(11):2513–2527.

Mons, M., Van Egmond, H., and Speijers, G. (1998). Paralytic shellfish poisoning: a review. Report, National Institute of Public Health and the Environment.

Morel, A. (1988). Optical modeling of the upper ocean in relation to its biogenous matter content (Case I waters). *Journal of Geophysical Research*, 93:10–749–10–768.

Morel, A. and Berthon, J.-F. (1989). Surface pigments, algal biomass profiles, and potential production of the euphotic layer: Relationships reinvestigated in view of remote-sensing applications. *Limnology and Oceanography*, 34(8):1545–1562.

Morel, A. and Maritorena, S. (2001). Bio-optical properties of oceanic waters: A reappraisal. *Journal of Geophysical Research*, 106(C4):7163–7180.

Mos, L. (2001). Domoic acid: a fascinating marine toxin. *Environmental Toxicology and Pharmacology*, 9(3):79–85.

Nechad, B., Ruddick, K., Schroeder, T., Oubelkheir, K., Blondeau-Patissier, D., Cherukuru, N., Brando, V., Dekker, A., Clementson, L., Banks, A. C., Maritorena, S., Werdell, P. J., Sá, C., Brotas, V., Caballero de Frutos, I., Ahn, Y. H., Salama, S., Tilstone, G., Martinez-Vicente, V., Foley, D., McKibben, M., Nahorniak, J., Peterson, T., Siliò-Calzada, A., Röttgers, R., Lee, Z., Peters, M., and Brockmann, C. (2015). CoastColour Round Robin data sets: a database to evaluate the performance of algorithms for the retrieval of water quality parameters in coastal waters. *Earth System Science Data*, 7(2):319–348.

Nosho, T. (1999). *Western Regional Aquaculture Center, Waterlines*, 9(1).

Novaczek, I., Madhyastha, M., Ablett, R., Donald, A., Johnson, G., Nijjar, M., and

Sims, D. E. (1992). Depuration of domoic acid from live blue mussels *(Mytilus edulis). Canadian Journal of Fisheries and Aquatic Sciences*, 49(2):312–318.

Ohana-Richardson, A. (2007). *Population ecology of the diatom genus* Pseudo-nitzschia *within the South Slough, Charleston, Oregon.* Thesis.

O'Reilly, J. E., Maritorena, S., and Siegel, D. A. (2000). Ocean color chlorophyll-a algorithms for SeaWiFS, OC2, and OC4: Version 4. *SeaWiFS postlaunch calibration and validation analysis*, 3:9–23.

Pauly, D. and Christensen, V. (1995). Primary production required to sustain global fisheries. *Nature*, 374:255–257.

Perry, M. J., Sackmann, B. S., Eriksen, C. C., and Lee, C. M. (2008). Seaglider observations of blooms and subsurface chlorophyll maxima off the Washington Coast. *Limnology and Oceanography*, 53(5, part2):2169–2179.

Peterson, W. T. and Keister, J. E. (2003). Interannual variability in copepod community composition at a coastal station in the northern California Current: a multivariate approach. *Deep Sea Research Part II: Topical Studies in Oceanography*, 50(14-16):2499–2517.

Phillips, E., Zamon, J., Nevins, H., Gibble, C., Duerr, R., and Kerr, L. (2011). Summary of birds killed by a harmful algal bloom along the south Washington and north Oregon coasts during October 2009. *Northwestern Naturalist*, 92(2):120–126.

Picot, C., Nguyen, T., Roudot, A., and Parent-Massin, D. (2011). A preliminary

risk assessment of human exposure to phycotoxins in shellfish: a review. *Human and Ecological Risk Assessment*, 17(2):328–366.

Pierce, S., Shearman, R. K., Barth, J. A., and Erofeev, A. (2016). Underwater Glider Observations of the 2014-15 Northeast Pacific Warm Anomaly. In *AGU Ocean Sciences 2016, Poster ME44E-0897*, New Orleans, LA.

Pitcher, G. C., Figueiras, F. G., Hickey, B. M., and Moita, M. T. (2010). The physical oceanography of upwelling systems and the development of harmful algal blooms. *Progress in Oceanography*, 85(1-2):5–32.

Quilliam, M. A., Xie, M., and Hardstaff, W. R. (1995). Rapid extraction and cleanup for liquid chromatographic determination of domoic acid in unsalted seafood. *Journal of the Association of Official Analytical Chemists International*, 78(2):543–554.

Roesler, C. S. and Barnard, A. H. (2013). Optical proxy for phytoplankton biomass in the absence of photophysiology: Rethinking the absorption line height. *Methods in Oceanography*, 7:79–94.

Sackmann, B. S., Perry, M. J., and Eriksen, C. C. (2008). Seaglider observations of variability in daytime fluorescence quenching of chlorophyll-a in Northeastern Pacific coastal waters. *Biogeosciences Discussions*, 5(4):2839–2865.

Saldías, G. S., Kipp Shearman, R., Barth, J. A., and Tufillaro, N. (2016). Optics of the offshore Columbia River plume from glider observations and satellite imagery. *Journal of Geophysical Research: Oceans*, 121(4):2367–2384.

Schofield, O., Kohut, J., Aragon, D., Creed, L., Graver, J., Haldeman, C., Kerfoot,

J., Roarty, H., Jones, C., Webb, D., and Glenn, S. (2007). Slocum Gliders: Robust and ready. *Journal of Field Robotics*, 24(6):473–485.

Scholin, C., Jensen, S., Roman, B., and Massion, E. (2006). The Environmental Sample Processor (ESP)-an autonomous robotic device for detecting microorganisms remotely using molecular probe technology. In *OCEANS 2006*. IEEE.

Scott, B. A. (2007). *The relationship between upwelling, shellfish toxicity, and the distribution of toxic cysts in Oregon*. Thesis.

Shanks, A. L. and McCulloch, A. (2003). Fornightly periodicity in the abundance of diatom and dinoflagellate taxa at a coastal study site. *Journal of Experimental Marine Biology and Ecology*, 296:113–126.

Shanks, A. L., Morgan, S. G., MacMahan, J., and Reniers, A. (2014). Onshore transport of plankton by internal tides and upwelling-relaxation events. *Marine Ecology Press Series*, 502:39–51.

Siegel, D. A., Maritorena, S., Nelson, N. B., Behrenfeld, M. J., and McClain, C. R. (2005). Colored dissolved organic matter and its influence on the satellite-based characterization of the ocean biosphere. *Geophysical Research Letters*, 32(20):L20605.

Slade, W. H., Boss, E., Dall'Olmo, G., Langner, M. R., Loftin, J., Behrenfeld, M. J., Roesler, C., Westberry, T. K., Slade, W. H., Langner, M. R., and Loftin, J. (2010). Underway and moored methods for improving accuracy in measurement of spectral particulate absorption and attenuation. *Journal of Atmospheric and Oceanic Technology*, 27(10):1733–1746.

Smayda, T. and Trainer, V. (2010). Dinoflagellate blooms in upwelling systems: Seeding, variability, and contrasts with diatom bloom behaviour. *Progress in Oceanography*, 85(1):92–107.

Stewart, J., Marks, L., Gilgan, M., Pfeiffer, E., and Zwicker, B. (1998). Microbial utilization of the neurotoxin domoic acid: blue mussels *(Mytilus edulis)* and soft shell clams *(Mya arenaria)* as sources of the microorganisms. *Canadian Journal of Microbiology*, 44(5):456–464.

Sullivan, J. M., Twardowski, M. S., Ronald, J., Zaneveld, V., and Moore, C. C. (2012). Measuring optical backscattering in water. In *Light Scattering Reviews 7*, pages 189–224. Springer Berlin Heidelberg, Berlin, Heidelberg.

Thomas, A. C., Brickley, P., and Weatherbee, R. (2009). Interannual variability in chlorophyll concentrations in the Humboldt and California Current Systems. *Progress in Oceanography*, 83(1-4):386–392.

Tomas, C. R. (1997). *Identifying marine phytoplankton*. Academic Press.

Trainer, V. and Hickey, B. (2002). Biological and physical dynamics of domoic acid production off the Washington Coast. *Limnology and Oceanography*, 47(5):1438–1446.

Trainer, V. L., Adams, N. G., and Wekell, J. C. (2001). Domoic acid-producing *Pseudo-nitzschia* species off the U.S. West Coast associated with toxification events. In Hallegraeff, G. M., Blackburn, S. I., Lewis, R. J., and Bolch, C. J., editors, *Proceedings of the Ninth International Conference on Harmful Algal Blooms*, pages p. 46–48. Intergovernmental Oceanographic Commission of UNESCO.

Trainer, V. L., Bates, S. S., Lundholm, N., Thessen, A. E., Cochlan, W. P., Adams, N. G., and Trick, C. G. (2012). *Pseudo-nitzschia* physiological ecology, phylogeny, toxicity, monitoring and impacts on ecosystem health. *Harmful Algae*, 14:271–300.

Trainer, V. L., Hickey, B. M., Lessard, E. J., Cochlan, W. P., Trick, C. G., Wells, M. L., MacFadyen, A., and Moore, S. K. (2009). Variability of *Pseudo-nitzschia* and domoic acid in the Juan de Fuca eddy region and its adjacent shelves. *Limnology and Oceanography*, 54(1):289–308.

Trainer, V. L., Pitcher, G. C., Reguera, B., and Smayda, T. J. (2010). The distribution and impacts of harmful algal bloom species in eastern boundary upwelling systems. *Progress in Oceanography: Special Issue on Harmful Algal Blooms in Upwelling Systems*, 85(1–2):33–52.

Trainer, V. L. and Suddleson, M. (2005). Monitoring approaches for early warning of domoic acid events in Washington State. *Oceanography*, 18(2):228.

Twardowski, M. S., Claustre, H., Freeman, S. A., Stramski, D., and Huot, Y. (2007). Optical backscattering properties of the "clearest" natural waters. *Biogeosciences Discussions*, 4(4):2441–2491.

Tweddle, J. F., Strutton, P. G., and Foley, D. G. (2010). Relationships among upwelling, phytoplankton blooms, and phycotoxins in coastal Oregon shellfish. *Marine Ecology Press Series*, 405:131–145.

Uitz, J., Claustre, H., Morel, A., and Hooker, S. B. (2006). Vertical distribution of phytoplankton communities in open ocean: An assessment based on surface chlorophyll. *Journal of Geophysical Research: Oceans*, 111(C8):C08005.

Van Dolah, F. M. (2000). Marine algal toxins: origins, health effects, and their increased occurrence. *Environmental Health Perspectives*, 108(Suppl 1):133–141.

Van Egmond, H., Van Apeldoorn, M., and Speijers, G. (2004). Marine biotoxins. Report, Food and Agriculture Organization of the United Nations.

Venegas, R. M., Strub, P. T., Beier, E., Letelier, R., Thomas, A. C., Cowles, T., James, C., Soto Mardones, L., and Cabrera, C. (2008). Satellite-derived variability in chlorophyll, wind stress, sea surface height, and temperature in the northern California Current System. *Journal of Geophysical Research: Oceans*, 113(C3):C03015.

Villac, M., Roelke, D., Chavez, F., Cifuentes, L., and Fryxell, G. (1993). *Pseudonitzschia australis Frenguelli* and related species from the West Coast of the U.S.A.: Occurrence and domoic acid production. *Journal of Shellfish Research*, 12(2):457–465.

Wekell, J. C., Gauglitz Jr, E. J., and Barnett, H. J. (1994). The occurrence of domoic acid in razor clams (*Siliqua patula*), Dungeness crab (*Cancer magister*), and anchovies (*Engraulis mordax*). *Journal of Shellfish Research*, 13:587–593.

Wells, M. L., Trainer, V. L., Smayda, T. J., Karlson, B. S. O., Trick, C. G., Kudela, R. M., Ishikawa, A., Bernard, S., Wulff, A., Anderson, D. M., and Cochlan, W. P. (2015). Harmful algal blooms and climate change: Learning from the past and present to forecast the future. *Harmful Algae*, 49:68–93.

Werdell, P. J. and Franz, B. A. (2007). Approach for the long-term spatial and temporal evaluation of ocean color satellite data products in a coastal environment. In Frouin, R. J., editor, *Proceedings of SPIE*, pages 66800G–1–12.

Wetz, M. S., Hales, B., Chase, Z., Wheeler, P. A., and Whitney, M. M. (2006). Riverine input of macronutrients, iron, and organic matter to the coastal ocean off Oregon, U.S.A., during the winter. *Limnology and Oceanography*, 51(5):2221–2231.

White, A., Watkins-Brandt, K., McKibben, M., Wood, A., Hunter, M., Forster, Z., Du, X., and Peterson, T. (2014). Large-scale bloom of *Akashiwo sanguinea* in the Northern California Current System in 2009 . *Harmful Algae*, 37:38–46.

Wood, A., Shapiro, L., and Bates, S. (1994). Domoic acid: final report of the workshop, Oregon Institute of Marine Biology, February 21-23, 1992. *Oregon Sea Grant*, ORESU-W-94-001:22. http://www.meds-sdmm.dfo-mpo.gc.ca/sp-ps/eng/Publication/Details/129.

Wright, J. L. C., Boyd, R. K., de Freitas, A. S. W., Falk, M., Foxall, R. A., Jamieson, W. D., Laycock, M. V., McCulloch, A. W., McInnes, A. G., Odense, P., Pathak, V. P., Quilliam, M. A., Ragan, M. A., Sim, P. G., Thibault, P., Walter, J. A., Gilgan, M., Richard, D. J. A., and Dewar, D. (1989). Identification of domoic acid, a neuroexcitatory amino acid, in toxic mussels from eastern Prince Edward Island. *Canadian Journal of Chemistry*, 67(3):481–490.

Xing, X., Claustre, H., and Blain, S. (2012). Quenching correction for *in vivo* chlorophyll fluorescence acquired by autonomous platforms: A case study with instrumented elephant seals in the Kerguelen region (Southern Ocean). *Limnology and Oceanography Methods*, 10:483–495.

Yamada, S. B., Peterson, W. T., and Kosro, P. M. (2015). Biological and physical

ocean indicators predict the success of an invasive crab, *Carcinus maenas*, in the northern California Current. *Marine Ecology*, 537:175–189.

Zhang, X., Hu, L., and He, M.-X. (2009). Scattering by pure seawater: Effect of salinity. *Optics Express*, 17(7):5698–5710.

APPENDIX

A APPENDIX Retrospective calibration methods for 8 years of bio-optical data obtained via Slocum glider in a hydrographically dynamic region

Bio-optical datasets collected over long periods of time (years) via autonomous in-water platforms are becoming common in ocean waters worldwide, providing a wealth of *in situ* oceanographic observations unmatched by other sampling methods. With any in-water instrumentation, careful calibration is necessary to ensure a robust and accurate dataset. Considering the relative ubiquity of long-term deployments of bio-optical sensors, there are few research documents with thorough coverage of sensor calibration and characterization of sensor performance over long time frames. In this work the methods developed for, and results of, retrospective calibration of three WET Labs ECO Puck sensors mounted aboard two Slocum gliders (named "Jane" and "Bob") are presented.

The three WET Labs ECO Puck Triplet BB2FLSO sensors were used in routine glider surveys that followed an east-west transect line off of the central Oregon coast from 2006 to 2014 (see Chapter 4.2.1 and Figure 4.1), reaching depths up to 200 meters. Deployments occurred for 1-3 weeks at a time year-round, weather permitting, and spanned hydrographically disparate regimes with strong seasonality. Each ECO Puck Triplet was equipped with chlorophyll-a (chl-a) fluorescence (excitation 470 nm/ emission 695 nm), colored dissolved organic matter (CDOM) fluorescence (excitation 370 nm/ emission 460 nm), and scattering (660 nm) sensors. All three sensors follow a common blueprint of operation: light is emitted at a certain wavelength, a response is induced, and the magnitude of the response is received on a detector and recorded as photon counts. Calibration protocols apply

two values to convert these raw signals into units of the constituent of interest: 1) a baseline signal value, or dark signal offset, representative of the average counts observed in the absence of the parameter of interest (necessary to "zero" the signal); and 2) a scale factor to linearly convert the corrected signal into the desired units following this generalized formula: Output [calibrated units] = (Raw signal [counts] - dark offset [counts]) * scale factor [calibrated units * counts^{-1}].

The primary goals of this work were to determine dark offset and scale factor methods that were a best fit for this dataset and to characterize changes in the sensors over the 8-year time frame. Additionally, an in-lab case study was conducted to assess the uncertainty contributed to calibrated chl-a values by a photoprotective mechanism called nonphotochemical quenching (NPQ) on the chl-a fluorescence signal. Results provide the correction and evaluation needed to correct the Slocum glider dataset prior to the study conducted in Chapter 4.. Implications of these findings to calibration of other long-term bio-optical missions are discussed as well.

A1 Baseline signal response and dark count correction

Zeroing the raw signal through subtraction of the dark offset is a necessary first step in instrument calibration. Methods can be generalized into two categories: the dark offset may be assessed *outside* of deployment (termed "in-lab" here for simplicity) or *during* deployment of the glider platform (*in situ*). For the purposes of this study, in-lab methods are broadly defined as those that include cleaning the optical face, carefully applying opaque tape to the detectors to obscure entry or exit of light, then collecting 1-2 minutes of data. The mean is the dark offset and the standard deviation is the instrument resolution. In-lab methods differ according to:

1) location of data collection (in a lab, on the deck of a ship, etc), 2) whether or not the instrument is powered by the same source used during deployments (in this case the batteries that power the glider platform) and 3) whether or not the instrument is immersed in water.

The dark offset may also be determined using *in situ* methods, which extract a dark offset value, unique to each deployment, from the raw data to individually dark-correct all data points in the deployment. How the offset is defined separates the methods. Identification of a clear water offset (CWO) location for each deployment is one method; the CWO may be defined as the "clearest" average signal obtained at a pre-determined deep water depth and location (Perry et al., 2008). This requires a region that is consistently visited by successive deployments that is reliably lacking the constituents of interest.

All available measures of the dark offset were compared for the 8-year time frame, and the best method to dark-correct this dataset selected. Three in-lab dark signal offset methods were assessed: factory (in water, removed from glider with external power source) and with the instruments mounted in and powered by the glider as described in Cetnic et al. 2009). For i*n-situ* methods, we assessed whether a CWO region was reliably present over time in our region of study and ultimately developed a "deployment minimum" correction to dark-correct our data (described below).

A1.1 Methods: Evaluation of four metrics of baseline signal

Clear water offset: Whether or a CWO assumption could be applied in the area of study was assessed, i.e. whether a reliably clear region (or regions) existed in

depth and latitude/longitude space for all deployments. Due to north-south variability in bathymetry and glider path (Fig. 4.1), only data from 44.55 to 44.75°N were considered for this analysis (section 4.2.1) for consistency. For each deployment, the "reduced" dataset (described below) was used to create probability distributions as follows: a range, in counts, where the lowest signals in each deployment dataset could be found was defined. This range began at the reduced dataset minimum and ended at that minimum plus the factory-derived instrument resolution for each sensor (∼1 count) multiplied by 3 (total range spanned approximately ∼3 counts). Next, 100 values within that range were randomly selected and the depths and longitudes of these points were used to create the probability distributions. This was done for each deployment to determine where clear water regions were statistically most likely to occur for each sensor.

In-lab darks: Dark offsets performed by WET Labs were determined with the ECO Pucks outside of the glider platform, submerged in water, and powered by an external source. Offsets were also determined with the ECO Pucks mounted inside, and powered by, the glider as described in Cetinic *et al.* 2009, which includes lowering the glider onto a custom chamber of water designed to submerge the sensors while still mounted on the glider (Fig. 0.6). "On deck" dark counts were conducted out of water on the deck of a research vessel. For all methods, dark tape covered the sensors and the mean and standard deviation of 2 minutes of data were recorded as the dark offset and instrument resolution, respectively.

Deployment baseline signal: To determine the baseline signal, or dark offset, for each deployment, the filtered, raw dataset was reduced to exclude data

points that had the greatest likelihood of instrument or light-induced noise (e.g. power fluctuations during top/bottom of dives, light at or near the surface being detected by the optics due to wave focusing or extreme pitch or roll of the glider, etc.). Data points meeting the following criteria were omitted: daytime values (4am-10pm local), pitch angles indicative of the top or bottom of a dive (pitch ¿=-0.5 or ¡=0.5 and pitch between -0.3 and 0.3), and depth values less than 10 meters. For each deployment, the minimum of this reduced version of the deployment dataset was defined as the baseline signal for correction.

A2 Dynamic signal response and scale factor conversions

The dynamic signal can be defined as a sensor's response to a constituent of interest. Scale factors are derived through linear regression of this signal (after dark correction) against a standard solution at varying concentrations. The slope relating the counts to the constituent concentration is the scale factor. These values are provided by the factory, or can be determined by the user. Discussion of which scale factor methods were used is included in the results below, and the potential effects of age, changes in calebration method, and nonphotochemical quenching activity of a phytoplankton community on scale factors discussed.

A2.1 Methods

Changes over time: The dynamic response of the optical sensors can change over long periods of time (years) due to the cumulative effects of the aging of components (e.g., decreased LED output, yellowing epoxy on the optical face, or scratches that reduce the signal return, etc.), among other possibilities. All scale factors de-

termined during factory servising were compiled from the period of 2004 through 2012, and derived against consistent standards, providing a metric of change in the instruments' dynamic range over time.

In-lab nonphotochemical quenching effects on the scattering to chl-a fluorescence relationship: In-lab dilution experiments were conducted to investigate how much variability in the scattering to chl-a fluorescence ratio may be caused by NPQ (described below and in chapter 1.2.1). Dark-corrected scattering and chl-a fluorescence counts were recorded during two dilution experiments: one with a light-adapted, and the other with a dark-adapted, phytoplankton monoculture of *Thalassiosira weissflogii*. Dilution series were conducted using a custom calibration chamber as described in Cetinic et al. 2009. Two minutes of data were collected for each dilution step to determine a mean value and standard deviation.

A3 Results and discussion

The power source utilized, whether the unit was immersed in water or not, changes in the glider platform or ECO Pucks over time (due to aging, upgrades, etc.), electromagnetic interference, and temperature or pressure at the time of data collection all potentially affect the dark offset value, introducing uncertainty into the final measurements (Boss et al., 2008; Cetinić et al., 2009; Twardowski et al., 2007; Cullen and Davis, 2003; Sullivan et al., 2012). Based on this, all available dark signal offsets were compared.

Routine monitoring of dark offsets during surveys that span years at a time is ideal to detect unexpected changes which may occur due to changes in the sensors

themselves or instrumentation and power configuration differences in the platform that they are integrated with (Twardowski et al., 2007; Cetinić et al., 2009). For for this retrospective study, there were relatively few "in-lab" offsets compared to the very long dataset, so *on situ* methods were also explored as options to dark-correct each deployment and assess instrument changes over time.

Baseline response: Seasonal patterns were similar for each sensor, but distributions of most statistically likely clear-water locations showed distinct differences among sensors (Fig. 0.1). The clearest waters viewed by the CDOM fluorometer were typically in the surface bins at nearly all latitudinal bins; at depth and more offshore for chl-a fluorescence; and at midwater or depth and offshore for scattering. Collectively, the clear water offset (CWO) assumption was found to not apply to this region. While each sensor had locations in latitude and depth space that stood out as statistically more likely to have near-zero values (Fig. 0.1), there was no location guaranteed to provide a quality baseline offset all of the time for any of the sensors.

After this assessment, and because the available in-lab dark offsets were too limited in time to apply for correction purposes (Fig. 0.2 and 0.3), a "deployment minimum" method was developed to correct all three sensors. Essentially, the dark offset is the minimum of the raw signal after it has been filtered for instrument noise (section 4.2.2). This process is done for each deployment. Plots of these minima over time, along with all other available baseline metrics (Figs. 0.2 & 0.3) revealed unexpected changes in the offsets over time that were not captured by the other baseline metrics (Fig. 0.1), hence, they provided the best dark correction value. The pattern of change among the three ECO Puck Triplets for both glider Bob and Jane platforms were qualitatively similar, even in spite of a complete sensor rebuild

of glider Bob's ECO Puck in 2010. Differences across deployments can presumably be attributed to changes in the instrumentation, specifically the ground state and impedance of the instrument, and the environment; an example is if "clear" waters were not encountered by a deployment. This occurred during very short, less than 5-day, deployments that remained primarily in the nearshore zone. The large peak in dark offset values observed in glider Jane's scattering meter in 2011 (Fig. 0.2) is an example of one such transect. Peaks in the dark signal offsets are apparent for the other sensors, although they are smaller in magnitude. Both gliders were overhauled in 2010, coincident with marked shifts in the offsets and to more stable values for the following 1-3 years, depending on the sensor.

Observed changes in dynamic response over time: Factory-derived scale factors for "Jane" and "Bob" ECO Puck sensors show changes in dynamic response (Figure 0.4 a,c,e), which includes changes due to calibration methods, hardware, and presumably instrument age. Glider Bob's ECO Puck was rebuilt in 2010, effectively becoming a third ECO Puck this dataset. In September 2010 and July 2011, WET Labs' calibration protocol changed for the CDOM and chl-a fluorometers, respectively. Only glider Jane's scattering meter had two consecutive scale factors with consistency in hardware and calibration; the trend of 10% per year for the Jane's scattering scale factors is comparable to previously noted values (Sullivan et al., 2012) attributed to aging of the sensor. Figure 0.4b,d,f shows how changes in the scale factors over time translate to changes in the values of the calibrated constituent of interest. For example, a greater than two-fold increase in the scale factor (Figure 0.4c), and subsequently the volume scattering function (Figure 0.4d), for the Jane scattering meter in 2012 compared to 2004.

Calibration method determination: For all three bio-optical sensors, the deployment minimum method was deemed to be the ideal dark offset method since the others do not correct for the large changes in the baseline signals over time. Factory-provided scale factors were used to convert the dark-corrected signal to the units of interest. This is because factory recommendations do not indicate a need for calibrating the CDOM or scattering meters against *in situ* samples. Factory instructions do, however, suggest calibrating the chl-a fluorometer against coincident *in situ* samples or in-lab phytoplankton communities that are considered representative of the region surveyed. This was not possible for two reasons: 1) this was a retrospective calibration effort and no *in situ* data were collected coincident with glider deployments, and 2) the region these gliders observe spans a dynamic nearshore coastal zone to a lower chlorophyll open-ocean regime with strong seasonal variability and broad differences in community composition that, collectively, would prove difficult to adequately characterize with grab samples.

Nonphotochemical quenching experiment: Physiological variability is a well-known confounding factor in the assumed linear relationship between chl-a fluorescence and chl-a concentration. An in-lab dilution experiment was conducted to determine to what extent NPQ by light-adapted phytoplankton may affect the fluorescence signal. The slope of the scattering to chl-a fluorescence plot was 0.89 for the dark-adapted culture and two times greater, 1.67, for the light-adapted culture (Figure 0.5); this indicates that NPQ in similar phytoplankton communities and light environments could reduce chl-a fluorescence signal by up to 1/2.

A4 Conclusions

In this work calibration and correction methods, as well as instrumental change over time, were assessed for bio-optical sensors deployed aboard two Slocum glider platforms which surveyed a consistent region offshore of the central Oregon coast for 8 years. Calibration methods in the literature were surveyed and considered or tested with this dataset. "Best fit" methods were applied (e.g., factory scale factor) or new methods developed (e.g., deployment minimum) when previously-described protocols were found not applicable.

An unexpected pattern of change was observed in the dark offsets over time and was likely due primarily to changes in the glider platform over time. Significant change was also found in the sensor scale factors over time, although for both the chl-a and CDOM fluorometers it was impossible to determine to what extent instrument age or differing sensor calibration methods could be responsible for those differences. Collectively, these changes over time underscore the importance of routine, consistent assessments of scale factors and dark offsets for the lifetime of a sensor. Through the considerations described in this work, the originally planned calibration methods ended up being different than those ultimately applied. The bio-optical dataset is more accurately calibrated as a result of this exercise.

The most broadly-applicable results of this work is that routine calibration of bio-optical sensors–using consistent methods over time–is key to robust datasets; however there is no "one-size fits all" selection of calibration protocols that will apply to all long-term deployments of bio-optical sensors. Calibration methods should be based on careful consideration of 1) region of interest and its inherent variability (hydrographic, seasonal, biological) and how that variability may impact sensor

performance; 2) availability of coincident in-water or in-lab datasets for calibration; 3) planned application of the dataset; 4) change in sensor performance over time; and 5) assumptions made in calibration methods, such as the assumed linear relationship between chl-a fluorescence and concentration inherent in chl-a fluorometer calibration.

FIGURES

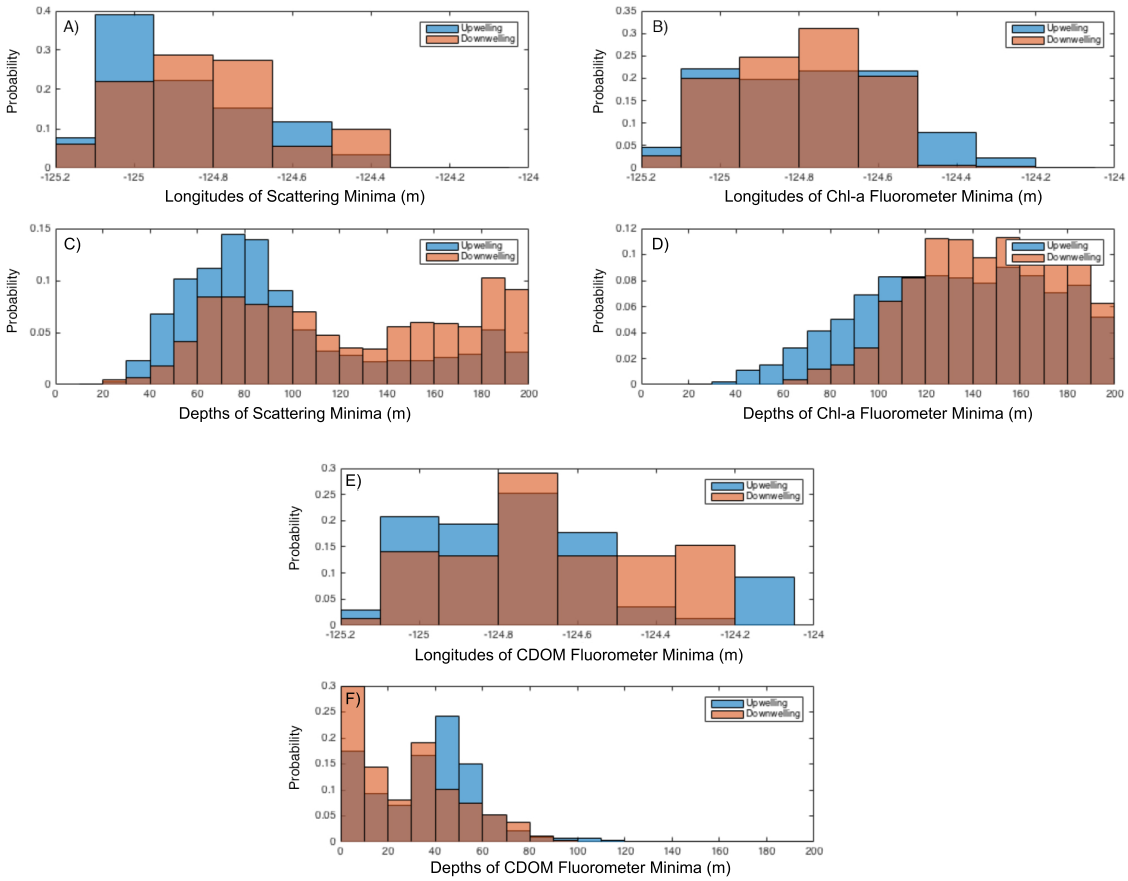

FIGURE 0.1: Probability distribution of lowest values in deployment

Does the "clear water assumption" hold in this region, i.e., does a consistent depth and offshore location reliably capture an accurate baseline signal? Probability distributions for a clear water location in longitude (top panels) and depth (lower panels) space for A) scattering, B) chlorophyll-a fluorescence, and C) CDOM fluorescence. Blue and red indicate up- and down-welling seasons.

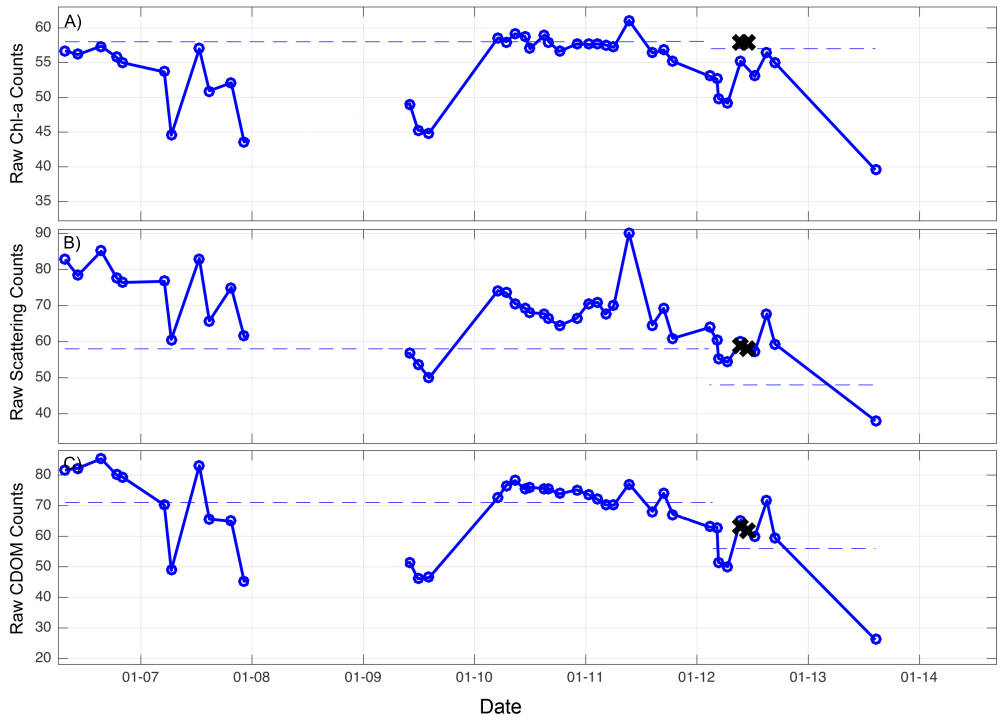

FIGURE 0.2: Trends in dark signal offsets for glider Jane over time

How do all available baseline signal metrics for glider Jane compare over time? Dark signal offsets for A,C) chl-a fluorometer, B,D) scattering, and E,F) CDOM fluorometer ECO Puck sensors aboard glider Jane over time. Dark offsets were calculated using each deployment minimum (blue solid line), factory (blue dashed line), and in-lab (black x symbols) methods. Note differences in y axes. Data for 2008 were unavailable for this study. Glider Jane was lost at sea in late 2013; no data available for 2014.

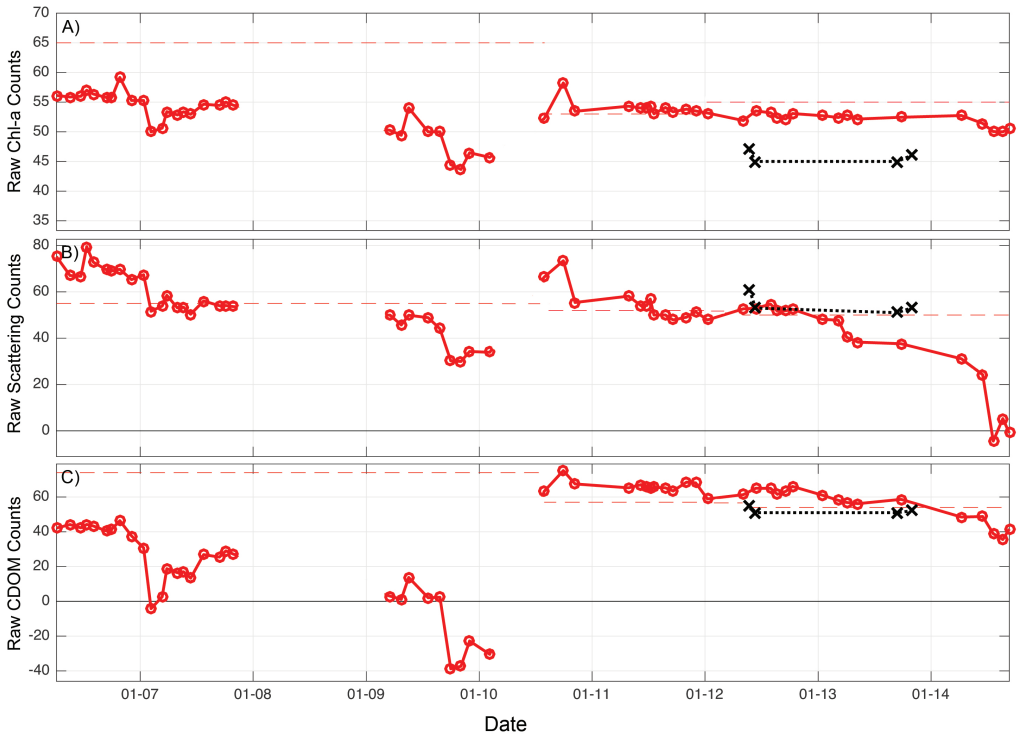

FIGURE 0.3: Trends in dark signal offsets for glider Bob over time

How do all available baseline signal metrics for glider Jane compare over time? Dark signal offsets for A) chl-a fluorometer, B) scattering, and C) CDOM fluorometer ECO Puck sensors aboard glider Bob over time. Glider Bob's ECO Puck was rebuilt in 2010 and was considered a new instrument, hence lines are not connected between the points in early 2010. Dark offsets were calculated using each deployment minimum (red solid line), factory (red dashed line), and in-lab (black x symbols) methods. Note differences in y axes. Data for 2008 were unavailable for this study.

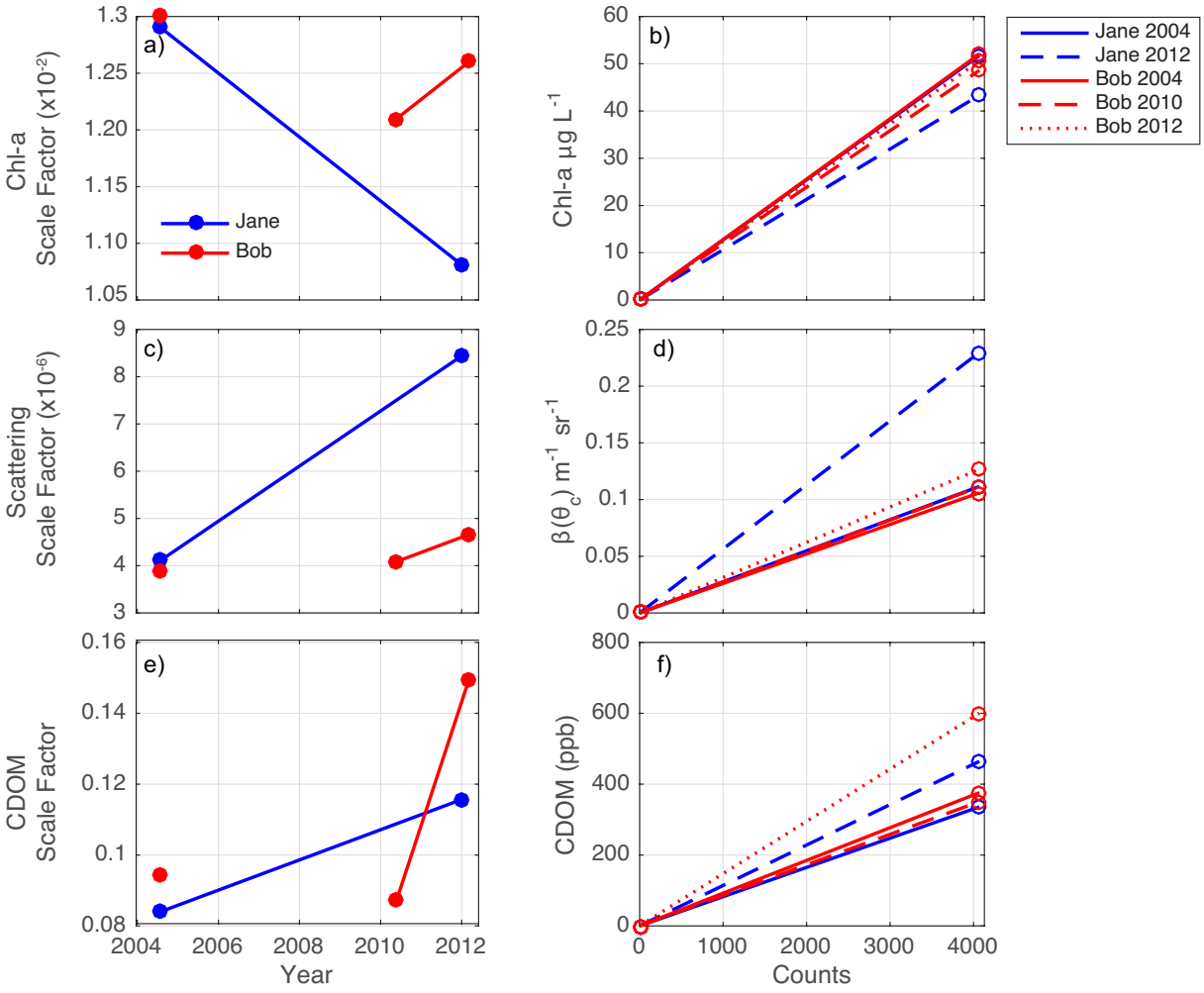

FIGURE 0.4: Changes in dynamic response over time

How did sensor baseline response change over time? Panels A, C, E show factory-derived scale factors for Jane (blue) and Bob (red) ECO Puck sensors. Glider Bob's ECO Puck was rebuilt in 2010 and was considered a new instrument, hence lines are not connected between the 2004 and 2010 data points (A,C,E). All scale factor values after 2004 are affected by method changes, except for scattering, see results section for details. Panels B, D, F show how changes in the scale factors translate to changes in values of the constituent of interest.

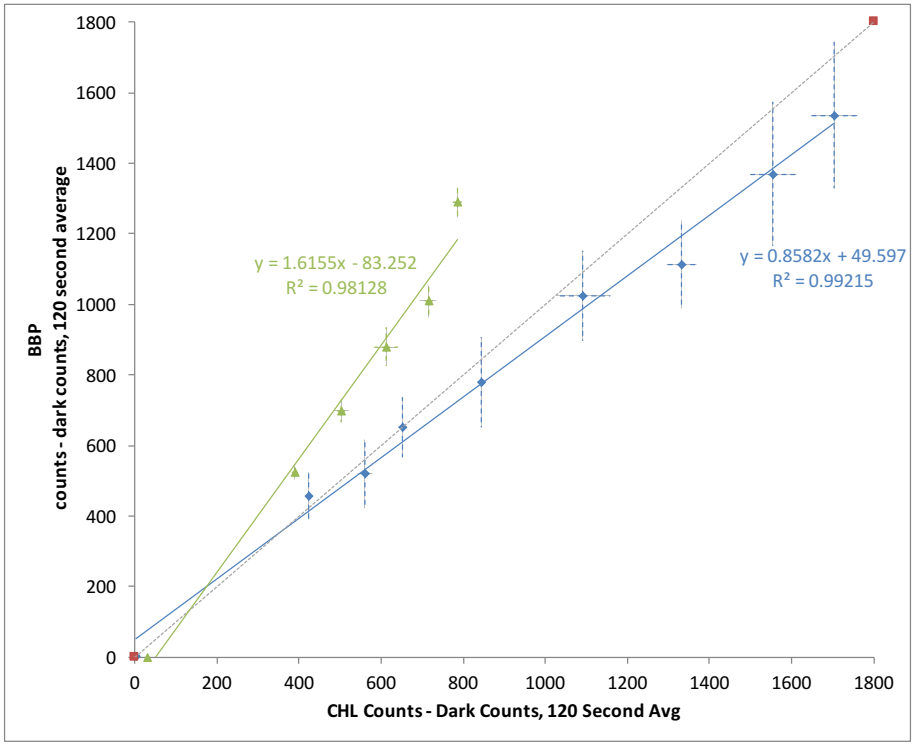

FIGURE 0.5: Chlorophyll-a to scattering ratio for light and dark-adapted phytoplankton

How much might nonphotochemical quenching affect the scattering to chl-a ratio? Dark-corrected scattering counts (y axis) versus dark correccted chlorophyll-a fluorescence counts (x axis) during dilution experiments with light- (green line) and dark-adapted (blue line) phytoplankton monocultures of *Thalassiosira weissflogii*. The slope for the light-adapted culture was twice the slope for the dark-adapted culture.

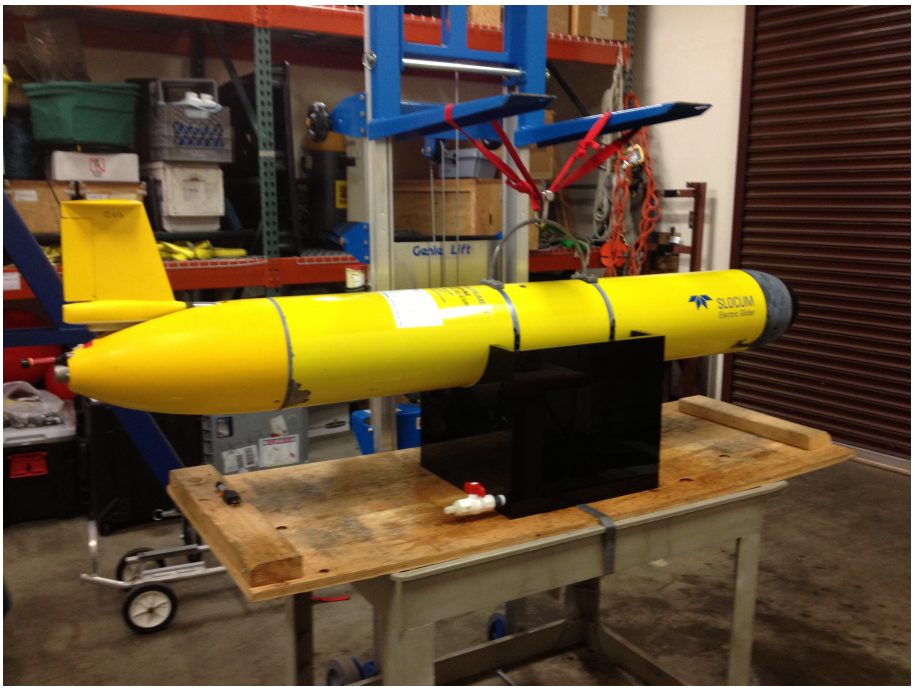

FIGURE 0.6: Setup for in-lab glider experiments

How much might nonphotochemical quenching affect the scattering to chl-a ratio? Experimental setup for in-lab experiments to quantify the effects of nonphotochemical quenching on the chl-a scale factor. Glider is placed on a custom-made dark chamber to submerge the optical instruments in a controlled parcel of water. Phytoplankton dilutions were conducted as described in (Cetinić et al., 2009), methods in Appendix A, and Fig. 0.5.